MOLECULAR ANISOTROPY AND LIQUID CRYSTALLINITY

BY

MARK JAMES WILSON

A Thesis submitted for the
degree of
MASTER OF PHILOSOPHY

Department of Chemistry
University of Southampton.

December 1991.

UNIVERSITY OF SOUTHAMPTON

ABSTRACT

FACULTY OF SCIENCE

CHEMISTRY

Master of Philosophy

Molecular Anisotropy and Liquid Crystallinity.

by Mark James Wilson

This thesis is concerned with the effect, on liquid-crystalline properties, of increasing the molecular anisotropy. In chapter one we give an introduction to liquid crystals; their phases, molecular structure and how this relates to their physical properties. This is followed by a quantitative description of the Maier-Saupe molecular field theory for rod-like molecules; the approximations made, the properties predicted and how these predictions compare with those of real systems. This chapter concludes with a purely qualitative description of how the Maier-Saupe theory can be extended to flexible molecules. The second chapter describes the synthesis and characterisation of the 4-n-alkoxy-4"-cyano-p-terphenyls. The properties of these new materials are compared with those of the analogous 4-n-alkyl-4"-cyano-p-terphenyls, as well as the 4-n-alkoxy and 4-n-alkyl-4'-cyanobiphenyls. The final chapter begins with a quantitative description of the molecular field theory for flexible molecules, as outlined qualitatively in chapter one. This is then used to predict the change in the properties of nematogens as the length of a terminal chain is increased. The chapter concludes with a comparison of these predicted thermodynamic properties of the 4-n-alkoxy-4"-cyano-p-terphenyls and 4-n-alkoxy-4'-cyanobiphenyls with those observed experimentally.

CONTENTS

ACKNOWLEDGEMENTS

Firstly I would like to thank my supervisor, Professor G.R. Luckhurst, for constant support and enthusiastic encouragement over the last year.
My thanks go to Dr J.M. Seddon for carrying out the X-ray diffraction experiments and Dr A.J.P. Emerson for the copy of his computer program used in the latter part of this work.

I wish to thank all the members of the liquid crystal group, both past and present, for the friendly atmosphere which makes study more enjoyable, lack of space prevents me naming them all. However, particular thanks must go to Mr O.T. Howell and Mr A.G. Douglass for their help with various aspects of synthetic chemistry, Mr K.E. Meacham for his assistance in computational areas, and Dr C.T. Imrie for proof reading this thesis.

My thanks go to Mrs. K. Hinton, the happiest member of the Chemistry department, for all her help over the last year.

I thank Merck UK (formerly BDH Ltd) and the Department of Chemistry for the maintenance award for the past year.

Finally, I am indebted to my family and my girlfriend, Amanda, for their constant understanding and encouragement.

TO

MY

GRANDPARENTS.

CHAPTER 1: Introduction to Liquid Crystal Phases and their Properties

It is a little over one hundred years since Friedrich Reinitzer communicated his unusual observations [1] on cholesteryl benzoate to Otto Lehmann. Reinitzer noted that the crystals would melt to form a turbid liquid which upon further heating would form a clear liquid. Optical studies by Lehmann showed this turbid phase to be birefringent, a property generally associated with crystalline materials but it flowed like a conventional liquid [2]. Consequently this turbid liquid was termed a liquid crystal phase or, more correctly, a mesophase, from the greek *meso-* meaning intermediate. Since Reinitzer's initial observations in 1888 many thousands of organic and, more recently, inorganic compounds have been found to exhibit mesophases [3]. All mesophases, of which many types have now been identified, show a degree of correlation of the molecular orientation which extends over much greater distances than in isotropic liquids, they possess a long range orientational ordering of the molecules. Combined with this is a positional ordering less than that found in crystalline phases, the mesophases possess short range positional order. Traditionally liquid-crystalline phases were classified as one of two types, thermotropic or lyotropic. Thermotropic phases are formed by pure compounds which upon heating melt from the crystalline state to a liquid crystal phase. Lyotropic mesophases result from molecular associations of amphiphilic molecules and self-organisation of the aggregates in systems of two or more components. This work will not deal with lyotropic systems any further, reviews of the subject being available in the literature [4]. In recent years, various developments [5] have meant that the two classifications now overlap to a considerable degree. It has been proposed that a better classification for mesophases is based on the basic unit being either a molecule, non-amphiphilic phases, or an aggregate, amphiphilic mesophases [6].

Liquid-crystalline materials are of great interest fundamentally because of the unusual combination of long range order and disorder in these systems and at a more practical level [7] for their many important industrial applications. In the case of thermotropic, non-amphiphilic compounds these include use in electro-optic display devices, temperature sensors, and for polymeric materials use as high strength materials. Lyotropic, amphiphilic liquid crystals are widely used as surfactants.

1.1 Description and Characterisation of Thermotropic Mesophases

1.1.1 The Nematic Phase (N)

The nematic is the least ordered of the mesophases [8] and is formed by anisotropic molecules, rod-like or disc-like molecules. The phase exhibits long range orientational order, over many molecular distances there is a statistical probability that the molecules will align with their long axes parallel to each

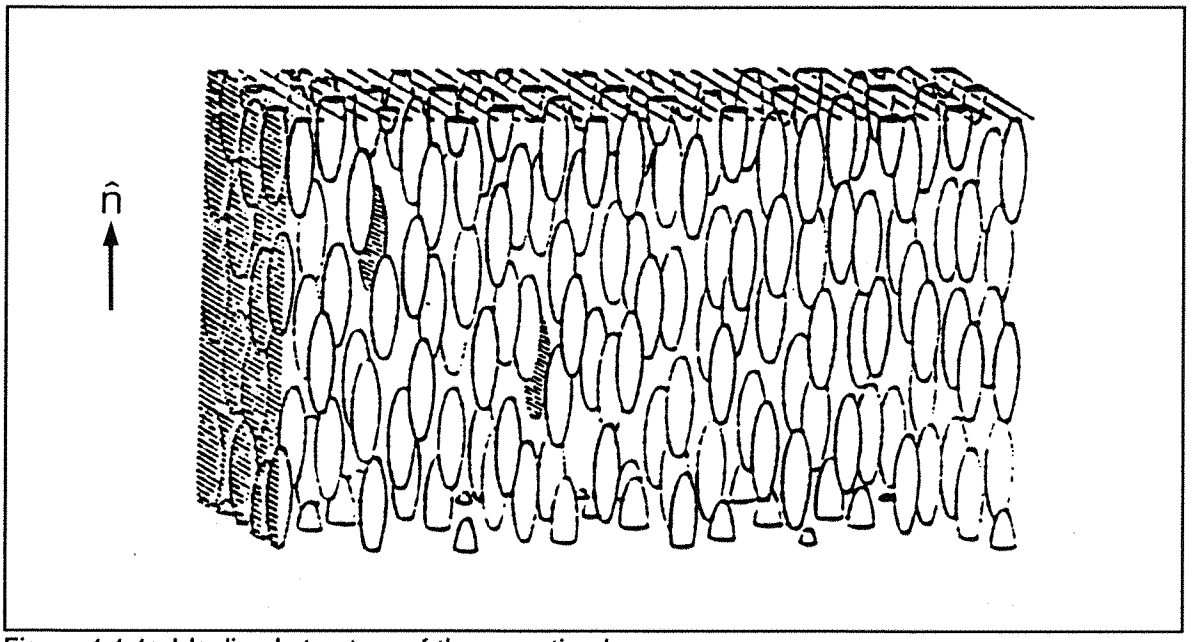

Figure 1.1.1a Idealised structure of the nematic phase.

other. The average direction of orientational alignment defines a unique direction known as the director,$\hat{n}$. Figure 1.1.1a shows an idealised structure of the nematic phase. This uniaxial phase shows correlations of the molecular centres of mass extending only over short distances, that is the phase has only short range positional order. This results in translational motion parallel to the director and free rotation about the molecular long axis.

The phase can show strong pretransitional effects, close to the phase transition

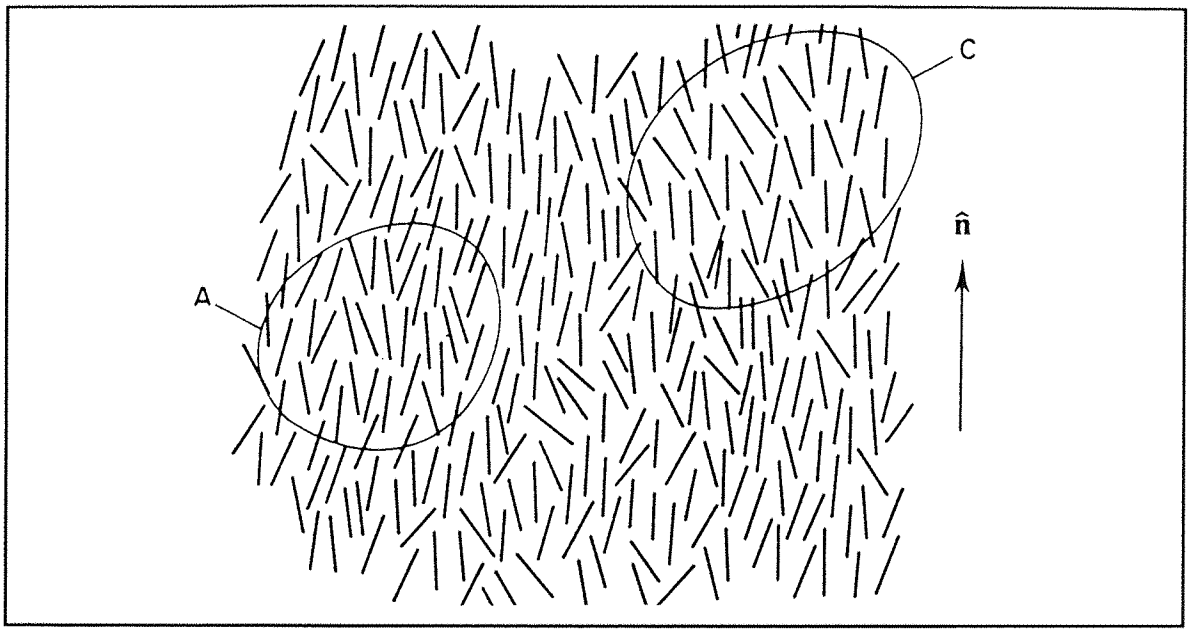

Figure 1.1.1b Areas of increased translational order within the nematic phase.

to a more ordered mesophase [9], areas of layered structure, similar to the smectic A or smectic C phase can be observed [10] (illustrated in figure 1.1.1b). The formation of such regions is the result of increases in the translational order.

The nematic phase can be identified via optical microscopy by the characteristic homeotropic and schlieren textures [11], as shown in plate 2.3(i). The homeotropic is produced by surface alignment of the director along the direction of the incident light beam and appears optically isotropic and dark. The schlieren texture is very mobile, highly coloured and has dark thread-like regions which meet at point singularities, arising from strong distortions in the director field. Both textures of the nematic phase flash when subjected to mechanical stress. The nematic schlieren texture occurs with both two and four point singularities, in contrast to the smectic C schlieren texture which only shows four point singularities.

1.1.2 Smectic Phases

The smectic phases [8][12] are more highly ordered than the nematic phase. They share with the nematic the tendency for alignment of the molecular long axes, but also show a degree of translational order which produces a layered structure. The layers, however, are not sharply defined. The positional singlet distribution function parallel to the director and layer normal being a sinusoidal density wave rather than a sum of delta functions.

As the structural details of the various smectic phases have been established some of the phases, namely E,G,H,J and K have been renamed crystal phases

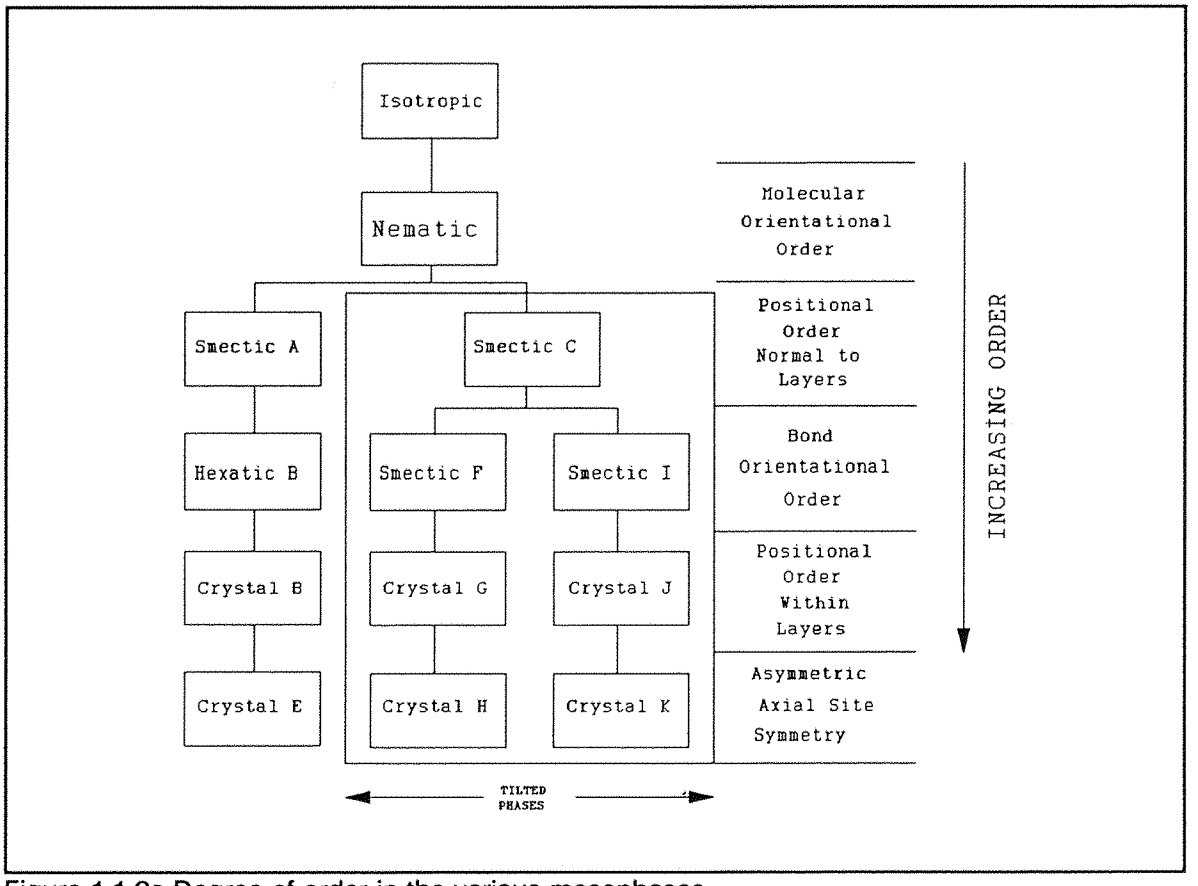

Figure 1.1.2a Degree of order in the various mesophases.

as they possess three dimensional correlations of molecular positions and consequently are structurally crystalline.

Optical studies of smectic phases can produce two types of phase texture, natural or paramorphotic. Natural optical textures are those formed on cooling directly from the nematic or isotropic phase. Paramorphotic textures are those inherited on cooling from a higher temperature smectic phase, eg the crystal E paramorphotic focal conic fan texture is a modified version of the similar texture formed by the smectic A phase.

The Smectic A phase (S_A)

The smectic A phase is the least ordered of the smectic phases and generally

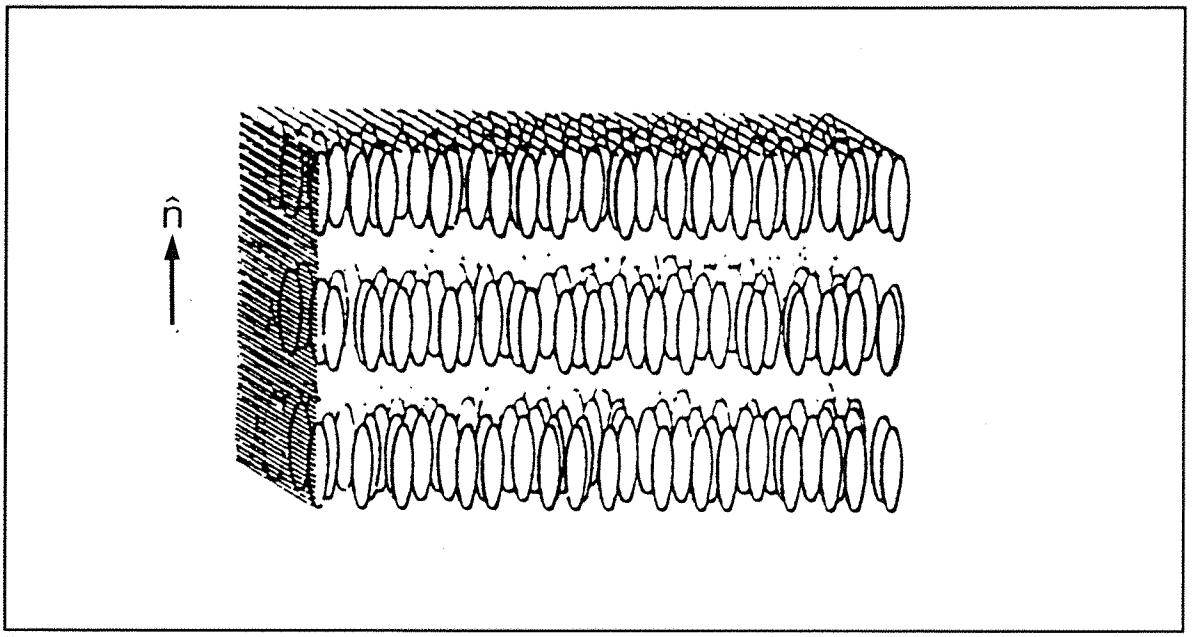

Figure 1.1.2b Idealised structure of the smectic A phase.

occurs as the highest temperature smectic phase. As in the nematic phase, there is a long range orientational correlation of the molecular long axes parallel to the director. The molecules also show a degree of long range positional ordering resulting in a layered structure. Within the layers the

structure is nematic like with no long range positional correlations, the molecules showing rapid rotation about their long axes. There is hindered translational motion of the molecules between layers and the layers freely slide over each other.

In recent years investigations have found that there are four modifications of the smectic A phase depending on the nature of the constituent molecules [10][13].

S_{A1} The conventional phase which shows a random head to tail disorder of the molecules. The layer spacing, as measured by X-ray diffraction, is of the order of 0.8 times the molecular length, less than the expected all *trans* length because of orientational fluctuations and conformational averaging across the distribution. (see figure 1.1.2c)

S_{A2} A bilayer phase showing antiferroelectric, alternate head to tail, ordering of the molecules. The measured layer spacing is of the order of 1.75 times the all *trans* molecular length. (see figure 1.1.2c)

S_{Ad} A semi-bilayer structure showing partial molecular associations, resulting in a layer spacing of the order of 1.25-1.50 times the all *trans* length. (see figure 1.1.2c)

$S_{\tilde{A}}$ Known as the antiphase, shows a modulated antiferroelectric ordering within the layers resulting in a ribbon type structure. (see figure 1.1.2c)

These four modifications can be distinguished by X-ray diffraction studies of monodomain samples, where the low angle region gives information on the layer spacing [14].

The smectic A phase can be identified by the two natural textures formed, the homeotropic and the focal conic. The homeotropic texture is optically isotropic and appears dark. This texture is the result of director alignment parallel to the incident light beam. The focal conic fan texture is characterised by the development of bâtonnets or needle shaped regions which merge to form a complete structure. The backs of the fans are crossed with faint lines.

Examples of both textures are shown in plates 2.3(ii) and 2.3(iii).

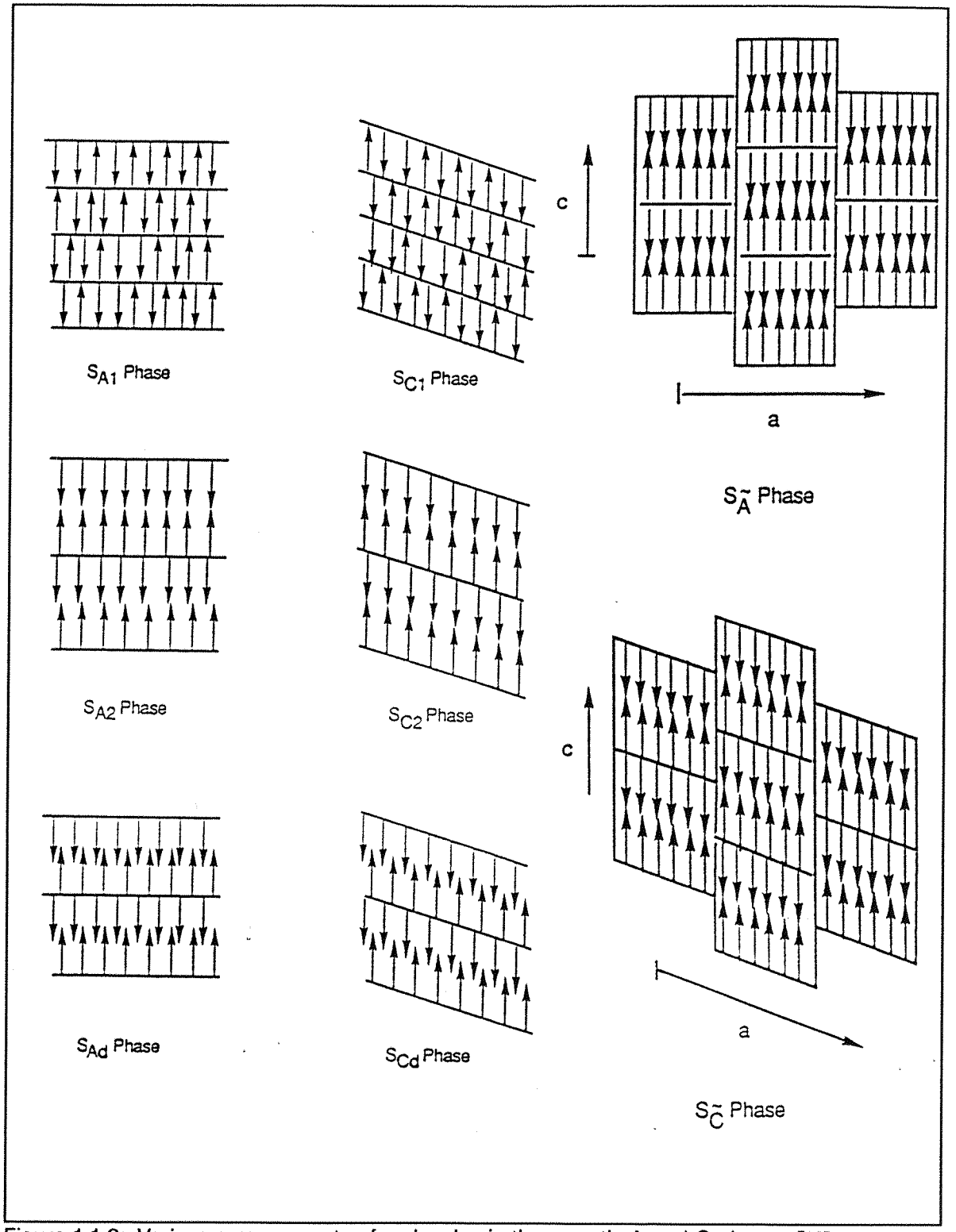

Figure 1.1.2c Various arrangements of molecules in the smectic A and C phases. [10]

The Smectic C phase (S_C)

The smectic C phase is closely related to the smectic A described in the last section, the main difference being that the director is tilted with respect to the layer normal resulting in the phase being biaxial. The tilt angle, measured between the director and the layer normal, will vary with temperature and between different compounds. Within the layers there is long range correlation of the tilt directors, there are however only short range correlations between layers and hindered movement of molecules between layers.

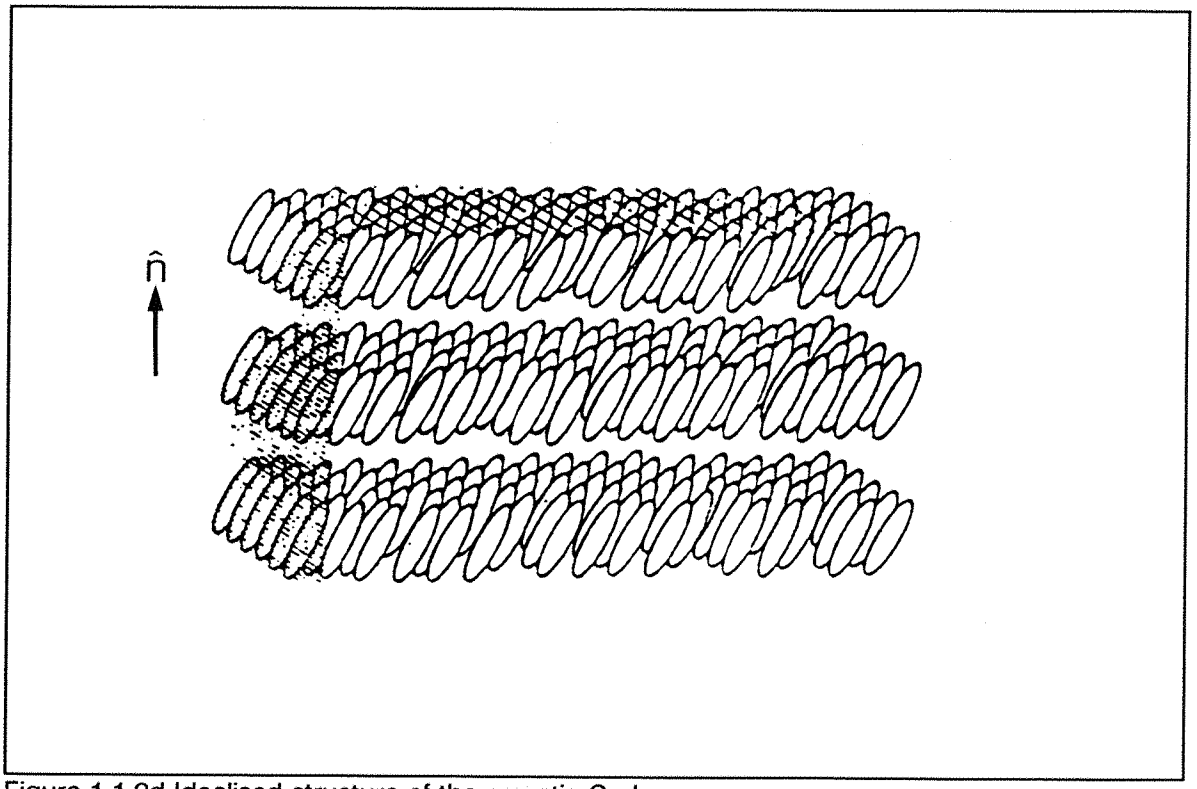

Figure 1.1.2d Idealised structure of the smectic C phase.

The smectic C phase again shows four modifications (S_{C1},S_{C2},S_{Cd},$S_{\tilde{C}}$) equivalent to those outlined for the smectic A phase [13], as illustrated in figure 1.1.2c.

The smectic C phase exhibits two natural textures the schlieren and the focal conic fan texture. The schlieren texture can be distinguished from that of the

nematic phase by the fact that it is less mobile, only consists of four point singularities and does not flash when subjected to mechanical stress. The focal conic fan texture is generally formed paramorphotically from the smectic A and is typically very broken and sanded resulting in an ill-defined appearance. The natural focal conic fan texture is rarely formed but when seen is less broken than that of the paramorphotic texture.

The Smectic B phase (S_B)

There are two forms of the smectic B phase, the hexatic B and the crystal B. The structure of the hexatic B phase is similar to that of the smectic A phase except for a hexagonal [15] packing of the molecules within the layers. The positional order is medium range with a correlation length an order of magnitude larger than for either the smectic A or C phases. Within the hexatic B there are no positional correlations between layers, but three dimensional long range bond orientational order is present [16]. In common with the S_A phase the director lies perpendicular to the layers and the molecules rotate rapidly [17] about their long axes. It has been shown that the hexagonal net on which the molecules are sited is small in comparison to the molecular size resulting in a cooperative rather than free rotation. The layers are of monolayer spacing except in the case of a few compounds containing very polar terminal groups, such as the cyano group [18], where a bilayer S_{B2} structure has been observed.

The crystal B phase shows long range layer correlations and long range positional ordering within the layers. The phase is truly crystalline but shows considerable thermal disorder, such as rapid rotation about the molecular long axes. The correlations between positions of molecules in adjacent layers gives rise to a variety of possible packing arrangements [19] such as **AAAA** monolayer, **ABAB** bilayer and **ABCA** trilayer (where **A**,**B** and **C** denote the highest symmetry positions of the molecules in adjacent layers).
The smectic B phase exhibits two natural textures the homeotropic and the mosaic and a single paramorphotic focal conic fan texture. The homeotropic texture is optically isotropic and appears dark as for the homeotropic S_A texture. The mosaic texture consists of interlocking platelets and is characterised by the presence of H-shaped platelets. The paramorphotic focal

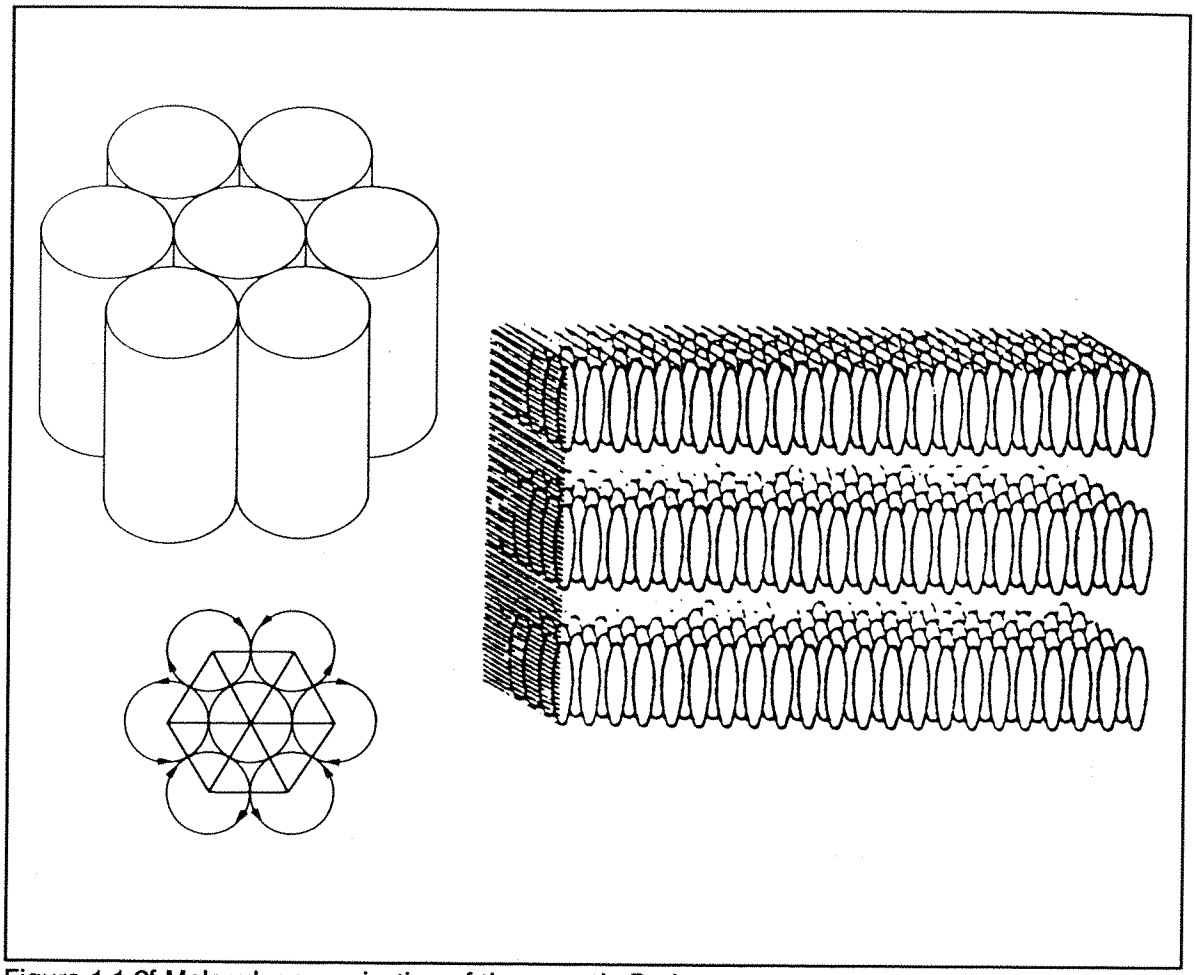

Figure 1.1.2f Molecular organisation of the smectic B phase.

conic fan texture is formed from the similar texture of the smectic A, but has very smooth fan backs unlike the S_A. The transition between S_A and S_B is characterised by the formation of transition bars across the backs of the fans. Although in some cases transition bars have been observed for the S_A to crystal B transition.

The D Phase (D)

The D phase, originally known as the smectic D, is a rarely observed phase. In all observations to date the phase shows an optically isotropic texture. The structure of the D phase is uncertain, however it has been clearly established as being based on a cubic unit cell and having three dimensional periodicity [20], with the possibility of micellar type formations.

The Smectic F and I phases (S_F,S_I)

The smectic F and smectic I phases are very similar in structure, both phases consist of layers of hexagonally packed molecules in which the director is tilted with respect to the layer normal. Within the layers there is no long range positional ordering of the molecular centres of mass and no long range interlayer correlations exist. These phases can, therefore, be considered as tilted analogues of the smectic B phase. The two phases differ in the direction of the director tilt with respect to the hexagonal net, in the smectic F the director is tilted towards the edge of the net whereas in the smectic I phase the tilt is towards the apex of the net, as illustrated in figure 1.1.2g.

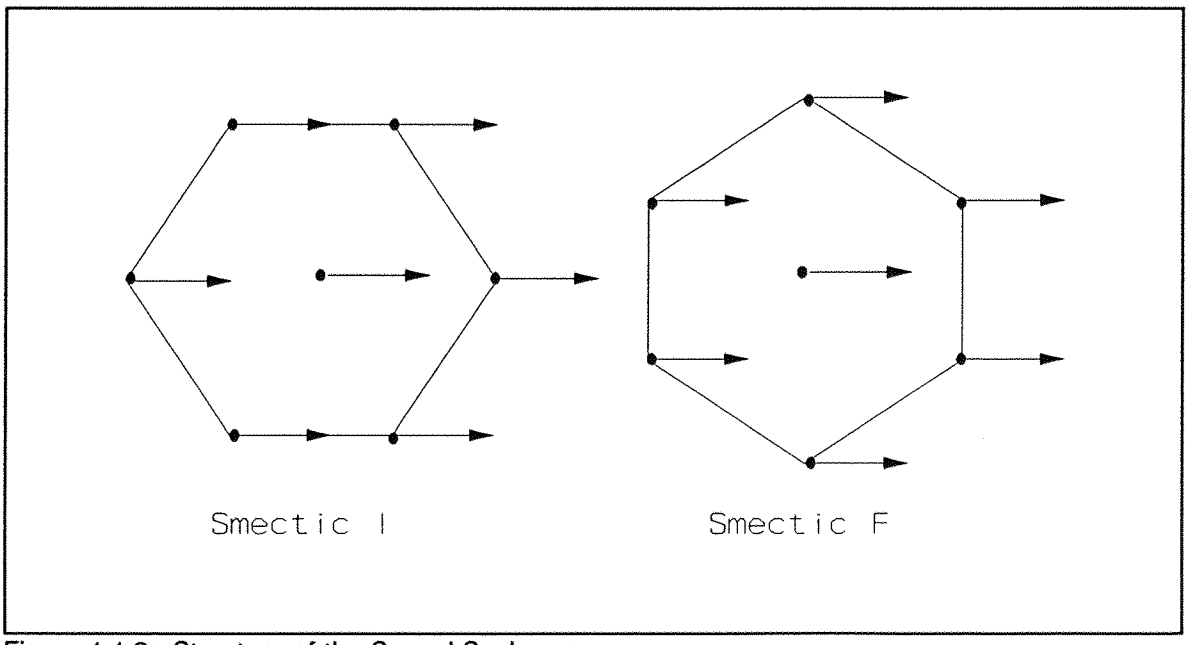

Figure 1.1.2g Structure of the S_F and S_I phases.

It should be noted, however, that there is some debate concerning the interlayer correlation length in the S_I phase, it has been suggested that a long range ordering exists within layers making this phase a series of weakly coupled two dimensional crystal layers [21].

1.1.3 Crystal phases

The Crystal E phase (E)

The crystal E or, as it is often still known, the smectic E phase has a long range ordering of both the molecular positions within the layers and interlayer correlations. The structure of the phase is that of the smectic B phase in which the cooperative rotation of the molecules about their long axes has been removed by the distortion of the unit cell from hexagonal to orthorhombic packing [19]. The motion of the molecules has been shown [17] to be a rapid but highly correlated flipping motion, a rotation of π about both long and short molecular axes. The resulting structure is a herringbone packing of the molecular cross sections within the layer, see figure 1.1.3a.

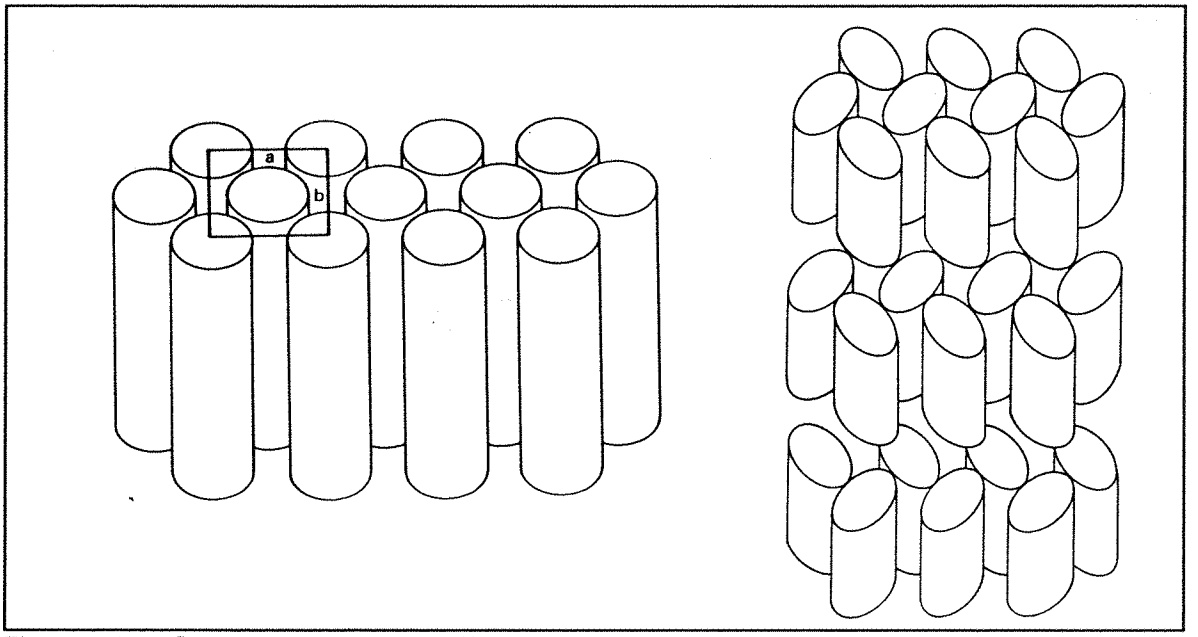

Figure 1.1.3a Structure of the crystal E phase.

There are very few examples of direct isotropic to crystal E transitions so it is difficult to determine the characteristics of the natural crystal E textures. However, the three paramorphotic varieties formed, the focal conic, the platelet

and the mosaic textures have been characterised. The focal conic fan texture shows very clear arcs across the backs of the fans which remain throughout the temperature range of the phase, in contrast to the S_A to S_B transition bars which can only be seen a few degrees either side of the transition. The platelets formed on cooling the homeotropic texture of the S_A or S_B phase appear grey-blue to yellow and ghost-like. The mosaic texture consists of interlocking well-defined platelets crossed with parallel lines. The platelet and focal conic fan textures of the crystal E phase are shown in plate 2.3(iv).

Other Crystal Phases

There are four further phases originally classified as smectics but in recent years they have been become known as crystal phases, as a result of the three dimensional long range order which they possess. The phases are best considered in pairs, the G and J phases are tilted analogues of the crystal B phase and as such crystal analogues of the S_F and S_I. They are hexagonally packed tilted phases that vary, as in the S_F and S_I, in the direction of the tilt. In the G phase the director is tilted towards the edge of the hexagonal net, the J phase towards the apex.

The crystal H and K phases are tilted analogues of the crystal E and thus can be considered as G and J phases with a loss of rotational freedom. The layers are composed of molecules packed in a herringbone arrangement with the director tilted with respect to the layer normal. The H and K phases vary in the tilt direction, in the crystal H the director tilts towards the edge of the orthorhombic net, in the K phase the director tilts towards the apex.

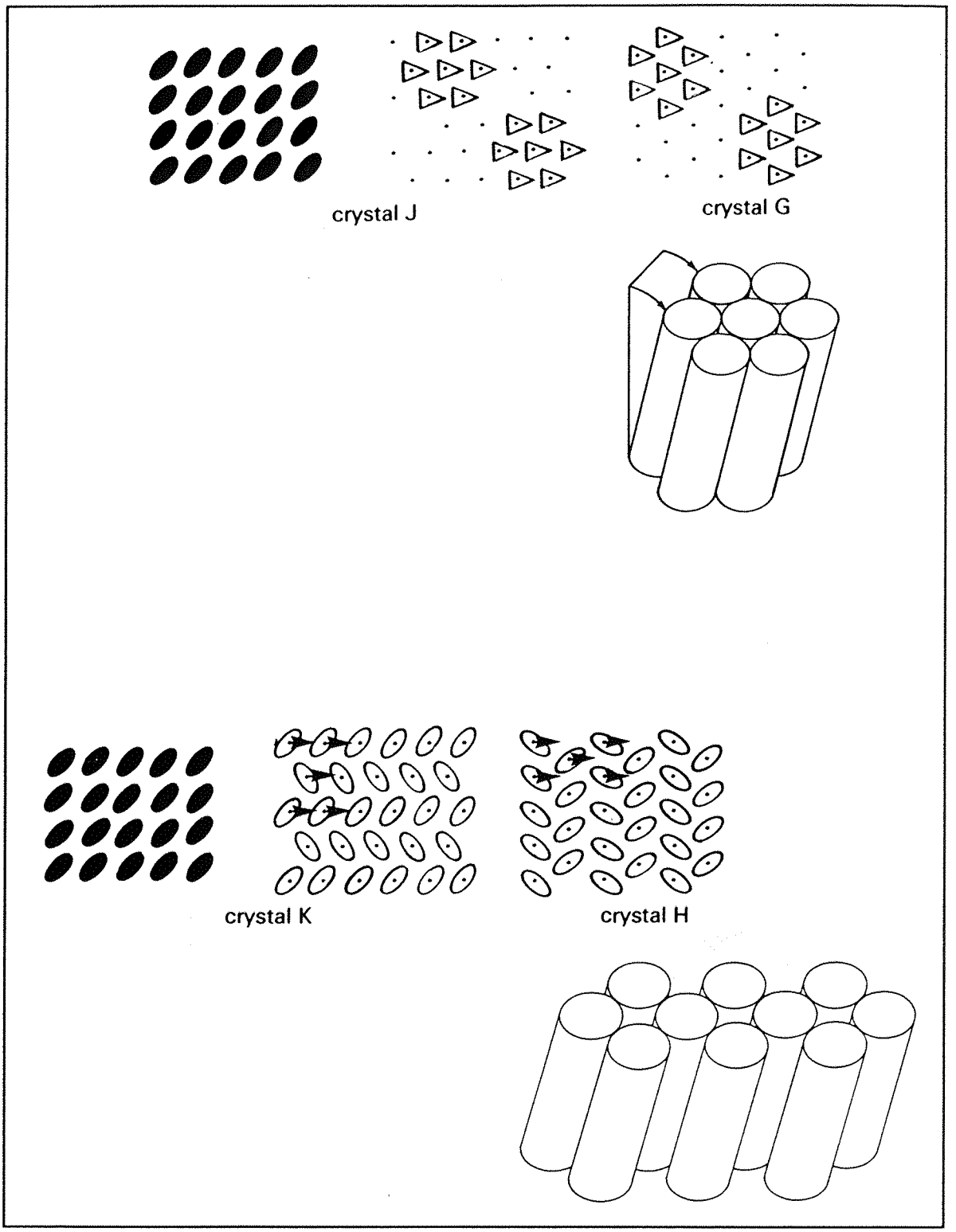

Figure 1.1.3b Schematic representations of the molecular organisation in the crystal G,J,H and K phases. [12]

1.2 Phase Transitions

Phase transitions can be classified according to a system proposed by Ehrenfest [22]. According to this scheme, which is widely used, the order of a phase transition is derived from considerations of the behaviour of the Gibbs free energy at the transition, where $\Delta G = \Delta H - T\Delta S$, where H is the enthalpy and S is the entropy.

A phase transition is said to be of n^{th} order if the n^{th} derivative of the Gibbs free energy with respect to temperature shows a discontinuity,ie. $(\partial G^n/\partial T^n)_p$ is discontinuous.

This classification [23] is a useful one as functions of the derivatives are equal to measurable physical properties. Thus the first derivative of G is the entropy, $S = -(\partial G/\partial T)_p$. The second derivative is related to the heat capacity at constant pressure, $C_p = -T(\partial^2 G/\partial T^2)_p$.

Figure 1.2a illustrates the variation of certain thermodynamic properties across first and second order phase transitions. It can be seen that a first order transition has a non-zero enthalpy and entropy change and an infinite heat capacity, indicating that heat energy is absorbed to disorder the system without increasing the temperature of the system. In contrast a second order transition shows enthalpy and entropy changes of zero and a finite change in the heat capacity of the system.

A useful technique in determining the enthalpy, entropy and heat capacity changes, and hence the order, of a transition together with the temperature at which it occurs is differential scanning calorimetry (DSC). A differential scanning calorimeter consists of sample and reference holders linked to an average temperature circuit which measures the temperatures of the two holders. The temperature is varied across a predetermined range and a temperature difference circuit adjusts the heaters of the two holders so that they remain at equal temperatures. When the sample undergoes a transition the two heaters require different power inputs to maintain the temperature

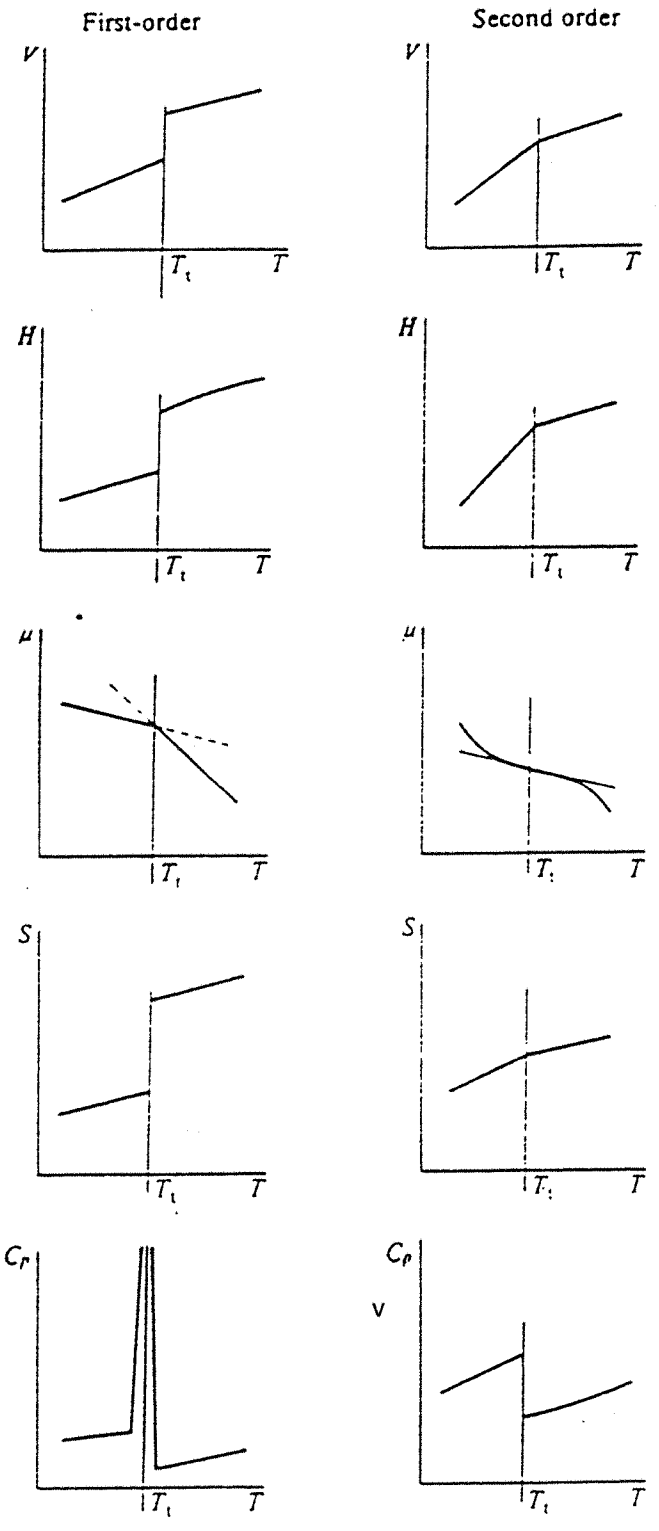

Figure 1.2a Variation of various properties across first and second order phase transitions[23]

equality. The power difference supplied to the heaters is plotted as a function of the temperture and the resulting graph gives information on any transitions that have occurred.

A first order transition is revealed by a peak, the area under which is proportional to the enthalpy change and the transition temperature is obtained by extrapolation of the leading edge to the baseline, see figure 1.2b. A second order transition is seen as a step in the baseline, the transition temperature is frequently taken as that at half height, see figure 1.2b, although other points can be used.

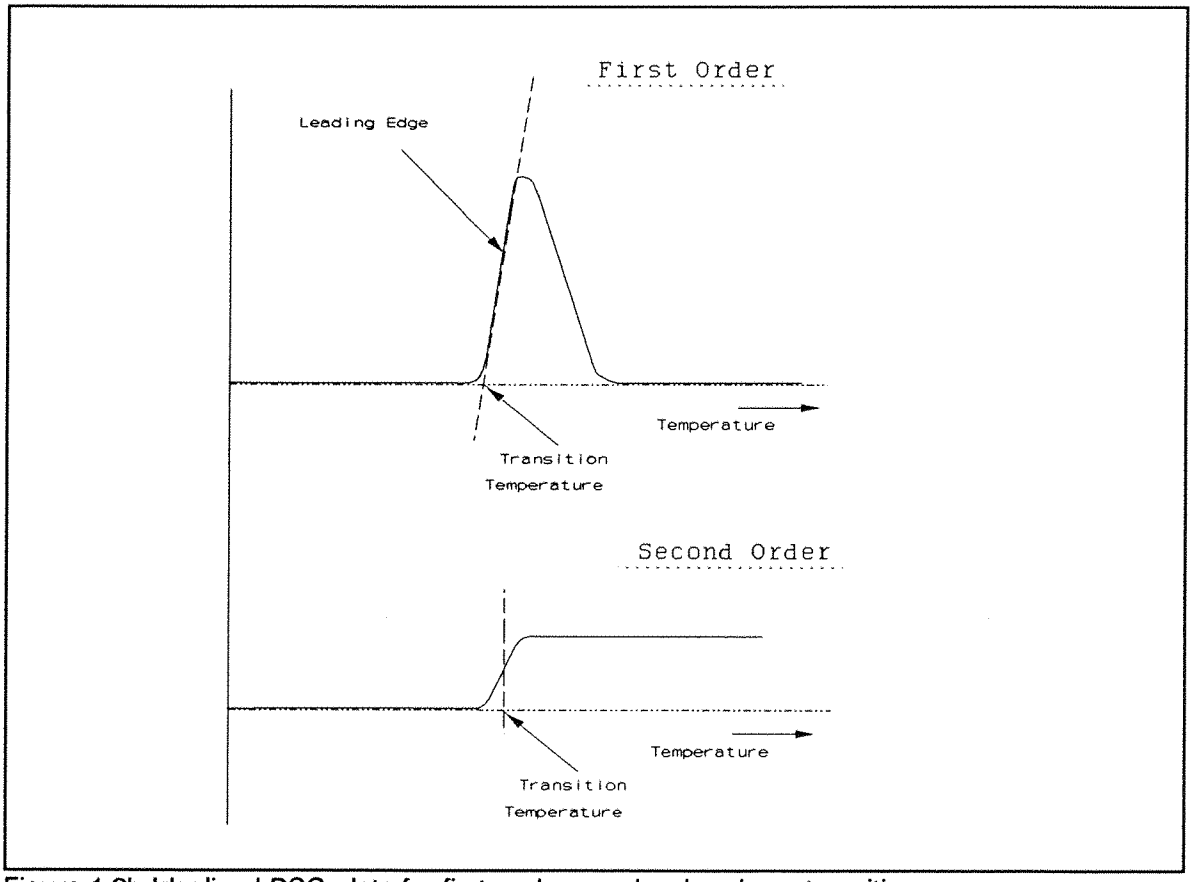

Figure 1.2b Idealised DSC plots for first and second order phase transitions.

1.3 X-ray Diffraction

X-ray diffraction is a powerful technique which can give information on the structural organisation of a phase [24]. In this work X-ray diffraction is used only to obtain an effective molecular length in the nematic phase and smectic layer spacings, in order to gain an insight into possible bilayer formation or interdigitation. As a result a relatively simple explanation of the technique will be sufficient [23].

Diffraction arises as a result of the interference between waves, there is an enhancement of the intensity if the waves are in phase and reinforce each other; constructive interference. Out of phase waves will cancel in destructive interference. The relative phases of waves originating from a single source depends on their path lengths. It is apparent from figure 1.3a that the path difference between the two waves illustrated is (AB+BC), simple trigonometry gives this path difference to be $2d \sin\theta$, where d is the layer spacing and θ the angle of incidence of the X-rays. In order for constructive interference to occur this path difference has to be equal to an integer number of wavelengths, bright reflections will only be observed when this Bragg condition is met, that is $n\lambda = 2d \sin\theta$. λ is known from the source characteristics and 2θ is measured in the experiment, the value of d the interlayer spacing can be obtained by assuming that the first bright reflection corresponds to the $n=1$, first order reflection.

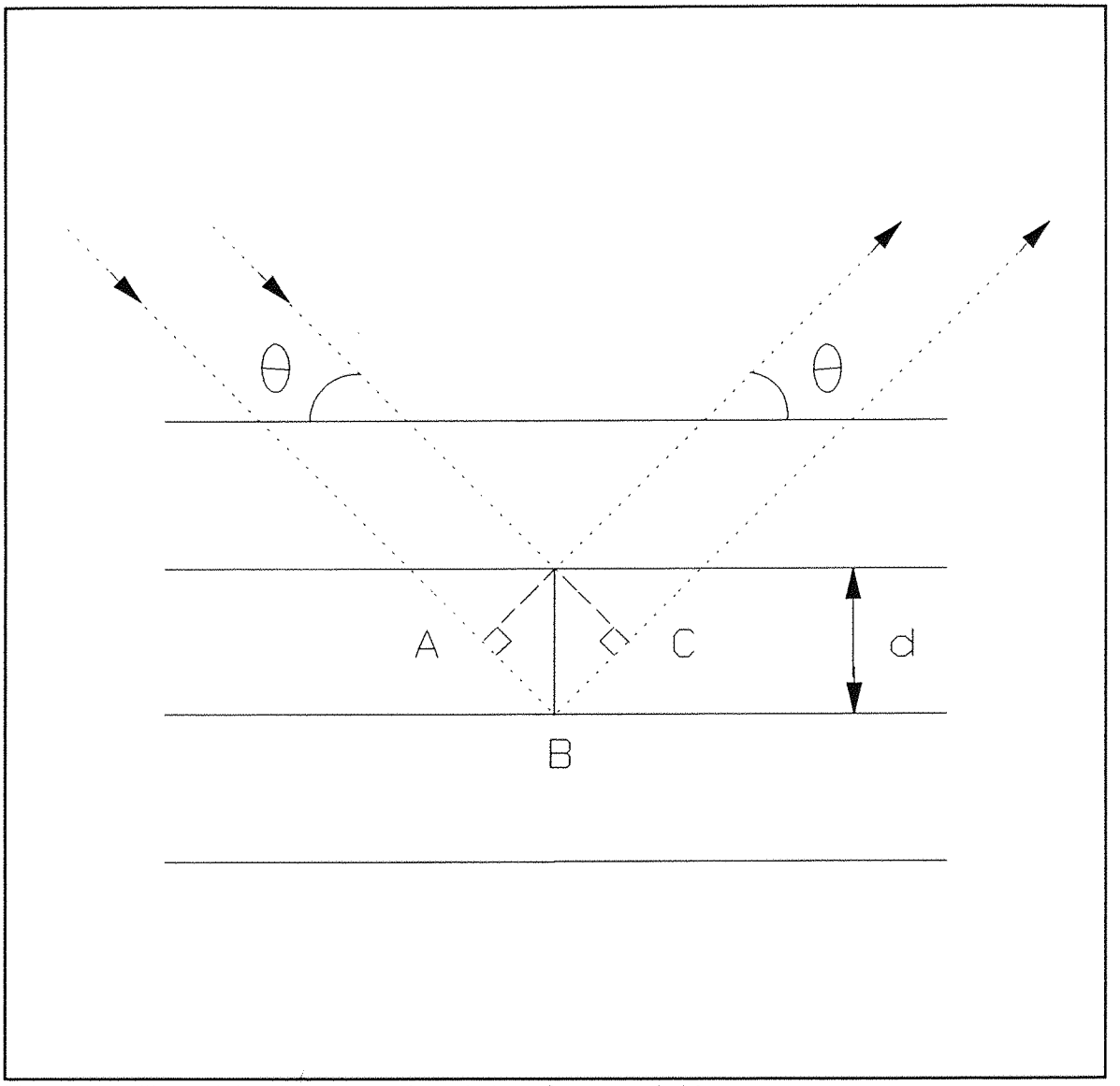

Figure 1.3a The origin of path length variations from parallel layers.

1.4 Structure-Property Relationships for Low Molar Mass Liquid Crystals

The formation of liquid crystal phases by low molar mass materials is dependent on a range of molecular properties, the most important of which is an anisotropic shape. This requirement can be met in a variety of ways [25] most commonly with a rod-like or more realistically, a lath-like molecule [26]. Molecules with a lath-like structure consist of a semi-rigid core, often containing aromatic rings, attached to which are terminal substituent groups, often alkyl or alkoxy chains, as illustrated below. The linking group -**A**-**B**- is normally an unsaturated unit thereby restricting rotation and preserving the rigidity and linearity of the core. In addition, an unsaturated core unit enhances the polarisibility anisotropy of the molecule through conjugation with the aromatic rings. A twist between the aromatic rings will reduce the contribution to the polarisibility, along the molecular long axis, from ring conjugation [27].

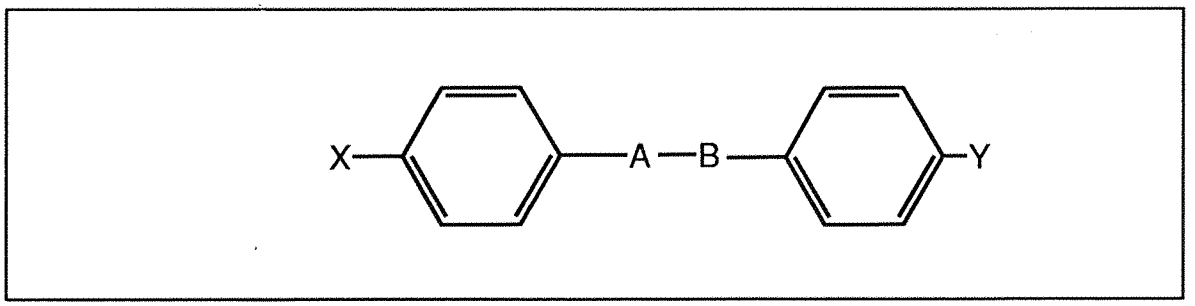

X,Y are terminal substituent groups
A-B a linking group.

Mesophase stability is dependent on an anisotropic intermolecular potential which is only possible if one or more of the constituent forces are themselves anisotropic. Electrostatic interactions (the resultant of dipolar, quadrupolar and larger multipolar terms) will be anisotropic in character. The nature of the dispersion forces (from induced dipole-induced dipole interactions) will depend

on the size and polarisibility of the molecule, but for molecules with a significant shape anisotropy, lath-like molecules, these forces will be anisotropic.

The enhancement of the thermal stability of the mesophase as a result of increased molecular anisotropy can be seen in figure 1.4a.

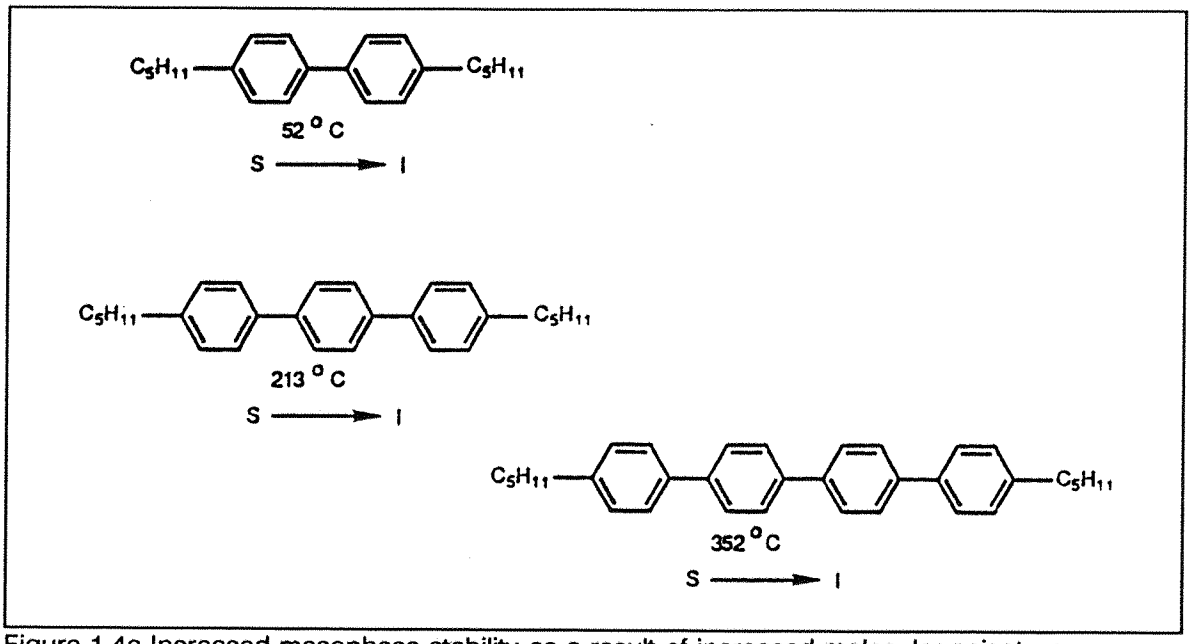

Figure 1.4a Increased mesophase stability as a result of increased molecular anisotropy.

The effect on the nematic to isotropic transition temperature (T_{NI}) of various linking groups sited between two phenyl rings has been studied [26] and an average efficiency order obtained, see figure 1.4b. The order of these groups can be explained in terms of enhanced molecular shape and polarisibility anisotropy. The high position of the bicyclooctane and cyclohexane saturated rings is surprising but is an indication that the preservation of molecular rigidity and linearity is of greater importance than the polarisibility considerations.

Attached to the semi-rigid core are one or more terminal substituents, one of which is generally an alkyl or alkoxy chain, which can affect mesophase stability in a number of ways. Alkyl and alkoxy chains are used as in general

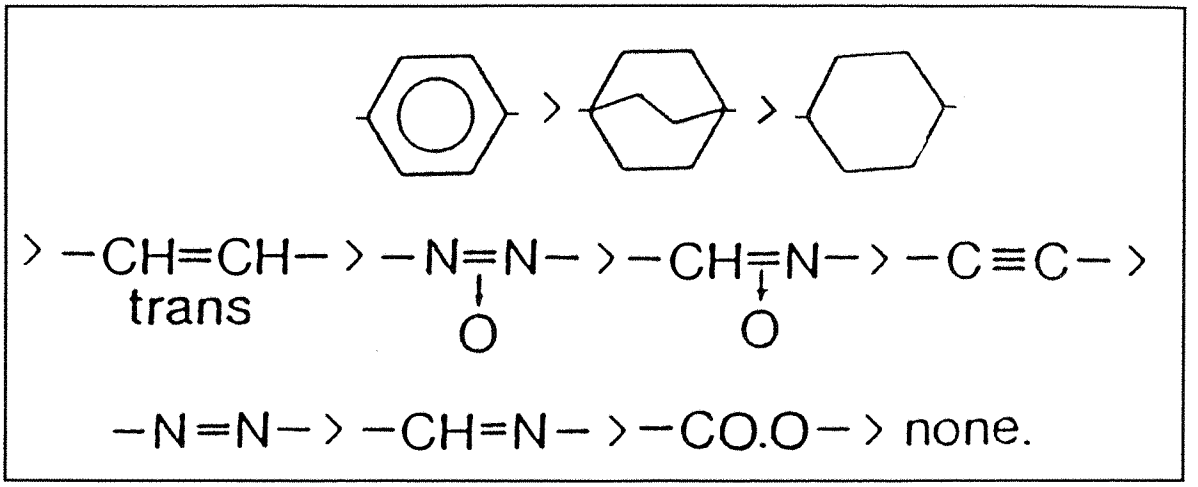

Figure 1.4b Average efficiency order of linking groups for enhancing T_{NI}.

$$Ph > NHCOCH_3 > CN > OCH_3 > NO_2$$

$$> Br > N(CH_3)_2 > CH_3 > F > H$$

Figure 1.4c Average efficiency order of terminal groups for enhancing T_{NI}.

the melting temperature falls as the chain length increases [26], exceptions to this include various biphenyl and Schiff's base materials. The efficiency of the terminal group at increasing T_{NI} has also been studied [26] and an average order obtained, as shown in figure 1.4c. Again this order can be explained in terms of the effect the substituent has on the molecular shape, polarity and polarisibility. Mesophase stability will be increased if a *para*-substituent can be easily integrated into the π electron system of the core, and increased to a lesser extent if the substituent introduces a permanent dipole to the molecule [27]. Introduction of a big group although increasing polarisibility will be detrimental to mesophase stability if the linearity of the molecule is reduced, changing a terminal halide from F, through Cl and Br, to

I will lead to a reduction in the stability of the mesophase generally to its exclusion.

It should be noted that the requirements for increased thermal stability of smectic phases are different from those for the nematic phase. For example, smectic phases are enhanced by groups such as -CO.NH_2, -CO.O-alkyl and CH=CH-CO.O-alkyl containing permanent dipoles in a transverse orientation, to the detriment of the nematic phase. Although the formation of smectic phases is thought to be the result of a separation, at a local level, of the aromatic cores and aliphatic chains in order to maximise the entropy of the system and not solely dependent on the presence of permanent dipoles [27]. By far the most common type of terminal substituents, and consequently the most studied, are the alkyl { -$(CH_2)_n$-CH_3 } and alkoxy { -O-$(CH_2)_n$-CH_3 } chains. A great number of homologous series have been made and characterised resulting in the observation of a number of common trends [26]: when the mesophase to isotropic transition temperature along a homologous series of compounds is plotted as a function of the terminal chain length, the transition temperatures for compounds with odd and even numbers of methylene units lie on two smooth curves that converge at long chain lengths (>8). In the case of alkyl substituents the odd members of the series have higher transition temperatures, for the alkoxy substituents the even members are higher. In the alkoxy systems the oxygen atom is geometrically similar to a methylene group, accounting for the effect reversal. The alternation, known as the *odd-even* effect, is largely a geometric effect arising in the alkyl chain systems because in odd members the terminal carbon-carbon bond lies parallel to the molecular axis while in even members it extends off the molecular axis, increasing the breadth of the molecule. This effect is illustrated in figure 1.4d. The attenuation of the curves is the result of a smaller proportional increase in the molecular anisotropy as the chain length is increased.

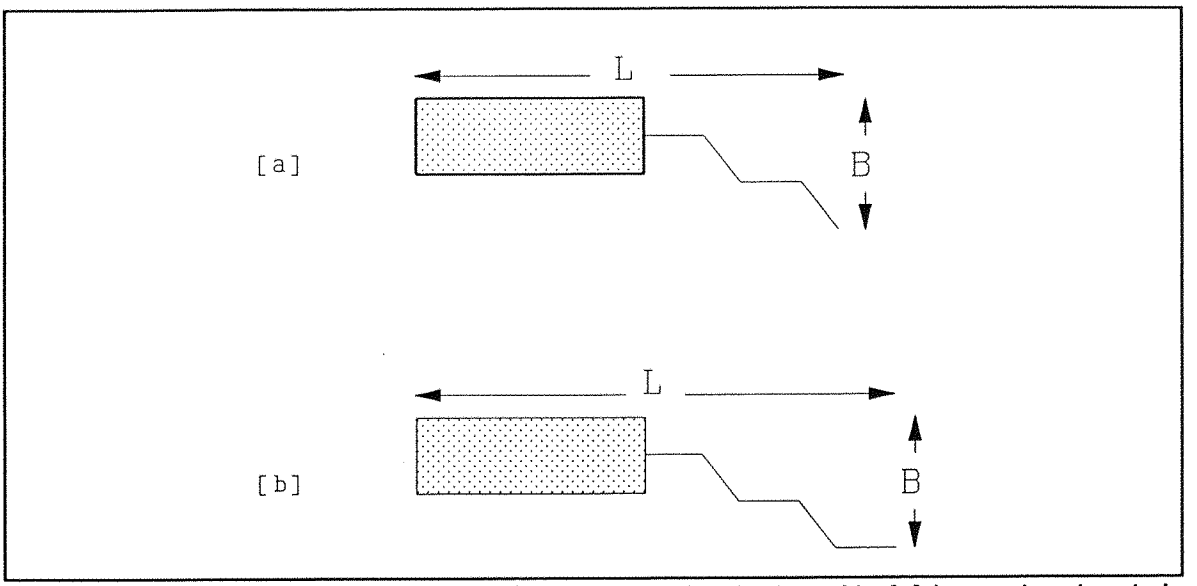

Figure 1.4d Effect of increased chain length on the molecular breadth. [a] Increasing the chain length produces a breadth increase. [b] Increasing the chain length only alters the molecular length.

An important feature observed in many homologous series is the increase in the stability of the smectic phases at the expense, eventually to the exclusion of, the nematic or cholesteric phase in compounds where more than one mesophase is present.

1.5 Molecular Field Theories of Nematics

In this section we briefly discuss the use of the molecular field approximation by Maier and Saupe [28] in the modelling of the nematic phase. The theory uses a simple anisotropic pair potential together with the mean field approximation to reduce the complex dependence of the internal energy of a liquid crystal on the positions and orientations of the constituent molecules to the sum of the single particle pseudo potentials. These potentials will represent the total interaction of a molecule with all others in the mesophase. The approximation can be introduced in a number of ways [29] but that used by Luckhurst [30] and by Woo and co-workers [31] is used here as the nature of the approximation made at each stage is particularly clear.

The Nature of the Problem.

In order to calculate the thermodynamic properties of a statistical mechanical system we need to evaluate the equilibrium configurational partition function,

$$Q_N = (1/N!) \int \{dX^N\} \exp [-U (\{X^N\}) /kT] , \qquad (1)$$

where $\{X^N\}$ denotes both the positional (r) and orientational (Ω) coordinates of the N particles in the system. This allows the calculation of the configurational Helmholtz free energy via

$$A = -kT \ln Q_N \qquad (2)$$

and from this the other thermodynamic properties can be obtained as derivatives of A with respect to T or V.

The problem in the nematic phase, or indeed any condensed phase, in calculating Q_N is that it requires the integration, over 6N coordinates, of a function of the energy dependent on the coordinates of the particles. In certain systems, such as an ideal gas, this problem is not encountered as the particles behave independently and the configurational partition function is then the product of the N single particle partition functions. The effect of the molecular field approximation is to reduce the total partition function to a product of single particle partition functions. To do this each particle is viewed as moving in the 'molecular field' generated by the interaction of every other molecule in the system with the molecule of interest. It is clear that this is an approximation, since no account is taken of the inevitable local variations in interparticle correlations at short distances: however, given that the characteristic of nematics is the long range ordering it is reasonable to expect that this method will be reasonably successful in predicting the behaviour of a nematogenic system.

The Molecular Field Approximation

The approximation can be introduced through the pair correlation function $g^{(2)}(X_1,X_2)$ which compares the value of the *n*-particle distribution function, in this case $n=2$ with the value expected at infinitely low density, the product of N single particle distribution functions. For a homogeneous phase this is defined by

$$P^{(2)}(X_1,X_2) = P^{(1)}(X_1)\, P^{(1)}(X_2)\, g^{(2)}(X_1,X_2)\ , \tag{3}$$

where X_1 denotes the positional and orientational coordinates of particle 1. In the nematic phase the singlet distribution function is, unlike that in a simple fluid where it is constant, related to the singlet orientational distribution function

$$P^{(1)}(X_1) = \rho\, f(\Omega)\ , \tag{4}$$

where ρ is the number density (N/V) and Ω denotes the orientational variables for particle i. This equation can be used to rewrite the pair distribution as

$$P^{(2)}(r_1\ \Omega_1 : r_2\ \Omega_2) = \rho^2\, f(\Omega_1)\, f(\Omega_2)\, g^{(2)}(\underline{r}_{12}\ \Omega_1\ \Omega_2)\ . \tag{5}$$

The pair correlation, $g^{(2)}(\underline{r}_{12}\Omega_1\Omega_2)$, is still dependent on the orientations of the particles, it is this dependence that the molecular field theory removes in order to simplify the problem. The molecules maintain their alignment parallel to the director by interaction with the molecular field rather than each other, thus

$$P^{(2)}(r_1\ \Omega_1 : r_2\ \Omega_2) = \rho^2\, f(\Omega_1)\, f(\Omega_2)\, g^{(2)}(r_{12})\ . \tag{6}$$

In order to proceed any further we need to introduce the Bogoliubov-Born-Green-Kirkwood-Yvon hierarchy of equations to describe the distribution functions [32]. This can be achieved starting from the singlet probability density $P^{(1)}(X_1)$ given by

$$P^{(1)}(X_1) = [(N/Z_N) \int \{dX_2^N\} \exp(-U\{dX^N\})/kT] \quad (7)$$

where $Z_N/N!$ is defined to be Q_N (equation (1)).
The total potential energy is replaced by a sum of pair potentials [32] as

$$U(\{X^N\}) = \sum U(X_i,X_j) . \quad (8)$$

This approximation may not be a valid one if $U(X_i,X_j)$ is the potential for two isolated molecules but appears to be useful if an effective pair potential is used. The substitution of equation (8) into the singlet probability density equation (7) followed by differentiation with respect to the coordinates of particle 1 yields

$$\nabla_1 P^{(1)}(X_1) = -1/kT \int dX_2 \nabla_1 U(X_1,X_2) P^{(2)}(X_1,X_2) . \quad (9)$$

Although apparently simpler we have made little progress as the pair distribution is given by another multidimensional integral

$$P^{(2)}(X_1,X_2) = \{N(N-1)/Z_N\} \int \{dX_3^N\} \exp[-U\{dX^N\})/kT] . \quad (10)$$

Equation (9) is the first in a hierarchy of equations each of which links the gradient of one distribution function to an integral involving the next distribution: in general

$$\nabla_1 P^{(N)}(\{X^N\}) = -1/kT \sum \nabla_1 U(X_1,X_2) P^{(N)}(\{X^N\}) \qquad (11)$$

$$- 1/kT \int dX_{N+1} \nabla_1 U(X_1,X_{N+1}) P^{(N+1)}(\{X^{N+1}\})$$

where ∇_1 is the operator defining the differentiation with respect to the coordinates of particle 1, $X_1=(r_1\ \Omega_1)$. In order to break the coupling we need to introduce a, so called, closure approximation [33]. Using the $n=1$ form of equation (11) and substituting for $P^{(1)}$ and $P^{(2)}$ using equations (4) and (6) respectively, gives

$$\nabla_{\Omega 1} f(\Omega_1) = -\rho/kT \int dr_2\, d\Omega_2 \nabla_{\Omega 1} U(r_{12}\Omega_1\Omega_2) f(\Omega_1) f(\Omega_2) g^{(2)}(r_{12}) . \qquad (12)$$

Division of both sides by $f(\Omega_1)$ gives

$$\nabla_{\Omega 1} \ln f(\Omega_1) = -\rho/kT \int dr_2\, d\Omega_2\, \nabla_{\Omega 1} U(r_{12}\ \Omega_1\ \Omega_2) f(\Omega_2) g^{(2)}(r_{12}), \qquad (13)$$

where $\nabla_{\Omega 1}$ denotes differentiation with respect to the angular coordinates of particle 1, (Ω_1). The use of the mean field approximation means the single particle distribution function is independent of the positional coordinates in the nematic phase, therefore we can ignore the differential with respect to r_1. Integration of equation (13) over Ω_1 gives

$$f(\Omega_1) = Z^{-1} \exp [\ -\rho/kT \int dr_2\, d\Omega_2\, U(r_{12}\ \Omega_1\ \Omega_2) f(\Omega_2) g(r_{12})]; \qquad (14)$$

this is the singlet orientational distribution function and Z is the single particle partition function, given by

$$Z = \int d\Omega_1 \exp(-U(\Omega_1)/kT) . \qquad (15)$$

We can use the orientation distribution function given in equation (14) to define an orientational pseudo-potential

$$U(\Omega_1) = \rho \int dr_{12}\, d\Omega_2\, U(r_{12}\, \Omega_1\, \Omega_2)\, f(\Omega_2)\, g(r_{12}) \,. \qquad (16)$$

This pseudo potential is obtained from the pair potential by averaging over all orientations of the intermolecular vector, intermolecular separations and orientations of the second molecule.

The Maier-Saupe Theory of Nematics

In their original work Maier and Saupe assumed that the existence of the nematic phase was due to anisotropic dispersion forces. However it is now known that dispersion forces make a minor contribution and a simple anisotropic potential is all that is required.

It is assumed in the theory that the molecules are rigid and possess $D_{\infty h}$ symmetry, an ideal that is never attained in real nematogens. The pair potential used consists of a scalar part and an anisotropic part, we shall only consider the latter as this will be sufficient to produce the essential properties of the model. The anisotropic potential is approximated by

$$U(r_{12}\ \hat{u}_1\ \hat{u}_2) = -U(r_{12})\ P_2(\hat{u}_1.\hat{u}_2) \qquad (17)$$

where $P_2(X)$ is the second Legendre polynomial, r_{12} is the scalar intermolecular distance $|r_1-r_2|$ and $\hat{u}_1\ \hat{u}_2$ are unit vectors parallel to the molecular symmetry axes of molecules 1 and 2, respectively, such that $\hat{u}_1.\hat{u}_2 = \cos\beta_{12}$ where β_{12} is the angle between the molecular symmetry axes, as shown in figure 1.5a.

The averages required to calculate the molecular field energy are over the coordinates of the second molecule. It is, therefore, convenient to separate the coordinates of the two particles, this is done using the spherical harmonic addition theorem [34] and gives the pair potential as

$$U(r_{12}\ u_1\ u_2) = -U(r_{12}) \sum C^*_{2,n}(\omega_1)\ \ C_{2,n}(\omega_2) \qquad (18)$$

where ω_1 and ω_2 are (α,β) the spherical polar coordinates of the two particles and $C_{2,n}(\omega)$ is a second rank spherical harmonic.

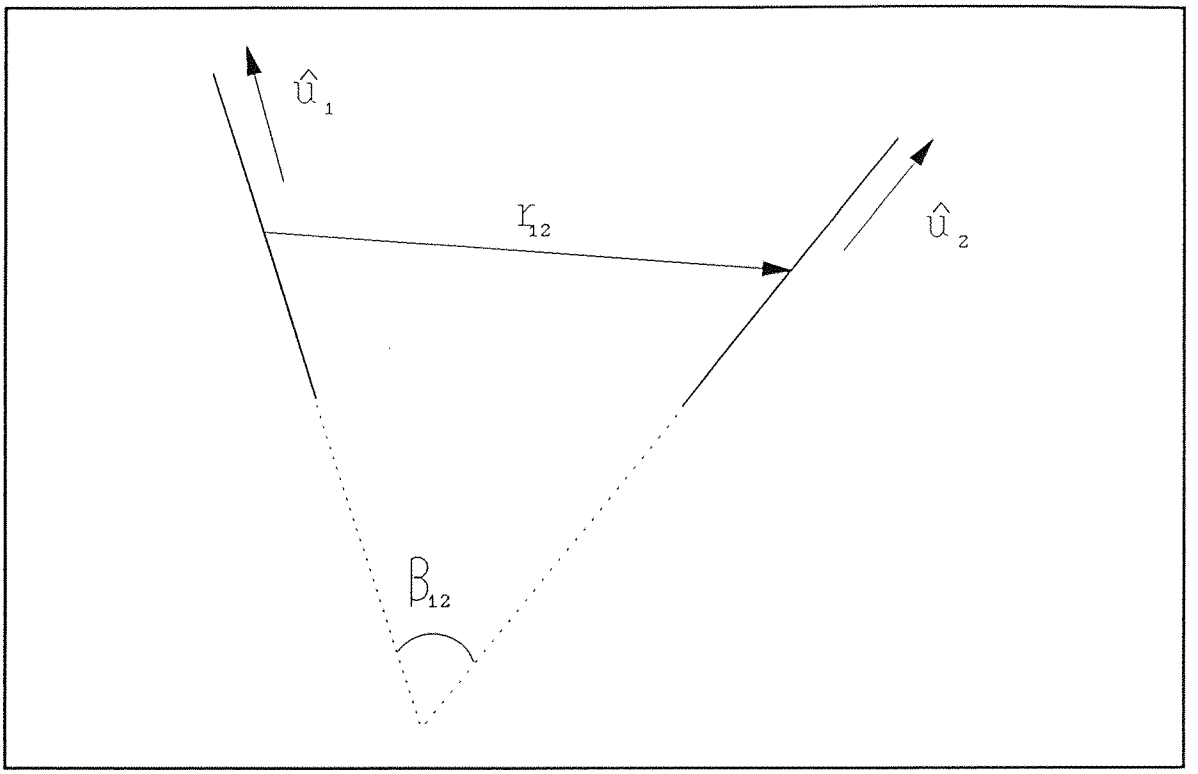

Figure 1.5a Schematic model of the molecules showing angles and distances referred to in the text.

At this point we introduce a further assumption. In a simple fluid $g^{(2)}(r_{12})$ depends only on the separation not the orientation of the intermolecular vector. In the nematic this orientation is expected to influence the pair correlation function, but it is not known to what degree. We assume the correlation function is independent of the orientation of the intermolecular vector, and replace $g^{(2)}(r_{12})$ with the radial distribution function $g(r_{12})$,

$$g(r_{12}) = g^{(2)}(r_{12}) /4\pi \ . \tag{19}$$

As a result of the assumed cylindrical symmetry and molecular rigidity $f(\Omega)$ depends only on the angle between the molecular symmetry axis and the phase symmetry axis, the director. If the phase symmetry axis is taken to be parallel to the space fixed z axis then

$$f(\beta) = f(\Omega)/4\pi^2 \ . \tag{20}$$

Equations (18), (19) and (20) can now be used to rewrite the pseudo potential, or potential of mean torque, given in equation (16) as

$$U(\beta)=-\sum \rho \int(d\omega_{12}/4\pi) \int dr_{12}\, 4\pi r^2_{12}\, U(r_{12})\, g(r_{12}) \qquad (21)$$

$$x \int d\alpha_2\, d\sin\beta_2\, d\beta_2\, d\gamma_2\, C_{2,n}(\omega_1)\, C^*_{2,n}(\omega_1)\, f(\beta_2)/4\pi^2$$

Evaluation of the three integrals in equation (21) gives the first to be unity; the second, because the radial distribution function is not known, gives an average strength parameter

$$\epsilon = \rho \int dr_{12}\, 4\pi r^2_{12}\, U(r_{12})\, g(r_{12}) , \qquad (22)$$

which is defined to be positive so the minimum energy is for a parallel alignment of the molecules. The third integral is evaluated using the orthogonality of the spherical harmonics and

$$\bar{D}^L_{mn} = \int D^L_{mn}(\Omega)\, f(\Omega)\, d\Omega , \qquad (23)$$

$$\bar{P}_L = \bar{D}^L_{OO'} ,$$

to give $\bar{P}_2\, P_2(\cos\beta_1)\, \delta_{on}$. (24)

The pseudo potential obtained from the simple anisotropic pair potential is

$$U(\beta) = -\epsilon\, \bar{P}_2\, P_2(\cos\beta) , \qquad (25)$$

and the singlet orientational distribution function is

$$f(\beta) = Z^{-1} \exp [\epsilon \bar{P}_2 P_2 (\cos \beta)/kT] , \quad (26)$$

where the partition function is given by

$$Z = \int \sin \beta \, d\beta \, \exp [\epsilon \bar{P}_2 P_2 (\cos \beta)/kT] . \quad (27)$$

Predictions of the Maier-Saupe theory

The properties of the nematogen can all be calculated from the key equation defining the orientational order, $\bar{P}_2$

$$\bar{P}_2 = \int d\cos\beta \; P_2(\cos\beta) \; f(\beta), \tag{28}$$

Using equation (26) defining the orientational distribution function, we obtain

$$\bar{P}_2 = Z^{-1} \int d\cos\beta \; P_2(\cos\beta) \exp [\epsilon \bar{P}_2 P_2 (\cos \beta)/kT] . \tag{29}$$

This is called the self consistency equation because of the presence of $\bar{P}_2$ on both sides, and is used since a value for which it is satisfied at a given temperature represents a local minimum in the orientational free energy with respect to $\bar{P}_2$.

The orientational contribution to the Helmholtz free energy is given by

$$A= (N\epsilon \bar{P}_2^2/2) - NkT \ln Z \tag{30}$$

where Z is given by equation (27). This is the free energy of the nematic phase and the free energy of the isotropic phase. As a consequence the free energy will vanish in the limit of complete disorder. The molecular field theory predictions for $\bar{P}_2$ and for A/kT are shown in figures 1.5b and 1.5c respectively. Figure 1.5b shows the variation of the order parameter as a function of the reduced variable kT/ϵ, by solving the self consistency equation, eq.(29). For all values of kT/ϵ the solution $\bar{P}_2=0$, corresponding to the isotropic phase, is obtained. Below $kT/\epsilon=0.222$ there are two further solutions, such that $\bar{P}_2\neq0$; these are the ordered states.

The graph of Helmholtz free energy shown in figure 1.5c, shows that above

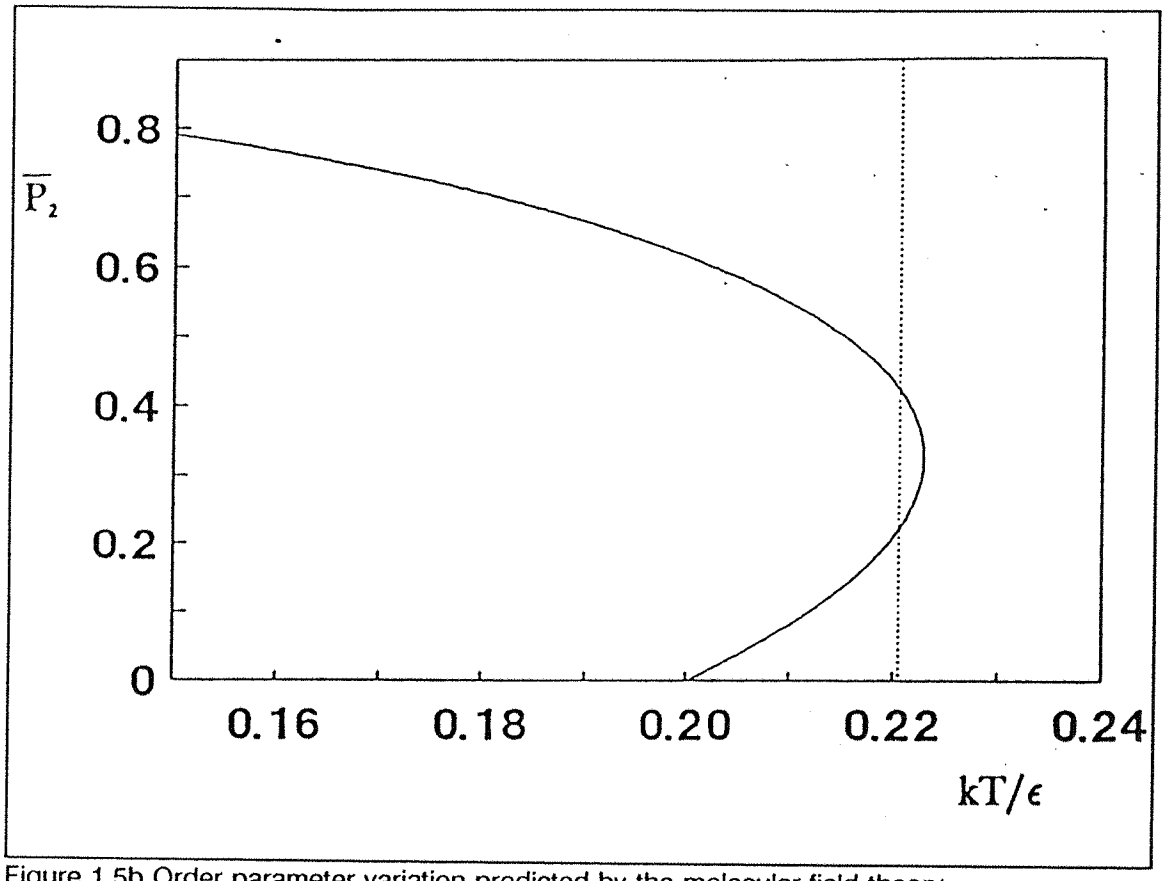

Figure 1.5b Order parameter variation predicted by the molecular field theory.

$kT/\epsilon=0.2203$ the solution $\bar{P}_2=0$, the isotropic phase, is thermodynamically the more stable phase. Whilst below this value the solution with the larger orientational order parameter, the nematic phase, is the more stable. At the temperature given by $kT/\epsilon=0.2203$ the theory predicts a discontinuous first order phase transition between the ordered, $\bar{P}_2\neq0$, state and the isotropic, $\bar{P}_2=0$ state.

The Maier-Saupe theory predicts the behaviour of a nematic liquid crystal quite successfully [30]. The phase transition is correctly predicted to be first order and the variation of the order parameter with temperature is well modelled. The problem with the theory comes in the entropies of transition which are predicted to be much higher than those found experimentally.

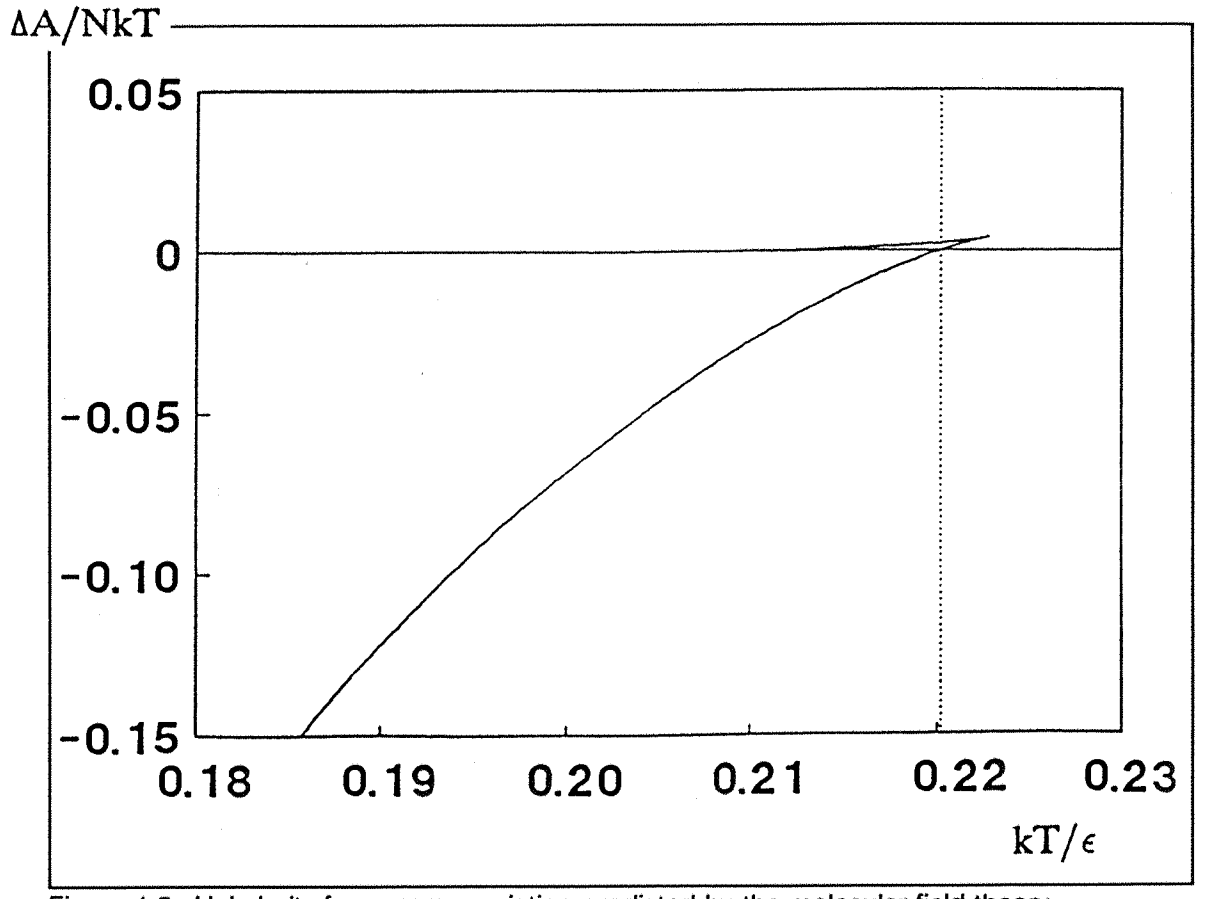

Figure 1.5c Helmholtz free energy variation predicted by the molecular field theory.

1.6 A Molecular Field Theory for Flexible Nematogens

In this section we outline the Marcelja [35] theory for flexible nematogens, an extension of the highly successful Maier-Saupe theory [28] for nematics, outlined in the previous section. The description given will be a qualitative one to compliment the more mathematical description of the theory, given in chapter 3. The theory consists of three essential elements, the first is a description of the conformations of the terminal alkyl/alkoxy chains together with their statistical weights. The next element is a description of the orientational dependent potentials responsible for conformer alignment and the use of segmental interactions to relate these potentials to the various conformers. The third element is the use of the molecular field approximation employed in the calculation of the Helmholtz free energy and hence all other configurational thermodynamic properties of the system.

Conformational States

In order to describe the many conformations which the alkyl chains can adopt we use the rotameric state model proposed by Flory [36]. In this model, in order to restrict the conformations considered to a reasonable level, only the rotations about the C-C and O-C bonds are considered and they are regarded as equivalent. The presence of the C-H bonds and the bond angle difference between the R-C-C and R-O-C bonds (where R is an aromatic unit) are ignored. The non-bonded interactions in the chain result in three conformations for which the internal or intramolecular energy is a minimum, as shown in figure 1.6a. The lowest energy of these is the *trans* conformer, with the two *gauche* conformers equal in energy but less stable than the *trans*. Only these three states are allowed in the rotameric state model, the conformation of the alkyl/alkoxy chain being defined by the number and position of the *gauche* linkages in the chain. The position of the *gauche* links, although having no effect on the internal energy in the isotropic phase, needs to be included because elongated conformations will be statistically favoured in the nematic phase. The compatibility of elongated conformations with the presence of orientational order is illustrated in figure 1.6b.

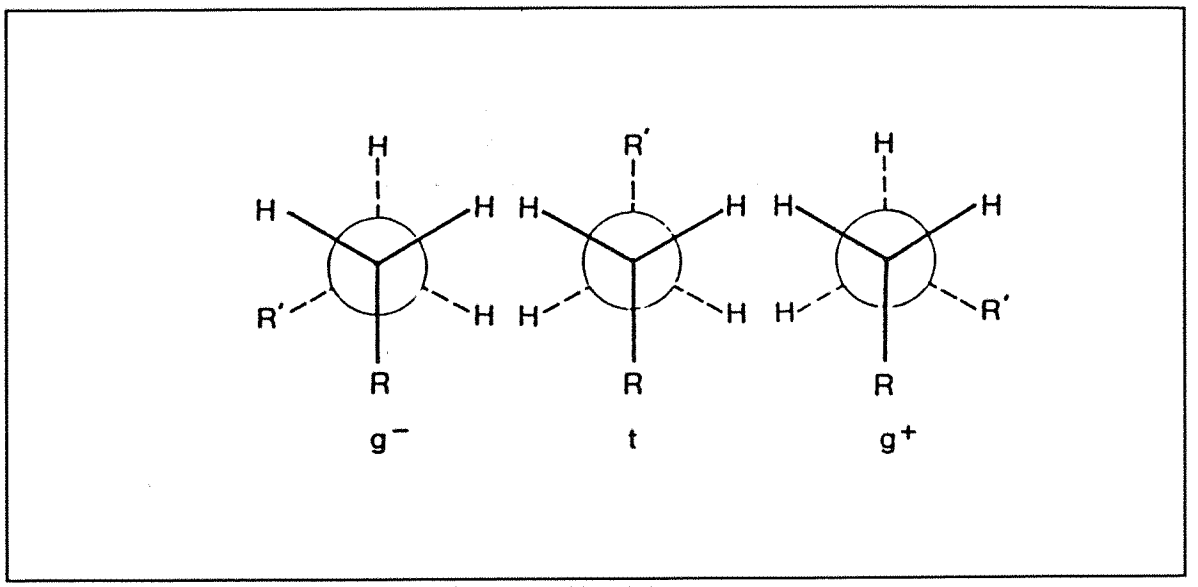

Figure 1.6a The three conformational states with minimum energy.

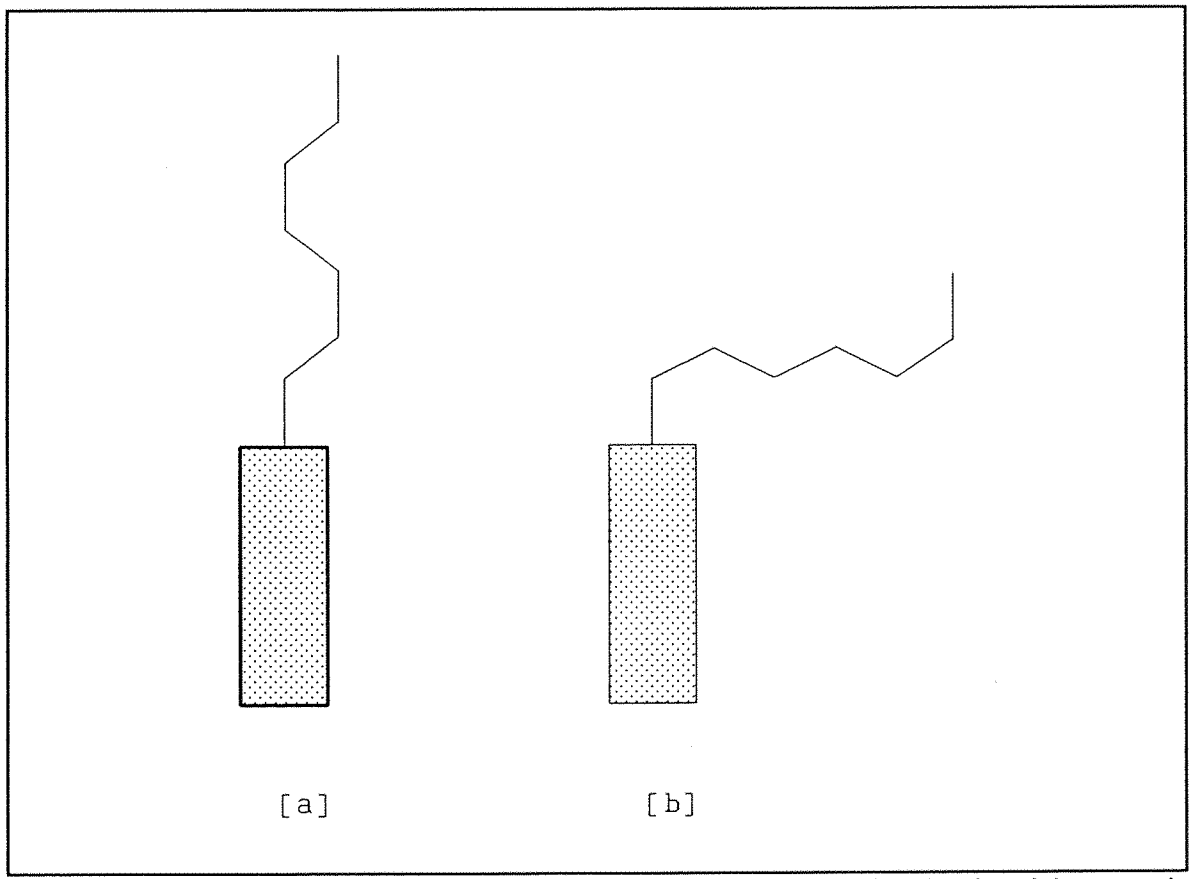

Figure 1.6b Compatibility of elongated conformers [a] with the orientational order of the nematic phase, the bent conformer [b] will be unfavourable.

Orientational Order

The extent of orientational fluctuations of the molecules about the director are characterised by orientational order parameters chosen so as to have a value of unity in the totally ordered crystal phase and a value of zero in the disordered, isotropic phase. The magnitude of the orientational fluctuations is controlled by the energy of the molecule as it reorientates with respect to the director. For cylindrical molecules this energy is dependent only on the angle between the molecular long axis and the director.

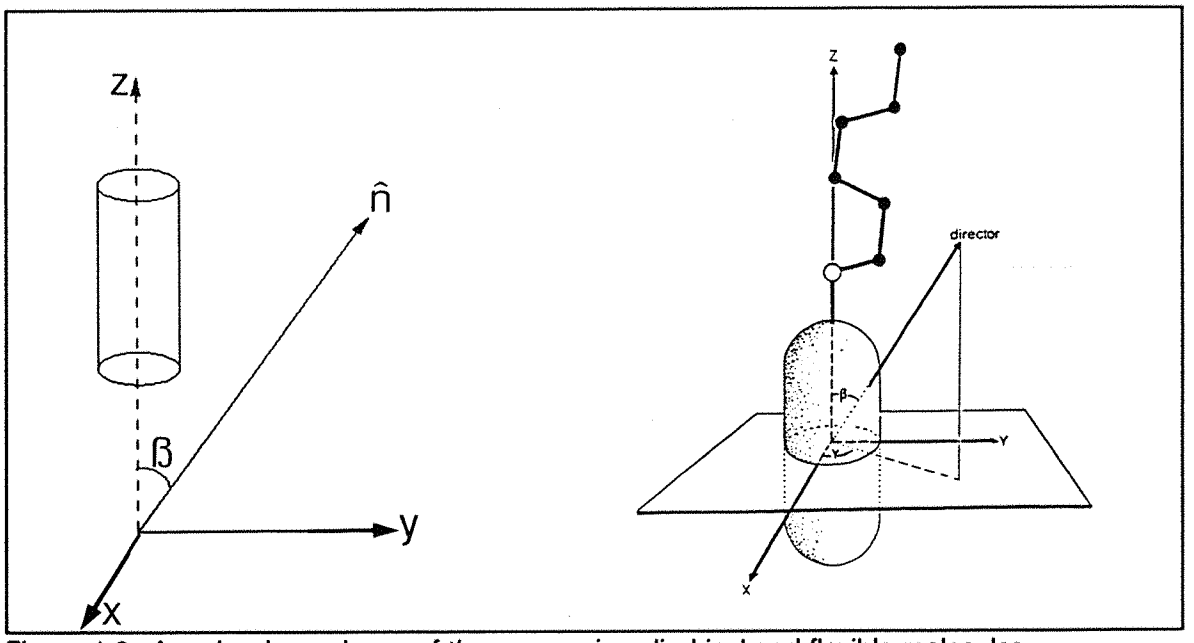

Figure 1.6c Angular dependence of the energy, in cylindrical and flexible molecules.

The orientational dependent energy or potential of mean torque, as it is known, is more complicated for a flexible molecule since no conformer is cylindrically symmetric. The potential of mean torque for each conformer is now dependent on two spherical polar angles as shown in figure 1.6c.

As we have seen the orientational energy results from the interactions of a molecule with its neighbours, this can be thought of as a single molecule fluctuating in the molecular interaction field generated by the rest of the molecules in the system. The strength of the molecular field will depend on

many different factors, including the molecular packing and orientational order in the system.

Figure 1.6d shows the potential of mean torque, the orientationally dependent energy, together with the singlet orientational distribution function for both a cylindrically symmetric molecule and a conformational flexible molecule. The latter is the function which, for a single molecule, defines the probability of finding the molecular long axis at a given angle to the director.

The orientational order parameters for the system can be evaluated from the singlet orientational distribution function.

NMR can be used to determine the order parameters however because conformer exchange within the molecules is fast on the NMR time scale the values obtained are weighted conformational averages.

For the theory to be tractable we need to calculate the orientational order parameters for each conformer without the introduction of large numbers of arbitrary parameters. This can be done by considering the molecular field as the result of a limited number of segmental interactions, generally in the case of liquid crystals these are taken to be the semi-rigid core and the C-C bonds with different interaction strengths for the two types of segment. O-C bonds are considered equal to C-C bonds. From a knowledge of the appropriate interaction strength parameters the order parameters for each conformer can be obtained. In order to obtain the required conformational average of the orientational order parameters the conformational distribution is required, and this can be calculated from a knowledge of the difference in energy of the *trans* and *gauche* conformational states, available from experimental data.

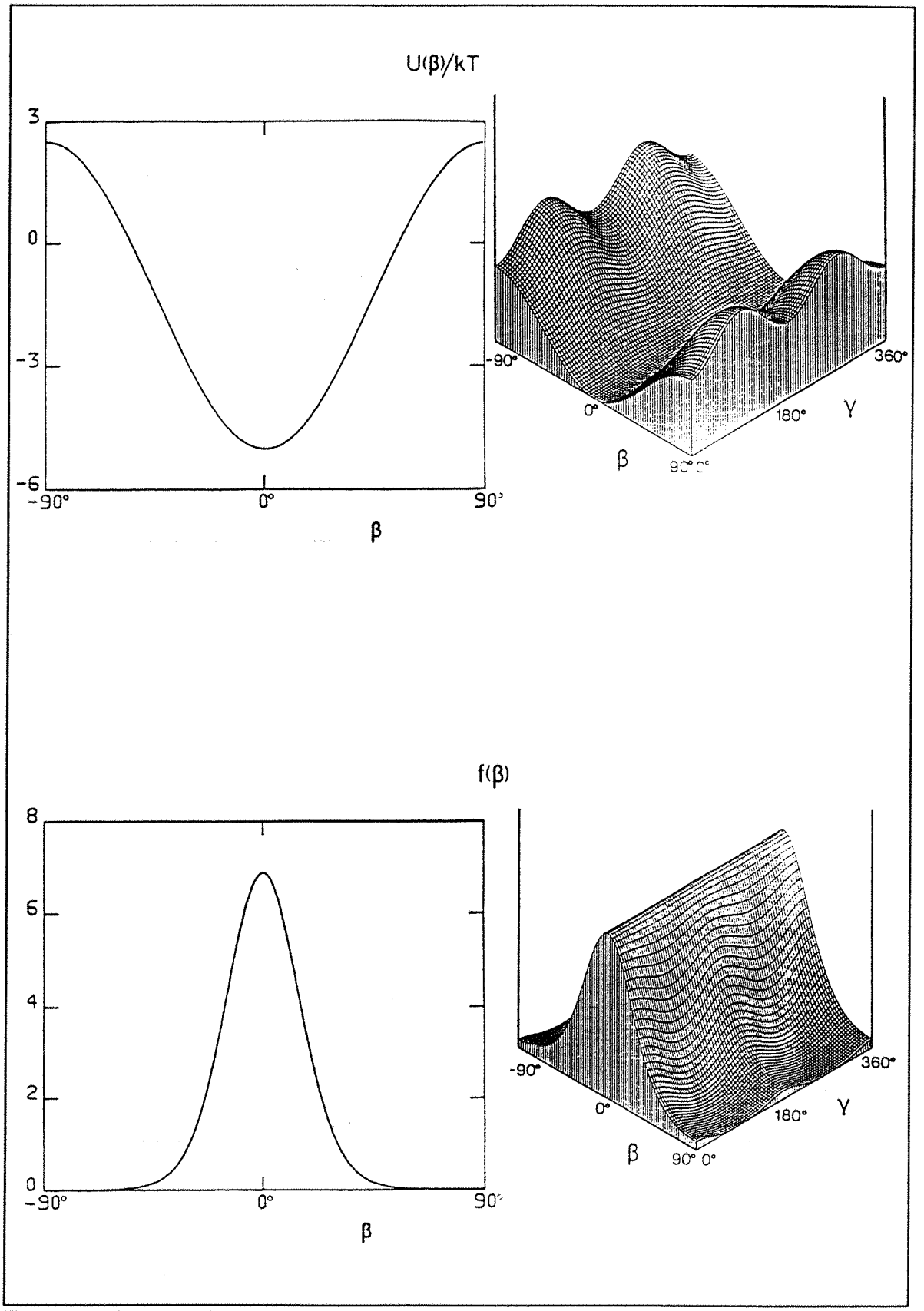

Figure 1.6d Potential of mean torque and singlet orientational distribution function for cylindrical and biaxial molecules.

Thermodynamic Properties

The thermodynamic properties of the system that will be of interest from a molecular field theory of a liquid crystal will be the mesophase to isotropic transition temperature, the entropy of transition and the second rank order parameter; properties which can readily be obtained from real systems allowing suitable values of parameters in the model to be determined and the success of the model to be evaluated. In order to obtain these properties we use the Helmholtz free energy to find the transition temperature. The free energies for the nematic and isotropic are equal at the transition. The statistical mechanical calculation of the free energy via the configurational partition function is relatively straightforward for a set of non-interacting particles, as outlined in section 1.5. By the replacement of the complex network of interactions by the molecular field acting on single particles the calculation is simplified considerably. Once the transition has been located the required properties can be calculated in a straightforward way as outlined in section 3.1.

CHAPTER 2: EXPERIMENTAL

In this chapter we describe the procedures used in the synthesis, purification and characterisation of the 4-*n*-alkoxy-4"-cyano-*p*-terphenyls. This is followed by a description of the mesophases observed, transition temperatures and transition entropies measured together with results of X-ray diffraction experiments. The chapter concludes with a discussion of the results in comparison to similar mesogenic systems.

The 4-*n*-alkoxy-4"-cyano-*p*-terphenyls are of interest for a variety of reasons. The similar 4-*n*-alkoxy and 4-*n*-alkyl-4'-cyanobiphenyls with a smaller mesogenic core have been extensively studied [37][38] and shown to exhibit a number of mesophases. Work by Gray [38],Leadbetter *et al.* [39] and Morrison *et al.* [40] on the 4-*n*-alkyl-4"-cyano-*p*-terphenyls has shown that the extension of the mesogenic core leads to increased interactions and the formation of further mesophases.

2.1 The Coupling Reaction

The synthesis of substituted terphenyl compounds has traditionally been carried out using *p*-terphenyl as a starting material and the required substituents added as appropriate [41]. For example, the 4-*n*-alkyl-4"-cyano-*p*-terphenyls used by Leadbetter *et al.* [39] were prepared by Friedel-Crafts acylation of *p*-terphenyl, the resulting ketone is reduced with lithium aluminium hydride then acylated at the other end of the molecule, using similar conditions. The resulting 4-*n*-alkyl-4"-acetyl-*p*-terphenyl is then converted to the final product. However, problems can be encountered with these methods as the conditions used can be quite harsh and reaction yields can be adversely effected by the presence of certain substituents. The synthetic

routes used in this work employ a relatively new organometallic coupling reaction [42], as used by Gray *et al.* [43], to build up the terphenyl ring system with the required substituents already in place. The reaction uses a catalytic amount of palladium tetra(triphenyl phosphine), $Pd(PPh_3)_4$, in the presence of base to couple an aryl boronic acid and a substituted arene.

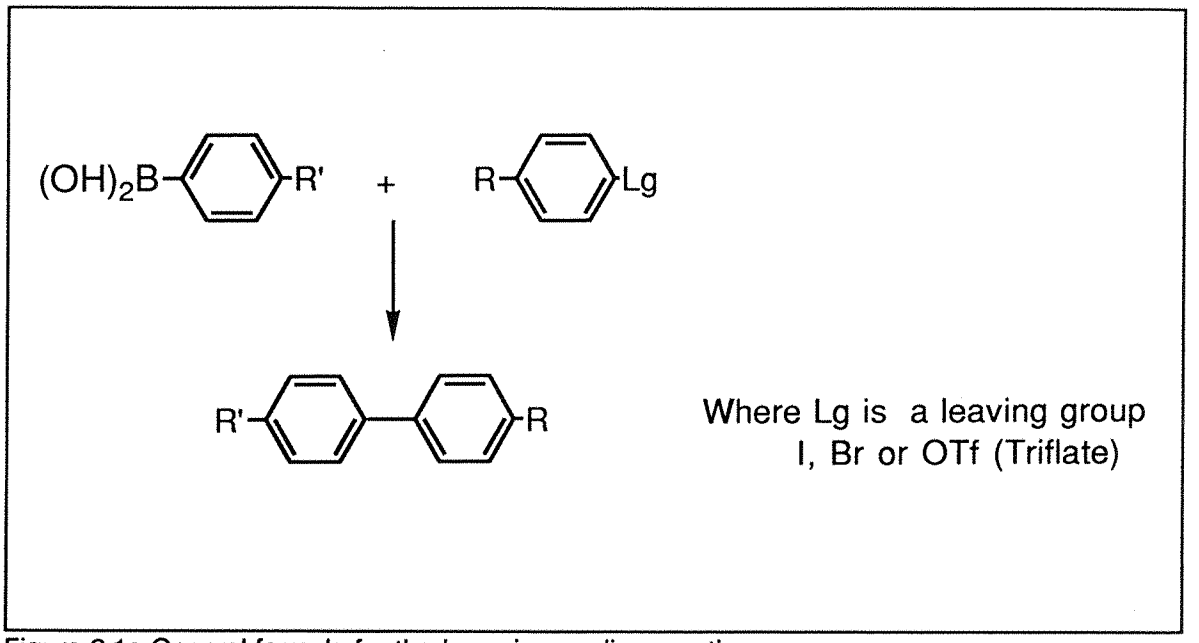

Figure 2.1a General formula for the boronic coupling reaction.

This reagent has the advantage, over many other organometallic reagents such as those used in the Grignard reaction, that it is quite inert to functional groups that often need protection-deprotection, in addition a reasonable degree of selectivity can be obtained. Studies by Gray *et al.* [44] have produced an order of reactivity for the arene substituents, see figure 2.1b. Studies by Miyaura *et al.* [42] have optimised the reagents used in the reaction. With regard to solvents, the higher reaction temperature produced by toluene, over benzene, gives higher yields when hindered bromoarenes are used. Table 2.1a shows the order of efficiency for the various bases employed.

If more than one leaving group is present in the molecule

I > OTf > Br

but where there is a single leaving group

Br > OTf

where OTf is a Triflate ($ArOSO_2CF_3$)

Figure 2.1b Order of reactivity of arene substituents.

Na_2CO_3	in H_2O
NaOH	in H_2O
NaOEt	in Ethanol
NaOAc	in H_2O

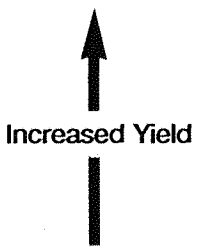

Table 2.1a

It should be noted that when strongly electron withdrawing groups are used protolysis, proton transfer from acid to base, can occur resulting in a dramatic reduction in the reaction yield. This problem, if encountered, can be alleviated by the use of the aryl boronic ester, $Ar\text{-}B(OBu)_2$, in place of the aryl boronic acid and with thallium carbonate, Tl_2CO_3, as the base [45].

2.2 Synthetic Procedure

The synthesis of the 4-*n*-alkoxy-4"-cyano-*p*-terphenyl compounds was carried out using two different routes. The first, as outlined in scheme 1, involves the synthesis of 4-hydroxy-4"-cyano-*p*-terphenyl, by a boronic acid coupling reaction, which is subsequently alkylated with the appropriate 1-bromoalkane except in the case of 4-methoxy-4"-cyano-*p*-terphenyl where the alkylation is performed using methyl iodide. Methyl iodide reacts quicker than the bromide analogue which under these conditions is prohibitively slow. The second route, as outlined in scheme 2, involves the coupling of benzonitrile to the appropriate 4-*n*-alkoxy-4'-bromobiphenyl, prepared by the alkylation of 4-hydroxy-4'-bromobiphenyl with the relevant 1-bromoalkane, using a boronic acid coupling reaction.

2.2.1 Preparation of 4-hydroxy-4"-cyano-*p*-terphenyl

The synthesis involves the coupling of the protected hydroxy compound, 4-acetoxy-4'-bromobiphenyl, with the boronic acid intermediate (4-cyanophenyl) boronic acid. This boronic acid intermediate is not commercially available and so it had to be made from 4-bromobenzonitrile.

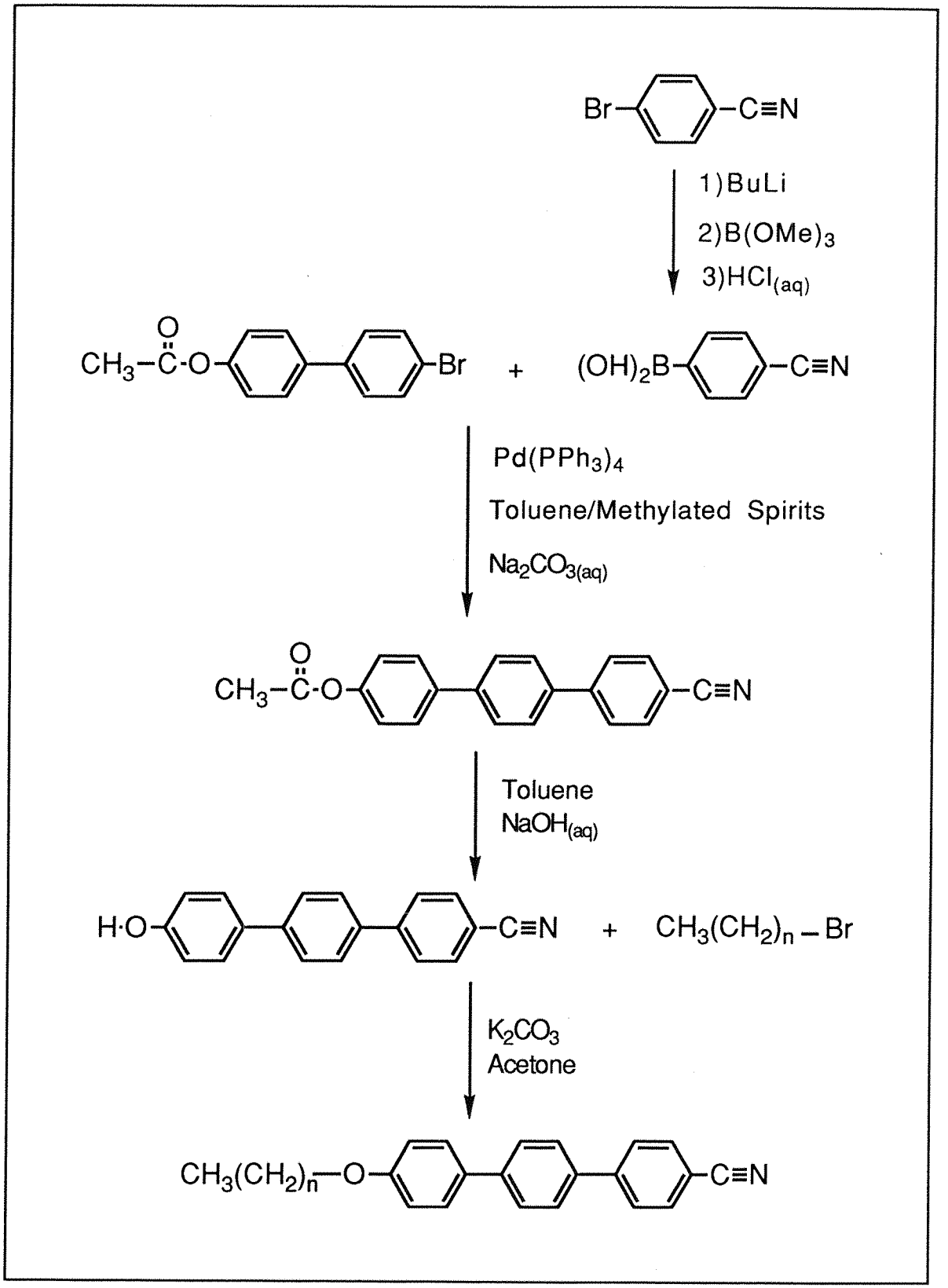
Br–C≡N
1)BuLi
2)B(OMe)3
3)HCl(aq)
CH3–C(=O)–O–Br
+
(OH)2B–C≡N
Pd(PPh3)4
Toluene/Methylated Spirits
Na2CO3(aq)
CH3–C(=O)–O–C≡N
Toluene
NaOH(aq)
H·O–C≡N
+
CH3(CH2)n – Br
K2CO3
Acetone
CH3(CH2)n–O–C≡N

Scheme 1.

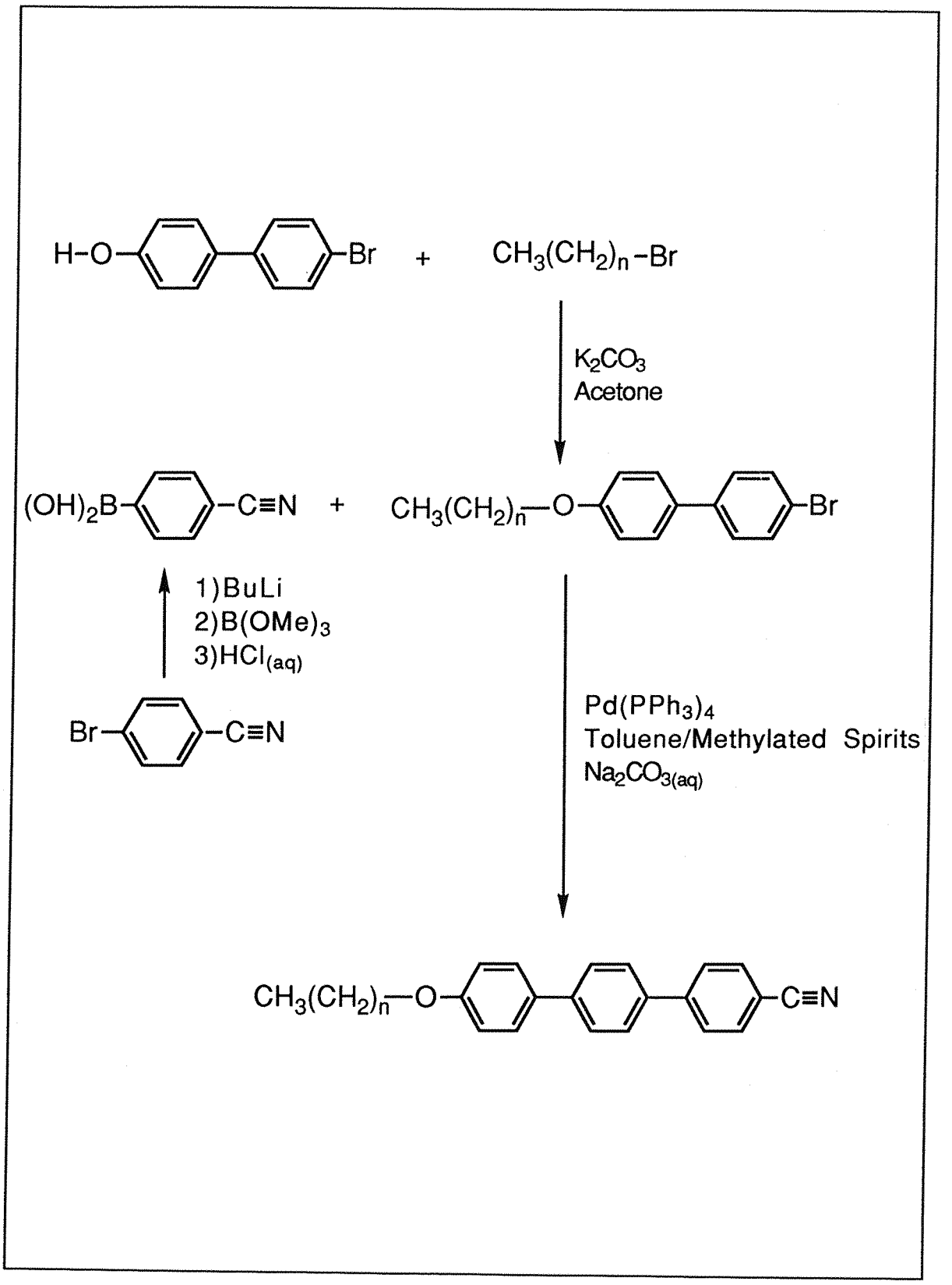
H-O
Br
+
CH3(CH2)n-Br
K2CO3
Acetone
(OH)2B
C≡N
+
CH3(CH2)n—O
Br
1)BuLi
2)B(OMe)3
3)HCl(aq)
Br
C≡N
Pd(PPh3)4
Toluene/Methylated Spirits
Na2CO3(aq)
CH3(CH2)n—O
C≡N

Scheme 2.

Preparation of (4-cyanophenyl) boronic acid

4-bromobenzonitrile (100g, 0.549 mol) was put into a 3l three neck flask fitted with an overhead stirrer, an electronic thermometer and a pressure equalising dropping funnel. The flask was placed in an insulated liquid nitrogen/ether bath and flushed with a stream of dry nitrogen. Dry tetrahydrofuran (1.2 l) and dry hexane (400 ml) were added and the mixture cooled to -100°C. Butyl-lithium (400 ml, 1.6M solution) was added as quickly as possible while maintaining the temperature below -95°C. Once the addition was complete, the mixture was stirred for 10 min. Trimethylborate (125 ml, 1.1 mol) was then added, again as rapidly as possible without allowing the temperature to increase significantly. The mixture was then allowed to attain room temperature and 15% hydrochloric acid solution added to acidify the mixture. The solution was transferred to a separating funnel and the aqueous layer extracted with two 150 ml aliquots of dichloromethane. The organic washings were combined, washed with water until acid free and then dried over magnesium sulphate. The solid was removed by filtration and the solution evaporated to dryness.

The product was checked for purity using thin-layer and gas chromatography.

Product yield= 76.7g, 95%.

Melting point= 384°C (decomposes)

IR /cm^{-1} : 3510.1, 3334.7 (B-OH); 2229.5 (Ar-C≡N) [46][47]

The Coupling Reaction

The coupling reaction uses the protected hydroxy compound, 4-acetoxy-4'-bromobiphenyl, as the hydroxy group in the starting material could react with the aryl boronic acid reducing the reaction yield and giving rise to unwanted products which could be difficult to remove.
4-acetoxy-4'-bromobiphenyl (50g, 0.172 mol), (4-cyanophenyl) boronic acid (30.3g, 0.206 mol) and the catalyst palladium tetra(triphenylphosphine) (0.1%mol) were put into a round-bottomed flask together with toluene (344 ml), methylated spirits (86 ml) and sodium carbonate solution (172 ml, 2M solution). The mixture was left to stir and reflux for 18hrs. under a nitrogen atmosphere. The progress of the reaction was monitored by thin layer chromatography. When the reaction was complete the mixture was poured into a separating funnel and the organic layer removed. The aqueous layer was extracted with dichloromethane, the organic washings combined, washed with water until neutral, dried over magnesium sulphate, filtered and evaporated to dryness.

The 4-acetoxy-4"-cyano-*p*-terphenyl was obtained in a crude state and the removal of the protecting group attempted before purification.

The 4-acetoxy-4"-cyano-*p*-terphenyl was dissolved in methylated spirits (500ml) using heat and stirring. Sodium hydroxide solution (2.4M solution) was then added and the mixture refluxed for 45 min. The resulting solid product was filtered, dried and recrystallised from a 1:2 butanone/toluene mixture.

NMR investigations showed that the removal of the protecting group had only been partially successful. Several attempts were made to obtain pure 4-hydroxy-4"-cyano-*p*-terphenyl. These involved the refluxing of 4-acetoxy-4"-cyano-*p*-terphenyl in aqueous ethanol (1l) for 1h, followed by the addition of

sodium hydroxide (3 mol equivalents) and refluxing for a further period of time (increased on successive attempts from 3-8h). The solution was then filtered to remove any undissolved 4-acetoxy-4"-cyano-*p*-terphenyl and then acidified with dilute hydrochloric acid. These attempts proved only partially successful with the resulting product as before being a mixture of the protected and deprotected materials. The problem is considered to be due to the low solubility of the 4-acetoxy-4"-cyano-*p*-terphenyl and time considerations dictated the use of an alternative route in preference to solving this problem.

2.2.2 Preparation of the 4-*n*-alkoxy-4"-cyano-*p*-terphenyl compounds.

Alkylation of 4-hydroxy-4'-bromobiphenyl

4-hydroxy-4'-bromobiphenyl (4g, 1 mol equivalents) and potassium carbonate (10 mol equivalents) together with Analar acetone (100 ml) were put into a round bottomed flask, fitted with a hotplate and magnetic stirrer. The mixture was refluxed for one hour then the appropriate 1-*n*-alkyl bromide (1.1 mol equivalents) added and the mixture refluxed for a further 18h. The mixture was filtered hot and the solid potassium carbonate washed with two 50ml aliquots of hot Analar acetone. The solution obtained was evaporated to dryness and the product recrystallised from absolute ethanol.

The Coupling Reaction

The coupling reaction is as described previously (section 2.2.1) but on a slightly smaller scale. The quantities used were

the appropriate 4-*n*-alkoxy-4'-bromobiphenyl (0.01mol)
(4-cyanophenyl) boronic acid (0.012 mol)
palladium tetra(triphenylphosphine) (0.1mol)
toluene (20ml)
methylated spirits (5ml)
sodium carbonate solution (10ml, 2M solution)

Product yields were in the range 65-88%.

The products were characterised by ^{1}H NMR and IR spectroscopy [46][47].

n=2 : ^{1}H NMR ($CDCl_3$) δ_H: 1.5(3H,t), 4.1(2H,Quartet), 6.95-8.0(12H,m)
IR: 2226 cm^{-1} (Ar-C≡N)

n=4 : IR: 2228 cm^{-1} (Ar-C≡N)

n=8 : IR: 2234 cm^{-1} (Ar-C≡N)

n=10 : ^{1}H NMR ($CDCl_3$) δ_H: 0.90(3H,t), 1.27(14H,s) 1.55(2H,s), 4.0(2H,t), 6.95-8.0(12H,m)
IR: 2231 cm^{-1} (Ar-C≡N)

Plate 2.3(i) Nematic phase formed by 8-OCT at 239.2°C.

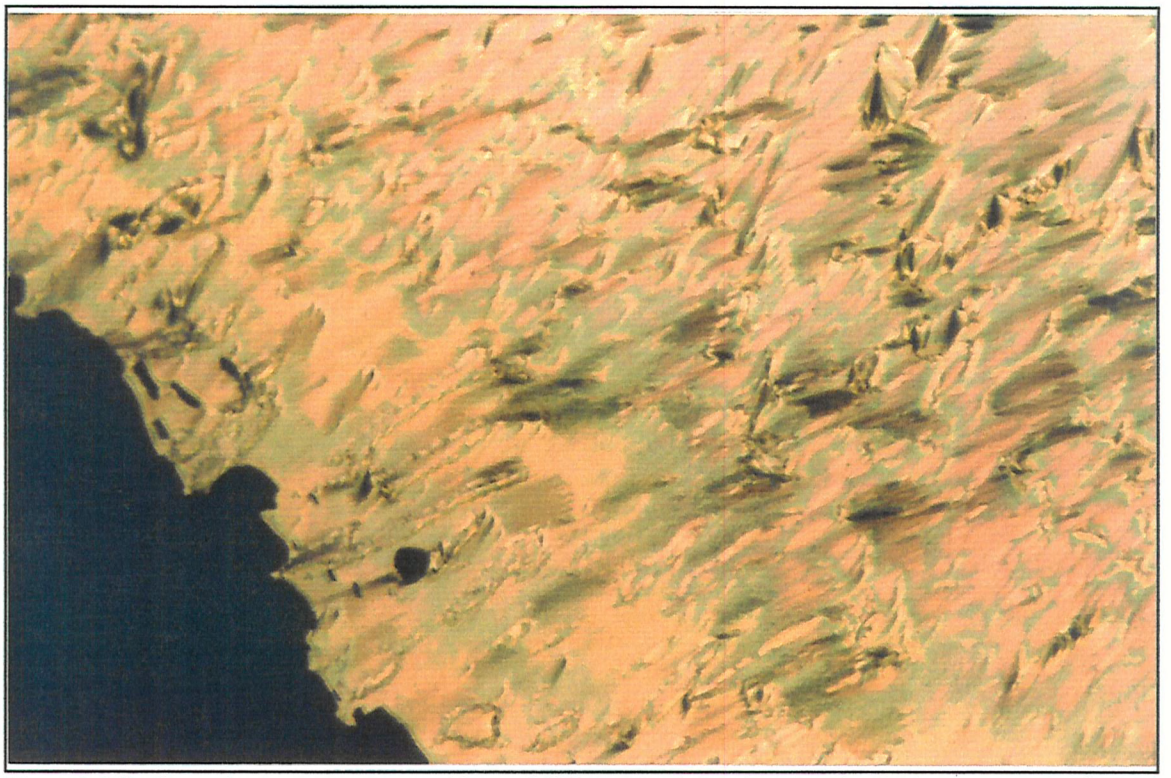

Plate 2.3(ii) Smectic A phase formed by 8-OCT at 205.1°C, showing both the homeotropic and focal conic fan textures.

Plate 2.3(iii) Smectic A phase formed by 8-OCT at 213.2°C, showing the focal conic fan texture.

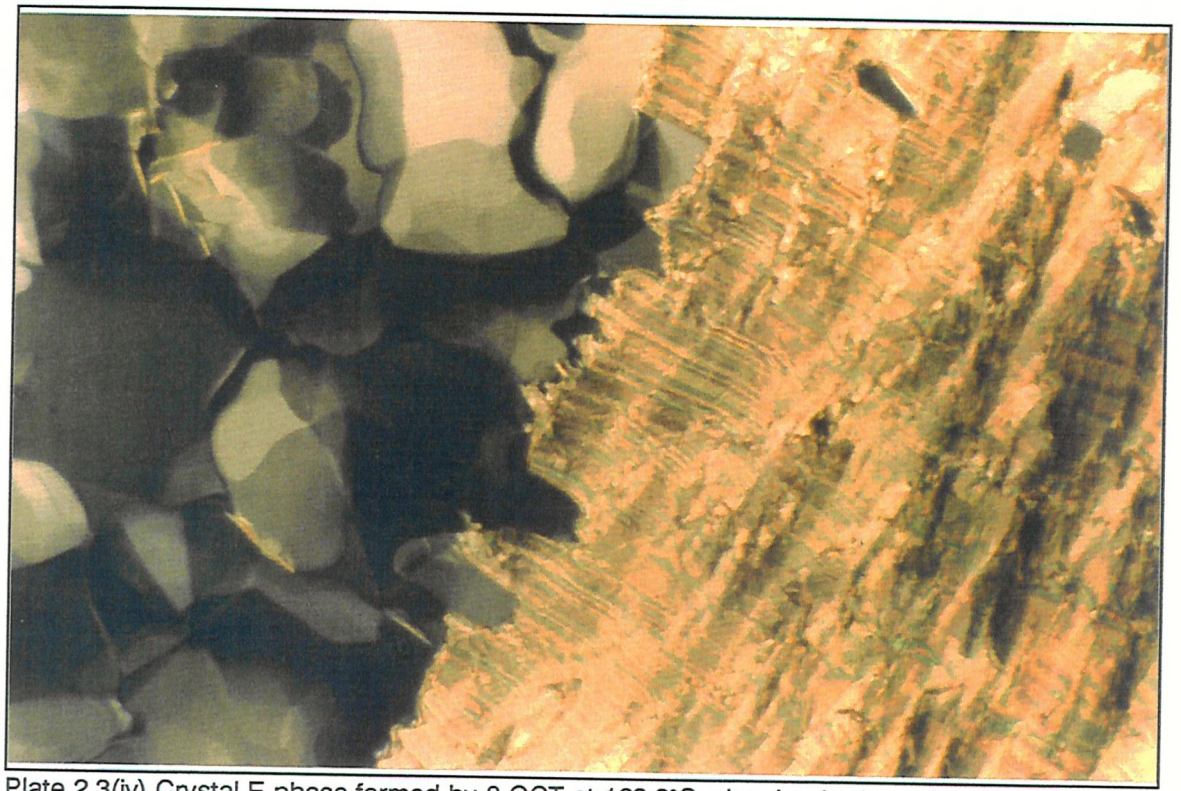

Plate 2.3(iv) Crystal E phase formed by 8-OCT at 163.2°C, showing both the focal conic fan and platelet textures.

2.3 Results and Discussion

The 4-*n*-alkoxy-4"-cyano-*p*-terphenyl compounds were characterised by optical microscopy, differential scanning calorimetry and by X-ray studies. The optical microscopy was performed using an Olympus BH-2 polarising microscope in conjunction with a Linkam THM-600 hot stage and Linkam TMS 90 control unit. The DSC measurements were performed using a Perkin Elmer DSC7. X-ray diffraction experiments to obtain an effective molecular length in the nematic phase and smectic layer spacings were kindly carried out by Dr. J.M. Seddon at the Imperial College of Science, Technology and Medicine.

The transition temperatures for the homologous series of 4-*n*-alkoxy-4"-cyano-*p*-terphenyl compounds (*n*-OCTs) are shown in table 2.3a, and graphically represented in figure 2.3a. It can be seen from the data that all homologues show enantiotropic phases, and for the first six members of the series only a nematic phase is observed. This being characterised by its highly mobile two and four point singularity schlieren and homeotropic textures, an example of the schlieren texture is shown in plate 2.3(i). Longer chain homologous also show smectic phases, with the stability of the nematic decreasing across the series to its eventual exclusion at 11-OCT. The high temperature smectic phase, the S_A is characterised by the focal conic fan texture and the optically isotropic homeotropic texture, examples of the S_A textures are shown in plates 2.3(ii) and 2.3(iii). The lower temperature phase observed is thought to be a crystal E phase because of the paramorphotic focal conic fan texture, the fans are clearly seen to be crossed with arcs that are present across the whole temperature range. Also observed on cooling the homeotropic texture of the S_A, are the ghost-like blueish-yellow platelets of the paramorphotic platelet texture, plate 2.3(iv) shows both the focal conic fan and platelet textures of the E phase.

n	$T_{CN/E}$/°C	T_{ESA}/°C	T_{SAN}/°C	$T_{SA/NI}$/°C
1	209.5			307.5
2	221.8			304.0
3	206.9			283.4
4	185.4			272.9
5	170.2			260.2
6	169.5			255.5
7	100.0	171.9	193.6	247.1
8	88.7	172.9	223.1	241.1
9	95.6	169.8	225.8	233.5
10	103.1	151.0	219.0	226.0
11	109.2	161.3		228.6
12	109.6	161.1		228.0

Table 2.3a

From figure 2.3a it is evident that the clearing temperature, the transition from the highest temperature mesophase to the isotropic liquid gradually falls with increasing terminal chain length, this is in accord with the observations of Gray outlined in section 1.4, and in accord with trends seen in compounds having relatively large mesogenic groups made up of three aromatic units [48]. This gradual fall is the result of two competing effects; the increasing terminal

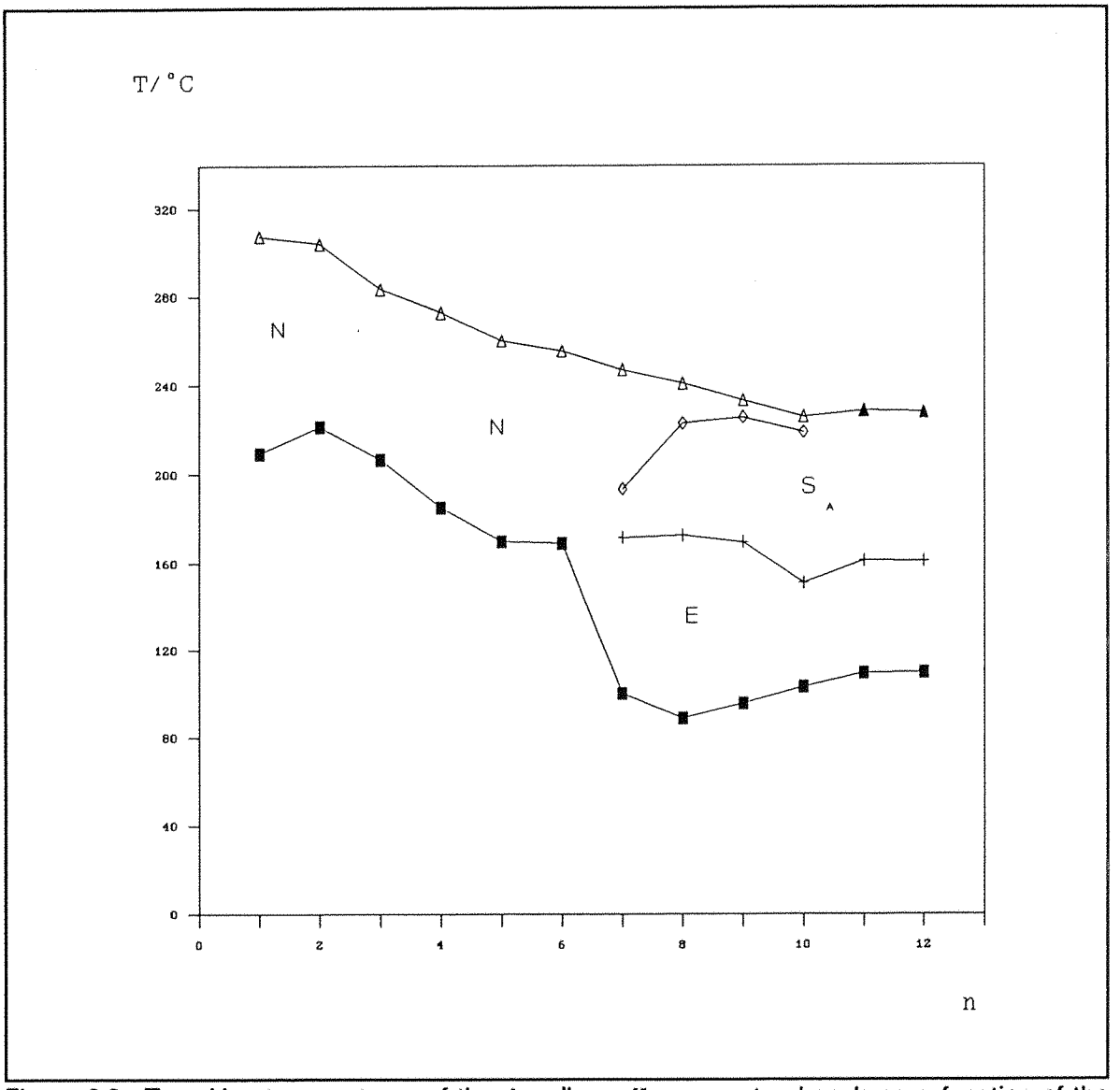

Figure 2.3a Transition temperatures of the 4-*n*-alkoxy-4"-cyano-*p*-terphenyls as a function of the chain length (n).

chain length increases the molecular anisotropy and so raises the clearing temperature and at the same time dilutes the interactions between mesogenic groups which lowers the clearing temperature. The behaviour of a system will depend on which of these effects dominates, in the *n*-OCTs the latter effect is dominant because of the large mesogenic core.

The stability range of the nematic remains approximately constant for the first six members of the series, until the formation of the smectic phases, where upon it rapidly decreases until its exclusion for $n=11$.

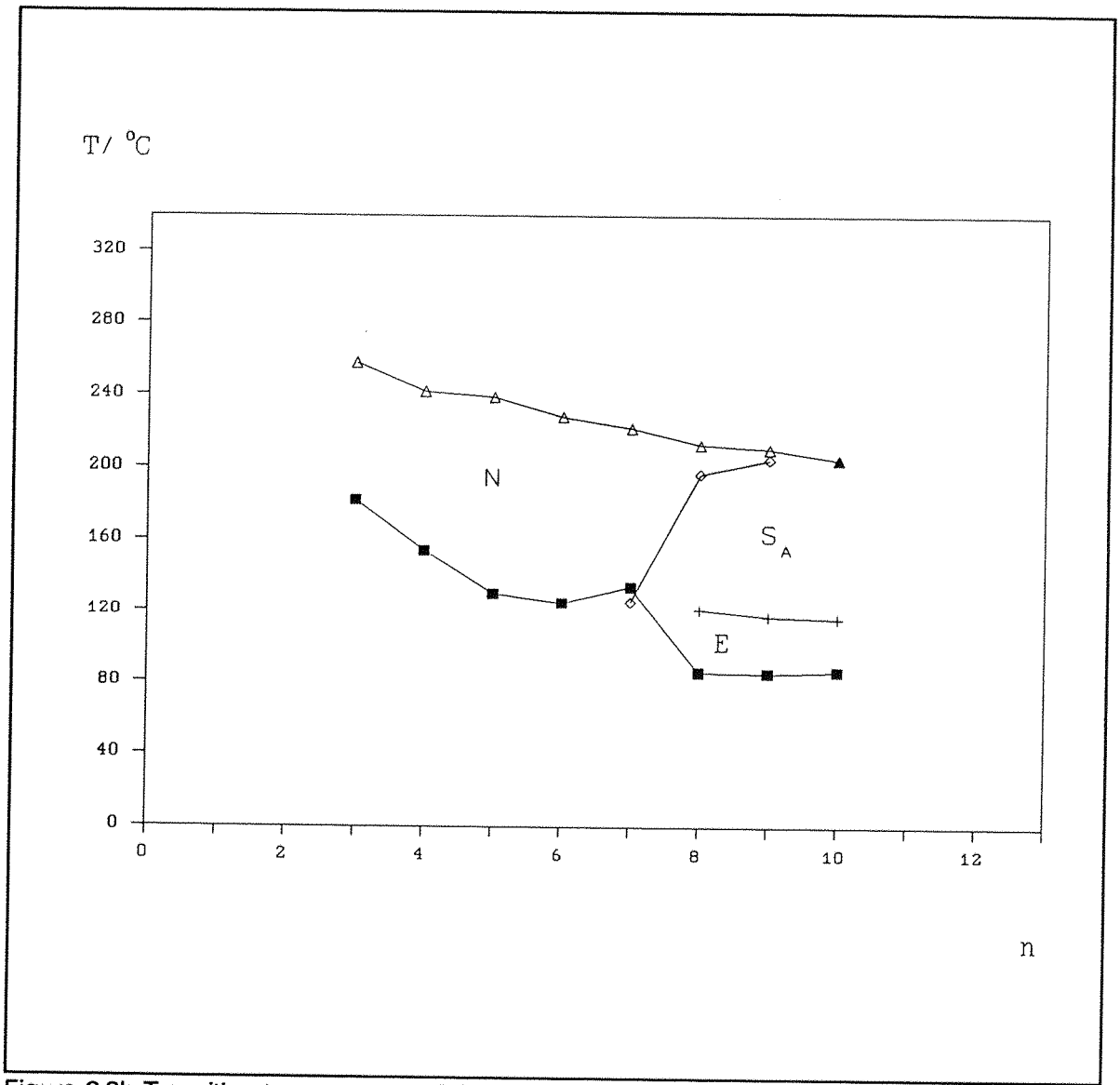

Figure 2.3b Transition temperatures of the 4-*n*-alkyl-4"-cyano-*p*-terphenyls as a function of chain length (n).

Comparison of the phase diagram with that of the analogous alkyl compounds [38,39,48], shown in figure 2.3b, reveals a high degree of similarity, as expected. The phases formed by the 4-*n*-alkyl-4"-cyano-*p*-terphenyl compounds (*n*-CTs), namely N, S_A and E, and general trends in the transition temperatures, the falling clearing point and the loss of the nematic stability in favour of the smectic phases, are the same. There are, however, notable differences the most apparent of which is that the alkoxy compounds have clearing temperatures approximately 20°C higher, the *n*-CTs having clearing

temperatures approximately 95% of the analogous *n*-OCT compound. The presence of the oxygen atom at the beginning of the chain has a marked effect on the geometry. In the alkoxy compounds the $C_{ar}OC_{al}$ bond angle is approximately 126.4°, significantly larger than the $C_{ar}C_{al}C_{al}$ bond angle this results in an increased molecular anisotropy and consequently an increased clearing temperature, as illustrated in figure 2.3c. A second less important effect is the conjugation of the oxygen lone pairs extending the mesogenic core. A difference in the clearing temperatures is also seen for the analogous biphenyl compounds (*n*-OCBs and *n*-CBs), as shown in figure 2.3d. In these compounds the smaller mesogenic unit produces a larger effect, the alkyl compounds having clearing temperatures approximately 90% of the analogous alkoxy compound.

The onset of smectic behaviour occurs at different points in the series, the *n*-OCT compounds showing enantiotropic smectic phases from 7-OCT, the alkyl compounds showing a very narrow monotropic S_A at 7-CT do not show enantiotropic smectic phases until 8-CT.

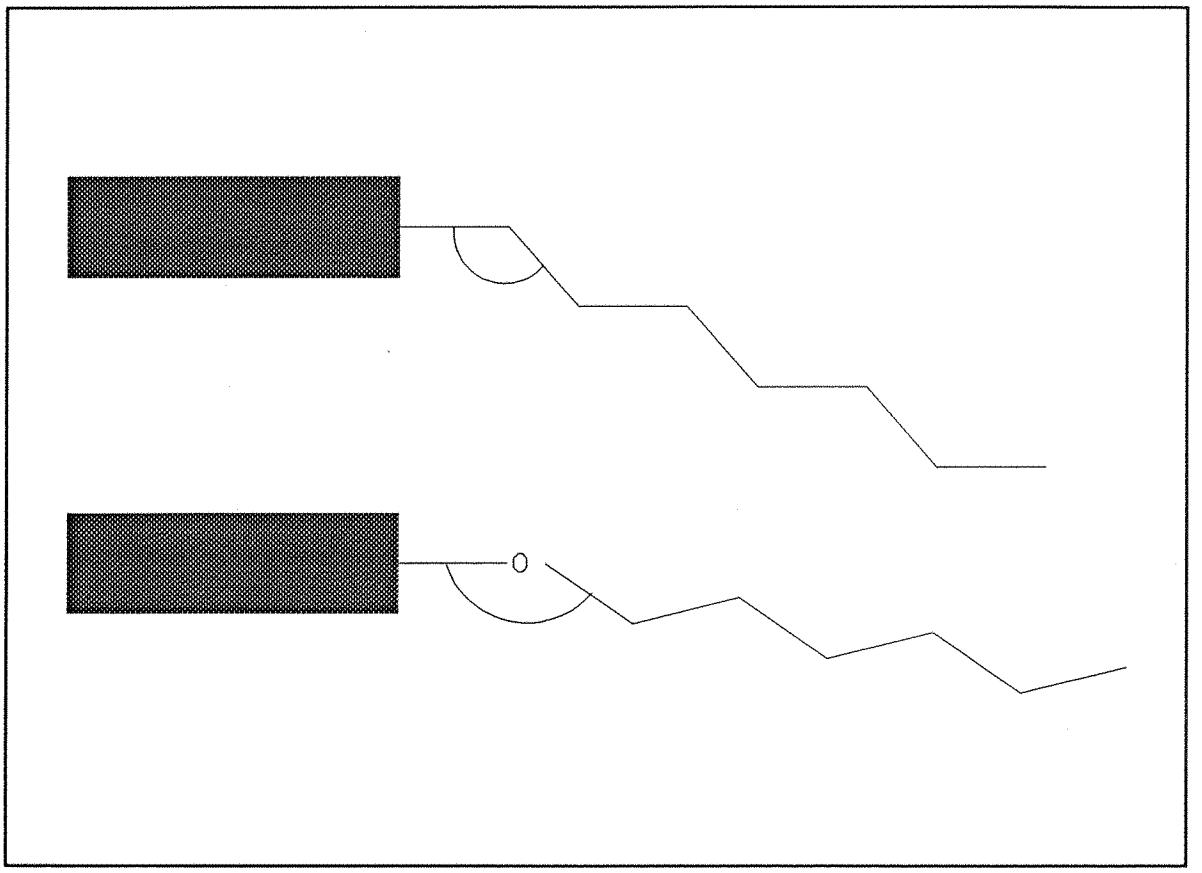

Figure 2.3c A sketch showing the difference in the molecular anisotropy resulting from differing bond angles in alkyl and alkoxy chains.

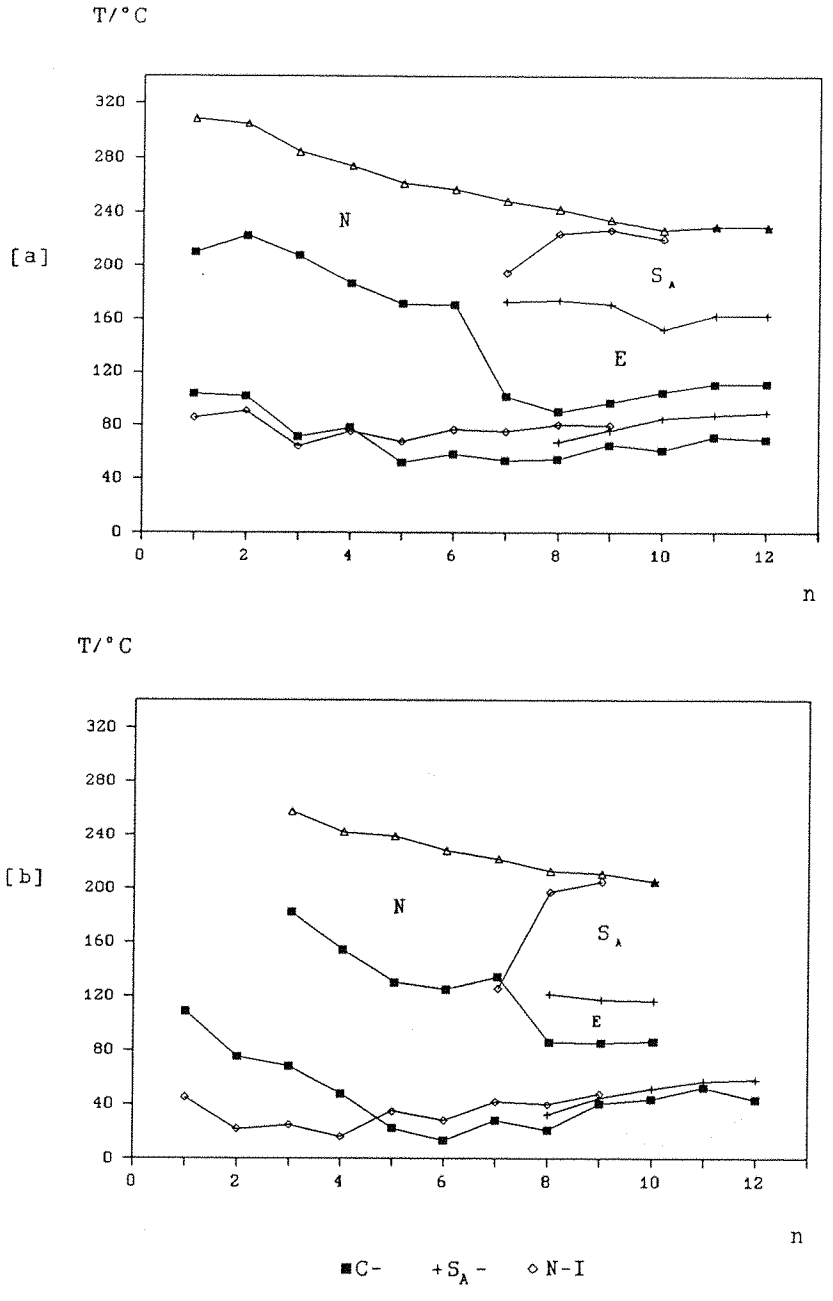

Figure 2.3d Transition temperatures for the (a) 4-*n*-alkoxy and (b)4-*n*-alkyl-4-cyanobiphenyl compounds as a function of chain length (n). Graphs show the appropriate terphenyl transition temperatures on the same axes.

A comparison of the 4-*n*-alkoxy- and 4-*n*-alkyl-4'-cyanobiphenyls with the analogous terphenyl compounds (shown in the upper portion of the appropriate graph in figure 2.3d) shows a number of interesting points. The onset of smectic mesomorphism in the *n*-OCB/CBs occurs at the $n=8$ homologue. In contrast the larger terphenyls show smectic phases, although monotropic in the case of the 7-CT homologue. Both types of mesogen form nematic and smectic A phases, however, it is only the larger terphenyl systems which exhibit the highly order crystal E phase. The 4-*n*-alkoxy and 4-*n*-alkyl-4'-cyanobiphenyls both show an observable *odd-even* alternation, although the effect is reversed for the reasons explained in section 1.4. The terphenyl compounds show no great alternation, exhibiting a gradual fall in the nematic to isotropic transition temperature. These differences can be explained in terms of the relative contributions to the total interaction energy from the core and chain units, as explained in greater detail in chapter 3.

Table 2.3b shows the molar entropy of transition measured for the 4-*n*-alkoxy-4"-cyano-*p*-terphenyl compounds, with graphical representations given in figures 2.3e and 2.3f.

		ΔS/R		
n	C-N/E	E-S_A	S_A-N	S_A/N-I
1	3.19			0.25
2	3.48			0.20
3	4.61			0.16
4	3.27			0.20
5	1.78			0.17
6	2.64			0.22
7	1.48	2.72	*	0.19
8	3.00	2.61	0.06	0.32
9	8.91	2.35	0.12	0.25
10	9.57	2.07	#	0.80*
11	12.21	2.21		1.05
12	9.96	1.84		1.17

Table 2.3b

* No peak was observed for the smectic A to nematic transition.

Peaks coincided so the value given * is the combined change for the S_A-N-I transitions.

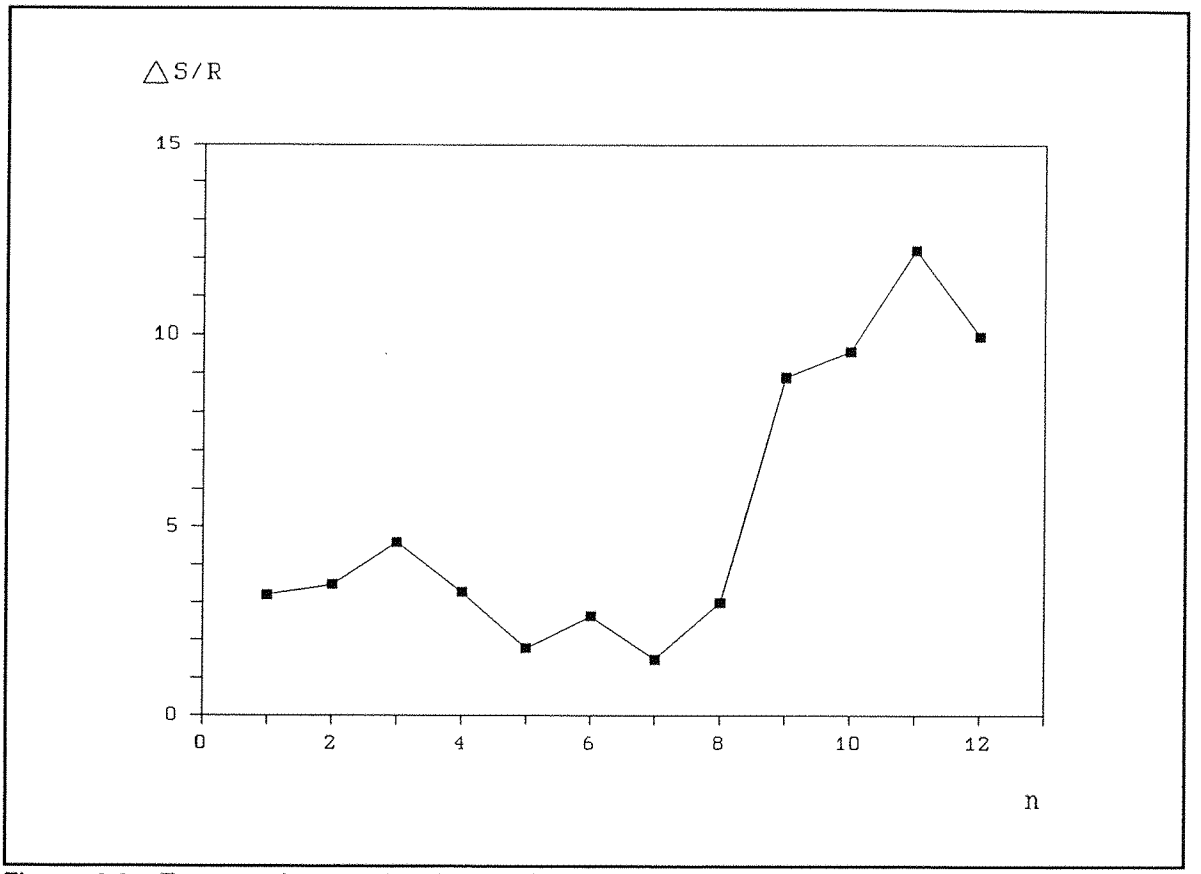

Figure 2.3e Entropy changes for the melting transitions in the 4-*n*-alkoxy-4"-cyano-*p*-terphenyl compounds.

In general, the transitions with the largest entropy change are the crystal to mesophase transitions, that is the crystal melting. This is as expected, as there is a significant increase in disorder on going from, the three dimensional positional and orientational order of the crystal to a phase with interlayer positional and orientational order in the case of the E phase or simply orientational order in the nematic phase. The values show no real trend across the series, but the last four members show significantly higher entropy changes than the lower members because of the increase in conformational freedom of the chains on going from the all *trans* arrangement of the crystal to the E phase. Comparison with the available data for the *n*-CTs [39] show good agreement. The entropy change values for the *n*-OCB and *n*-CB compounds,

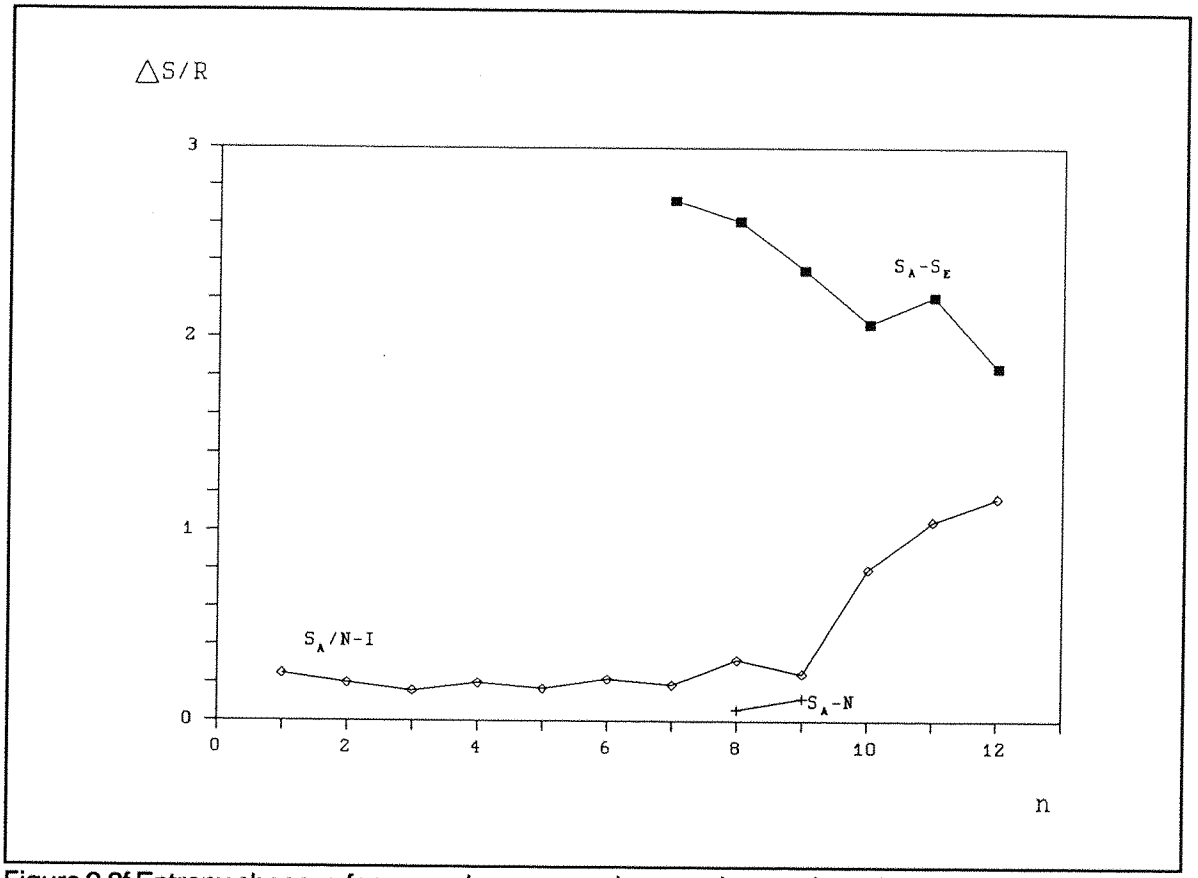

Figure 2.3f Entropy changes for mesophase-mesophase and mesophase-isotropic transitions in the 4-*n*-alkoxy-4"-cyano-*p*-terphenyl compounds.

shown in figure 2.3g [49], indicate that the irregular behaviour is reasonable, however they do show a more noticeable upward trend across the series.

The entropy changes found for the E to S_A transition show a slight downward trend with increasing chain length, varying between 2.9 and 2.5 from 7-OCT to 12-OCT. These values are, as expected, higher than those for the S_A/N to isotropic transition, but considerably smaller than the values obtained for the 4-*n*-alkyl-4"-cyano-*p*-terphenyl compounds by Leadbetter *et al.* [39] given in table 2.3c.

The values obtained for the clearing transition, figure 2.3f, remain approximately constant across the series up to the 9-OCT homologue, the last

	C-E	E-E'	E'-S_A	S_A-N	S_A/N-I
8-CT	5.52	0.63	1.06	0.05	0.24
9-CT	6.78	0.54	1.01	0.13	0.25
10-CT	9.71	0.48	1.00	-	1.04

Table 2.3c [39]

compound to show a reasonable nematic range, after which the value increases significantly. In the case of the 10-OCT compound the value recorded is a combined **N**-S_A-I, as the peaks recorded overlap considerably. The general upward trend, increasing dramatically at the smectic phases, in the entropies of the clearing transition is in agreement with the analogous biphenyl compounds. The rationale for these observations is the fact that the transition from the layered S_A to the isotropic liquid involves the loss of translational order not found in the nematic and so the increase in disorder is greater.

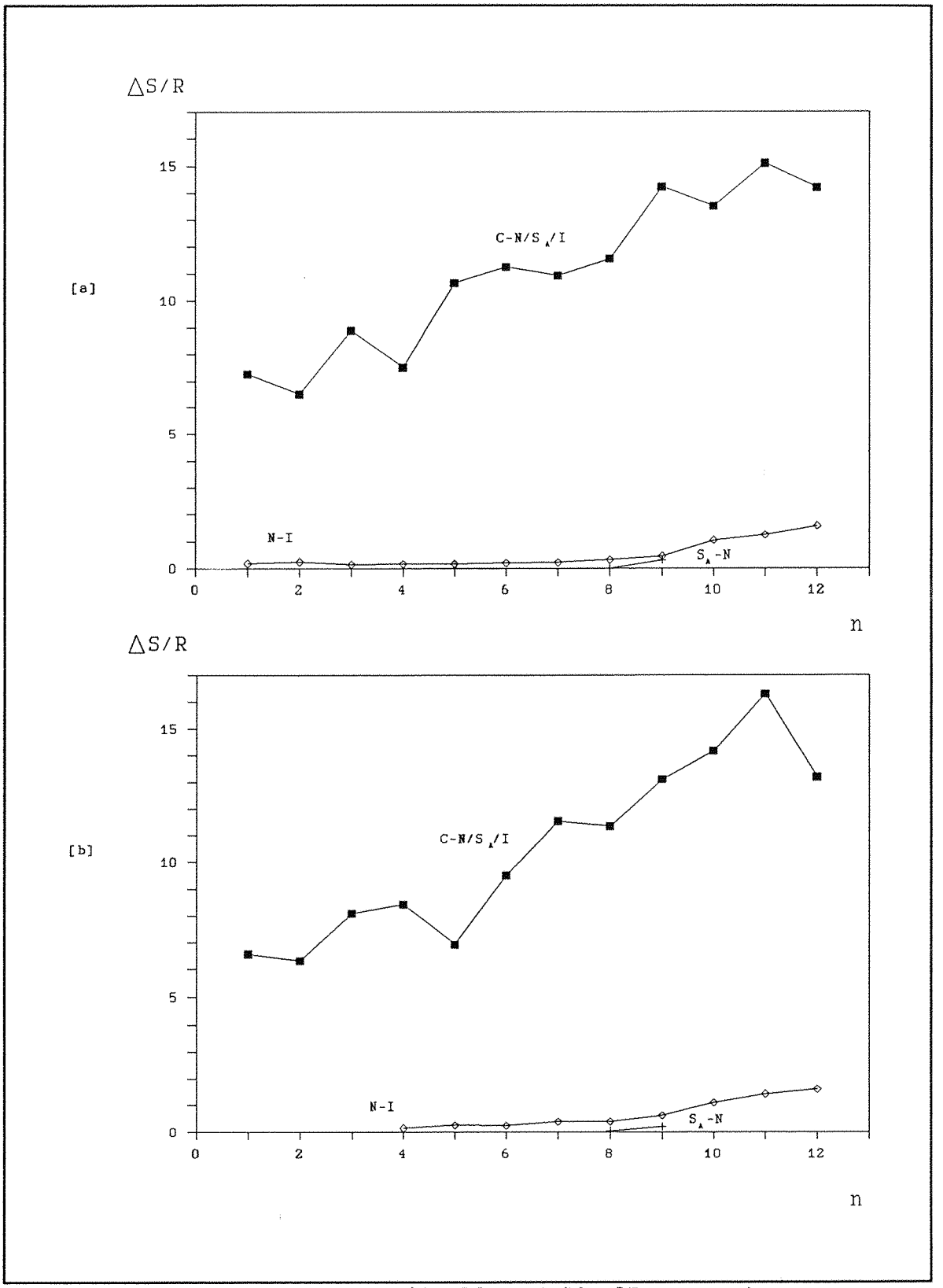

Figure 2.3g Entropies of transition for the (a) *n*-OCB and (b) *n*-CB compounds.

X-ray Diffraction Experiments

X-ray diffraction experiments were carried out on powder samples of two members of the *n*-OCT series, namely the $n=7$ and $n=8$ homologues. These compounds were chosen because they exhibit all three of the mesophases seen in this homologous series. The layer spacings for the S_A and E phases and the repeat distance for the nematic phase are shown in table 2.3d.

	E	S_A	N	Molecular length/Å
7-OCT	27.4Å 4.53Å (*110*) 4.03Å (*200*) 3.24Å (*210*)	33.6Å	≈35 Å	24.8
8-OCT	29.2Å 4.54Å (*110*) 4.03Å (*200*) 3.24Å (*210*)	35.7Å	≈36Å	26.1

Table 2.3d

The molecular lengths given in table 2.3d are the fully extended molecular lengths obtained from a projection of the all-*trans* conformation onto the director. The all-*trans* molecular lengths were obtained using Polygen Quanta software on an IBM RISC 6000 computer. The numbers given in parenthesis, (*hkl*), represent the Miller indices for the Bragg peaks, assigned using information given by Doucet [50], Leadbetter *et al.* [39] and Morrison *et al.* [40]. The wide angle scattering observed for the E phase is consistent with computer simulation studies by Luckhurst *et al.*[51] and studies by Doucet on PBAPC (*p*-phenylbenzylidene-*p*-amino *n*-pentyl cinnamate) [50]. Using

these wide angle reflections and the indexing shown in table 2.3d the orthorhombic cell dimensions [23] are obtained as

	a/Å	*b*/Å	*c*/Å
7-OCT	8.06	5.48	27.4
8-OCT	8.06	5.49	29.2 .

The values obtained for the cell dimensions *a* and *b* are in agreement with those found in the *n*-CT compounds. They do, however, represent a significant distortion of the hexagonal arrangement on which the orthorhombic unit cell is based. The *c* dimension corresponds, assuming a mean thermal displacement along the director of approximately 3Å, to a monolayer arrangement. Within the S_A phase the layer spacing shows an unusual inverse temperature dependence, the layer spacing increasing with reduced temperature. The layer spacings observed corresponding to approximately the length of the aromatic core plus two alkoxy chains, a layer spacing to molecular length (*d*/*l*) ratio of ≈1.4. This phase in both cases is a S_{Ad}, an interdigitated smectic A phase, similar to those found in the *n*-CT compounds by Leadbetter *et al.* [39] and Morrison *et al.* [40] and in 8-CB by Leadbetter *et al.* [52]. The value given in table 2.3d for the repeat distance in the nematic phase is measured as the distance between the central points of the diffuse spots observed. As expected because of the reduction in the order of the phase this repeat distance is larger than the layer spacing seen in the S_A phase. This distance is the average molecular repeat distance on a local level, and corresponds to approximately 1.4 times the molecular length.

2.4 Conclusions

In this chapter we have described the preparation and characterisation of the homologous series of 4-*n*-alkoxy-4"-cyano-*p*-terphenyl compounds. The phase diagram for this series of compounds shows the presence of nematic, smectic A and crystal E phases. The trends observed in the phase diagram, are the formation of exclusively nematic phases by homologues up to, and including, the sixth member and for higher homologues the formation of smectic A and crystal E phases. Also seen is a gradual fall in the clearing temperature to higher members of the series, with the melting transition temperature falling to a minimum at 8-OCT then rising again.

The entropy change values for the transitions, obtained by differential scanning calorimetry, although lacking any detailed regular feature, show the expected alternation in the nematic to isotropic transition values and a dramatic increase as the transition becomes smectic to isotropic. There is an increase in the entropy change observed for the melting transition on going from a crystal to nematic transition to a crystal to crystal E transition.

These observations are in agreement with the phase diagrams and entropy change variations found in the similar 4-*n*-alkyl-4"-cyano-*p*-terphenyl (*n*-CT), 4-*n*-alkoxy-4'-cyanobiphenyl (*n*-OCB) and 4-*n*-alkyl-4'-cyanobiphenyl (*n*-CB) systems.

CHAPTER 3: Application of the Molecular Field Theory to Nematics Composed of Flexible Molecules.

In this chapter we give a mathematical description of the Marcelja-Luckhurst theory [53] for flexible molecules as outlined qualitatively in section 1.6. The theory is then used to predict the thermodynamic properties of the 4-*n*-alkoxy-4"-cyano-*p*-terphenyls and 4-*n*-alkoxy-4'-cyanobiphenyl compounds; these values are compared with the experimental values given in chapter 2.

3.1 Mathematical Description of the Theory for Nematics Composed of Flexible Molecules

Conformational States

Using the rotameric state model of Flory [36] the simplest form of the internal energy $U_{INT}(n)$ of the n^{th} conformer is given by

$$U_{INT}(n) = n_g E_{tg} , \qquad (1)$$

where n_g is the number of *gauche* linkages and E_{tg} is the energy difference between the *trans* and *gauche* states. A second term can be included to discriminate against $g\pm g\mp$ sequences, which lead to unfavourable 1-5 methylene interactions

$$U_{INT}(n) = n_g E_{tg} + n_{g\pm\, g\mp} E_{g\pm\, g\mp} , \qquad (2)$$

where $n_{g\pm\, g\mp}$ is the number of these sequences and $E_{g\pm\, g\mp}$ is the energy penalty relative to a pair of *gauche* links ($2E_{tg}$). Extended sequences of *gauche* links which for a strict tetrahedral geometry result in the overlap of one or more atoms are excluded completely from the calculation. In calculations

involving the real geometries it is necessary to introduce a proximity criteria to remove unacceptable extended sequences of *gauche* links, those where unbonded atoms approach 154pm (a carbon-carbon bond length).
The probability of finding the chain in its n^{th} conformer in the isotropic phase is

$$p_n = \exp \{ -U_{INT}(n)/kT \} / Z_{INT} , \quad (3)$$

where the partition function is given by

$$Z_{INT} = \sum \exp \{ -U_{INT}(n)/kT \} . \quad (4)$$

In an orientationally ordered phase such as a nematic this expression will not be valid as it is necessary to consider the potential of mean torque, U_{EXT}, responsible for the existence of the phase since this favours the more elongated conformers. This potential will depend on both the conformational state of the molecule and its orientation with respect to the director. The total energy can be approximated by

$$U(n,\omega) = U_{INT}(n) + U_{EXT}(n,\omega) , \quad (5)$$

where ω denotes the spherical polar coordinates of the director in the molecular frame, as illustrated in figure 1.6a. This expression is approximate because $U_{INT}(n)$, the energy of the conformer resulting from intramolecular interactions, is assumed to be independent of the molecular orientation. The normalized probability of finding the n^{th} conformer with an orientation ω with respect to the director is

$$f(n,\omega) = \exp\{ -U_{INT}(n)/kT \} \exp \{ -U_{EXT}(n,\omega)/kT \}/Z , \quad (6)$$

where the conformational-orientational partition function, Z, is given by

$$Z = \sum \exp \{ -U_{INT}(n)/kT \} Q_n . \quad (7)$$

Here Q_n is the orientational partition function for the n^{th} conformer and is given by

$$Q_n = \int \exp \{ -U_{EXT}(n,\omega)/kT \} d\omega . \quad (8)$$

Integration of $f(n,\omega)$ over all orientations gives the probability of finding a molecule in the n^{th} conformer irrespective of its orientation,

$$p_n = \exp \{ -U_{INT}(n)/kT \} Q_n/Z . \quad (9)$$

The orientational partition function Q_n causes a variation in the statistical weights p_n for the nematic phase, from those in the isotropic phase. The statistical weights, p_n, will be enhanced for well ordered, linear, conformations for which $U_{EXT}(n,\omega)$ is large. In the isotropic limit the orientational partition functions are 4π because the potential of mean torque vanishes and so equation (9) reduces to equation (3).

Orientational Order

In a uniaxial phase, such as a nematic, composed of rigid particles the orientational order is characterised by an infinite set of order parameters [54] defined as the averages of even rank modified spherical harmonics

$$\bar{C}_{L,m} = \int C_{L,m}(\omega) f(\omega) d\omega , \quad (10)$$

where the bar indicates an ensemble average and $f(\omega)$ is the normalised singlet orientational distribution function, as illustrated in figure 1.6c. Of the infinite set of order parameters only the second rank quantities $\bar{C}_{2,m}$, of which there are five corresponding to $m=0,\pm1,\pm2$, can readily be measured. In addition these second rank order parameters tend to be dominant, especially close to the nematic-isotropic transition.

For a flexible molecule we need to define an ordering tensor for each rigid sub-unit within the molecule so as to characterise the orientational ordering [55]. The sub-units chosen should remain unchanged by geometric and conformational changes within the molecule. The ordering tensor takes a similar form to that in equation (10) but the joint conformational-orientational singlet distribution function is required because the orientation of the director in the segmental axis system will change as a result of fluctuations in both conformational state and molecular orientation;

$$\bar{C}_{2,m} = \sum \int C_{2,m}(\omega)\, f(n,\omega)\, d\omega \ . \qquad (11)$$

We can using our previous assumption concerning the separation of the total energy into internal and external contributions, (see equation (5)), write the conformational-orientational singlet distribution function as the product

$$f(n,\omega) = p_n\, f_n(\omega) \ , \qquad (12)$$

where p_n is the probability of the molecule being in the n^{th} conformer and $f_n(\omega)$ is the singlet orientational distribution function for the n^{th} conformer. Assuming that the internal energy is only dependent on the conformational state in equation (5) gives

$$\begin{aligned} \bar{C}_{2,m} &= \sum p_n \int C_{2,m}(\omega)\, f_n(\omega)\, d\omega \ , \qquad (13) \\ &= \sum p_n\, \bar{C}^n_{2,m} \ , \end{aligned}$$

where $C^n_{2,m}$ is the ordering tensor for the n^{th} conformer.
Calculation of $C^n_{2,m}$ requires use of the potential of mean torque in order to determine the orientational distribution function for the n^{th} conformer

$$f_n(\omega) = \exp \{ -U_{EXT} (n,\omega)/kT \}/Q_n . \quad (14)$$

Formally the potential of mean torque can be expanded in a complete basis set of modified spherical harmonics, however the expansion includes coefficients dependent on the anisotropic molecular interactions, of which we have little knowledge. Consequently the summation, restricted to even values by the symmetry of the nematic phase, is truncated at the second rank term, to give

$$U_{EXT}(n,\omega) = -\sum x^n_{2,m} C^*_{2,m}(\omega) , \quad (15)$$

where $x^n_{2,m}$ is the conformationally dependent interaction tensor. It can be constructed from the sum of segmental interactions for the molecule. When considering a flexible molecule an ordering tensor for each rigid sub-unit within the molecule is required to characterise the orientational order. The best choice of sub-unit for typical rod-like mesogenic molecules as used by Marcelja [35] and Luckhurst [53] are the aromatic core and the carbon-carbon bonds as this provides a realistic physical picture of the molecule and remain unchanged by geometric or conformation changes. However Photinos *et al.* [56] have introduced additional contributions associated with chords joining the mid-point of adjacent bonds, an approach applied in early work by Marcelja for lipids [57]. The use of rigid segments is useful to relate the conformationally dependent $x^n_{2,m}$ to a small number of variables and the geometry. The contribution of each segment or chord in the molecule to $x^n_{2,m}$ expressed in a common reference frame varies with the orientation of the segmental axis systems in this frame. The total interaction tensor is related to the segmental interactions by

$$x^{n}_{2,m} = \sum D^{2}_{m,P} (\Omega_{n,j}) X^{j}_{2,P} , \qquad (16)$$

where $D^{2}_{m,P} (\Omega_{n,j})$ is a Wigner rotation matrix used to transform from the local segmental frame to the global reference frame for the conformer. The Euler angles relating the two frames are $\Omega_{n,j}$. The segmental interaction tensors $X^{j}_{2,P}$ are considered to be independent of the molecular conformation; in addition it is convenient but not necessary to assume, for compounds such as the 4-*n*-alkoxy-4"-cyano-*p*-terphenyls and 4-*n*-alkoxy-4'-cyanobiphenyls that the segmental interactions are cylindrically symmetrical about the carbon-carbon bond or mesogenic *para* axis. The total interaction tensor consequently reduces to

$$x^{n}_{2,m} = \sum C_{2,m}(\omega_{n,j}) X_{j} , \qquad (17)$$

where X_j is the component of $X^{j}_{2,P}$ for the j^{th} sub-unit and $\omega_{n,j}$ denotes the orientation of the assumed segmental symmetry axis in the reference frame. Diagonalisation of the conformational interaction tensor gives the principal components $x^{n}_{2,0}$ and $x^{n}_{2,2}$ used to define the reference frame. This diagonalisation is also of considerable value in the evaluation of the ordering tensor, $C^{n}_{2,m}$ as we shall now see. In the principal axis system the potential of mean torque becomes

$$U_{EXT}(n,\omega) = -\{x^{n}_{2,0} P_2(\cos\beta) + x^{n}_{2,2} (3/2)^{1/2}\sin^2\beta \cos 2\gamma\} , \qquad (18)$$

where $P_2(\cos\beta)$ is the second Legendre polynomial. The principal axes of $x^{n}_{2,q}$, are also the principal axes of the ordering tensor $C^{n}_{2,q}$, whose components are given by

$$C^{n}_{2,q} = Q_n^{-1} \int P_2(\cos\beta) \exp \{ U_{EXT} /kT \} \sin\beta \, d\beta \, d\gamma \qquad (19)$$

the integration over γ is analytical, this however is not the case if $x^n_{2,1}$ terms are present.

The resulting principal components are given by

$$C^n_{2,0} = 2\pi/Q_n \int P_2(\cos\beta)\, I_0\{(3/8)^{1/2} b_n \sin^2\beta\} \times \exp\{a_n P_2(\cos\beta)\} \sin\beta \, d\beta \quad (20)$$

and

$$C^n_{2,2} = C^n_{2,-2} = 2\pi(3/8)^{1/2}/Q_n \int \sin^2\beta \, I_1\{(3/8)^{1/2} b_n \sin^2\beta\} \times \exp\{a_n P_2(\cos\beta)\} \sin\beta \, d\beta \, . \quad (21)$$

Here the orientational partition function, Q_n, for the n^{th} conformer is

$$Q_n = 2\pi \int I_0\{(3/8)^{1/2} b_n \sin^2\beta\} \exp\{a_n P_2(\cos\beta)\} \sin\beta \, d\beta \quad (22)$$

and $I_n(x)$ is an n^{th} order modified Bessel function

$$I_n(x) = 1/\pi \int \cos n\gamma \exp(x\cos\gamma) \, d\gamma \, . \quad (23)$$

The interaction parameters occurring in these equations for the order parameters of the n^{th} conformer a_n and b_n are $x^n_{2,0}/kT$ and $2x^n_{2,2}/kT$, respectively.

In order to make a comparison between the predicted orientational ordering tensors and those obtained experimentally, it is necessary to transform from the principal axis system to the local segmental axis system, this is achieved using

$$\bar{C}'_{2,n} = \sum D^2_{m,n}(\Omega) \, \bar{C}_{2,m} \, , \quad (24)$$

where the prime indicates the ordering tensor in the segmental frame. Using deuterium NMR spectroscopy we can obtain order parameters for the carbon-deuterium bonds, but because of the time scale of the experiment the result is a conformational average. The conformational averages of the segmental ordering tensors are evaluated using equation (9). This allows a direct comparison of experimental results with those obtained from the theory and consequently optimisation of the parameters X_a/kT and X_c/kT for the system under study.

Thermodynamic Properties

In order to obtain the thermodynamic properties of interest, namely the nematic to isotropic transition temperature and the entropy of transition, it is first necessary to locate the phase transition. This is achieved by calculating the Helmholtz free energy of the two phases, the phase transition occurring when the free energies of the two phases are equal. The Helmholtz free energy is used because we are concerned with systems at constant volume, which is a convenient approximation.
The Helmholtz free energy for a system of N independent particles, such as an ideal gas, is given by

$$A = -NkT \ln Z \qquad (25)$$

where Z is the single particle partition function. When considering a system consisting of particles interacting with a molecular field, which they both generate and experience, this expression overcounts the internal energy by a factor of two. The Helmholtz free energy of a system of N particles interacting with a molecular field is

$$A = -NkT \ln Z - N \bar{U}_{EXT} /2 , \qquad (26)$$

where in order to evaluate this expression we need to calculate $\bar{U}_{EXT}$, the contribution to the internal energy from the anisotropic interactions. The starting point is equation (15) for the potential of mean torque of the n^{th} conformation; this can be rewritten in terms of the segmental interactions,

$$U_{EXT}(n,\omega) = -\sum x^{n}_{2,m}\, C^{*}_{2,m}(\omega) \ ,$$

where the complex conjugate of the modified spherical harmonic is required to ensure that the resultant scalar energy U_{EXT} is real.
Writing $x_{2,m}$ the interaction tensor as the sum over segments in the molecule gives

$$x_{2,m} = \sum X^{j(n)}_{2,m} \ , \qquad (27)$$

$$= \sum \sum D^{2}_{m,n}(\Omega_j)\ X^{j}_{2,n} \ , \qquad (28)$$

where $X^{j(n)}_{2,m}$ are the segmental interaction tensors for the n^{th} conformer and $D^{2}_{m,n}(\Omega_j)$ is a Wigner rotation matrix as in equation (16). Assuming that the segments have cylindrical symmetry,

$$X^{j}_{2,n} = X^{j}_{2,0}\ \delta_{0,n} \ , \qquad (29)$$

where $\delta_{0,n}$ is a Kronecker delta function such that $\delta=1$ for $n=0$ but $\delta=0$ for all other values of n. Using this assumption in equation (28) reduces it to

$$x_{2,m} = \sum C_{2.m}(\omega_j)\ X_j \ , \qquad (30)$$

where X_j is the interaction tensor for the j^{th} segment in the molecule. Substitution of this equation into equation (15) gives

$$U_{EXT}(n,\omega) = -\sum \sum\ C_{2,m}(\omega_j)\ X_j\ C^{*}_{2,m}(\omega) \ . \qquad (31)$$

Use of the spherical harmonic addition theorem gives

$$U_{EXT}(n,\omega) = - \{ x_a P_2(\cos\beta_a) + x_c \sum P_2(\cos\beta^j_c) \} , \qquad (32)$$

where β is the angle between the director and the symmetry axis for the segmental interaction tensor. The parameters x_a and x_c are the non-zero components, for the aromatic core and carbon-carbon bond units respectively, of the interaction tensor in the local segmental frame.
Averaging over both the orientations and conformations of the molecule gives the average energy per particle as

$$<\bar{U}_{EXT}> = - \{ x_a <\bar{P}^a_2> + x_c <\bar{P}^c_2> \} , \qquad (33)$$

where the angular brackets denote a conformational average and the bars indicate an orientational average. $<\bar{P}^c_2>$ the order parameter for the chain is defined as the sum of the order parameters for each carbon-carbon bond.
The contribution to the internal energy of the system of N particles is $N<\bar{U}_{EXT}>/2$ where the factor of 1/2 allows for the over-counting of the anisotropic interactions resulting from the molecular field approximation. The Helmholtz free energy for the nematic phase composed of N particles is then

$$A_N = N \{ x_a <\bar{P}^a_2> + x_c <\bar{P}^c_2> \}/2 - NkT \, ln \, Z , \qquad (34)$$

where Z is defined in equation (7). The phase transition, between the nematic and the isotropic phase, occurs when the free energies of the two phases are equal. The free energy of the isotropic phase is obtained by setting the order parameters in equation (34) to zero, giving

$$A_I = - NkT \, ln \, Z_I , \qquad (35)$$

where

$$Z_I = 4\pi \sum \exp\{-U_{INT}(n)/kT\} \qquad (36)$$

and 4π is the orientational partition function for a molecule in the isotropic phase. The difference in the free energy between the nematic and the isotropic is given by, equation (34) minus equation (35), namely

$$\Delta A = A_N - A_I$$

$$\Delta A = N\{ x_a\langle \bar{P}^a_2\rangle + x_c\langle \bar{P}^c_2\rangle \}/2 - NkT \ln Z_N / Z_I \, . \qquad (37)$$

We are unable to use this equation until we introduce a suitable description of the temperature dependence of the segmental interaction parameters x_a and x_c.

The entropy of transition is the change in the internal energy at the transition divided by the transition temperature. As well as the average orientational energy resulting from the anisotropic interactions we require the contribution from the intramolecular energy, obtained by averaging $U_{INT}(n)$ over all conformations. This gives

$$U_N = -N \{ x_a \langle \bar{P}^a_2\rangle + x_c \langle \bar{P}^c_2\rangle \}/2 + N\langle U_{INT}\rangle_N \qquad (38)$$

for the nematic phase and

$$U_I = N\langle U_{INT}\rangle_I \qquad (39)$$

for the isotropic phase. By evaluating these quantities at the nematic-isotropic transition we obtain the entropy of transition as

$$\Delta S/R = -\{ x^{NI}_a \langle \bar{P}^a_2 \rangle_{NI} + x^{NI}_c \langle \bar{P}^c_2 \rangle_{NI} \}/2kT_{NI} + \{\langle U_{INT} \rangle^{NI}_N - \langle U_{INT} \rangle^{NI}_I /kT_{NI} \, . \quad (40)$$

The entropy of transition depends, therefore, on the change in orientational order as well as the difference in the conformational distributions of the two phases.

Having determined the temperature dependence of the free energy, we need to consider the temperature dependence of the segmental interaction parameters x_a and x_c. This dependence arises as a result of the orientational order of the system and so it is reasonable to expect x_a and x_c to be proportional to the molecular order parameters.

For a mixture of rod-like particles the Humphries-James-Luckhurst molecular field theory assumes that the interaction parameters for species *i* is given by [58]

$$x_i = v^{-1}_{mi} \sum \epsilon_{i,j} \bar{P}^j_2 \, , \quad (41)$$

where v_{mi} is the molecular volume of species *i*. The parameters $\epsilon_{i,j}$ are determined by the average anisotropic interactions between particles *i* and *j*. If we consider the nematic phase composed of flexible molecules to be a mixture of aromatic core and chain units, we can write

$$x_a = \epsilon_{aa} v^{-1}_{ma} \langle \bar{P}^a_2 \rangle + \epsilon_{ac} v^{-1}_{mc} \langle \bar{P}^c_2 \rangle \, , \quad (42)$$

$$x_c = \epsilon_{ac} v^{-1}_{ma} \langle \bar{P}^a_2 \rangle + \epsilon_{cc} v^{-1}_{mc} \langle \bar{P}^c_2 \rangle \, . \quad (43)$$

The volume terms are available from tabulations in the literature [59]. The remaining unknowns are the three strength parameters ϵ_{aa}, ϵ_{ac} and ϵ_{cc} resulting from core-core, core-chain and chain-chain interactions, respectively. It is reasonable to remove one of the variables by assuming the Berthelot combining rule [53]

$$\epsilon_{ac} = (\epsilon_{aa} \ \epsilon_{cc})^{1/2} . \qquad (44)$$

Given this approximation the ratio x_c/x_a, the parameter controlling the relative contributions to the total interaction energy of the core and chain segments, reduces to

$$x_c/x_a = (\epsilon_{cc} / \epsilon_{aa})^{1/2} \qquad (45)$$

and so is temperature independent. This result removes much of the computational difficulty in solving the equations for the orientational order parameters and the Helmholtz free energy.
A temperature scale emerges if we divide equation (42) by kT, to give

$$X_a/kT = (\epsilon_{aa} v^{-1}_m/kT) \{<\bar{P}^a_2> + (\epsilon_{ac}/\epsilon_{aa}) <\bar{P}^c_2> \}$$

$$= (\epsilon_{aa} v^{-1}_m/kT) \{<\bar{P}^a_2> + (\epsilon_{cc}/\epsilon_{aa})^{1/2} <\bar{P}^c_2> \}$$

$$= (\epsilon_{aa} v^{-1}_m/kT) \{<\bar{P}^a_2> + X_c/X_a <\bar{P}^c_2> \} . \qquad (46)$$

The scaled temperature is then written as

$$T^* = v_m \, kT/ \epsilon_{aa} . \qquad (47)$$

Within the computer X_a/kT and X_c/X_a are input parameters, using these the order parameters for each segment are evaluated allowing the calculation of the scaled temperature from

$$T^* = (kT/X_a) \{<\bar{P}^a_2> + X_c/X_a <\bar{P}^c_2> \} . \qquad (48)$$

The important stage in the theory is the introduction of the Berthelot combining rule which considerably simplifies the calculation. Without this simplification the procedure would require the solution of N self consistent equations at each temperature, as in the original treatment by Marcelja [35].

This completes the mathematical description of the theory for nematics composed of flexible molecules.

3.2 Application to the 4-*n*-alkoxy-4"-cyano-*p*-terphenyls.

The molecular field theory outlined in sections 1.6 and 3.1 has been used to predict the nematic to isotropic transition temperatures and entropy of transition for the *n*-OCT and *n*-OCB compounds. The calculations were performed, using a modified version of a computer program written by Dr. A.P.J. Emerson [60], on the University of Southampton IBM 3090-195 computer.

3.2.1 Input Parameters for the Simulation

The computer program used in these simulations was designed to be as flexible as possible, allowing work on a variety of monomeric and dimeric systems [60] to be carried out using the same program. As such the program has a relatively large number of input parameters. In this section we describe those parameters and give an indication of the appropriate values for each.

Chain length: This is the length of the flexible chain attached to the mesogenic core. In this work the oxygen atom which in the theory is considered as being identical to a methylene unit is included as a group in the aliphatic chain, as illustrated below. The chain length was restricted to a value of about nine in order to limit use of computer resources.

X^*_a : The strength parameter for the mesogenic core scaled with kT (X_a/kT). This parameter indirectly controls the temperature of the system, via equation (46), such that a high value of X_a produces a low temperature and a low X_a a high temperature. In practice the value of

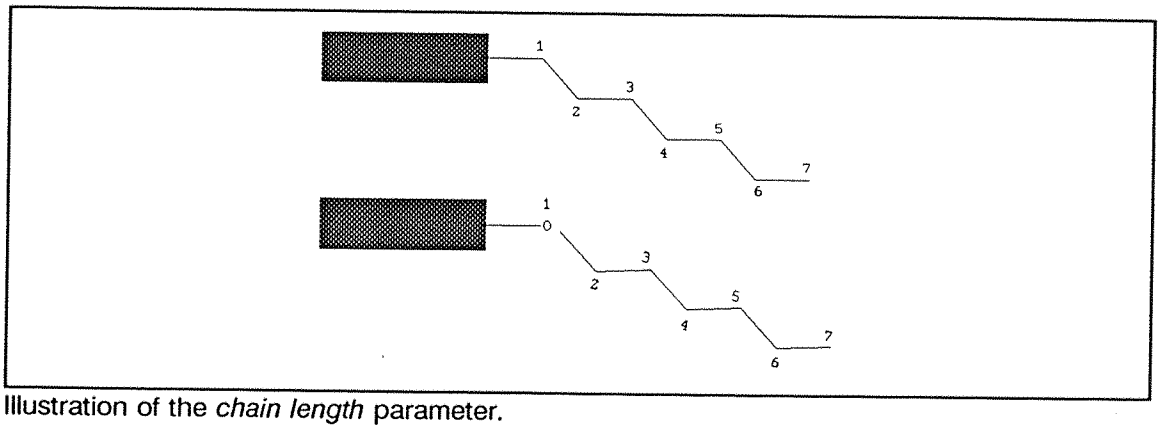

Illustration of the *chain length* parameter.

this strength parameter varies between zero and four, with the nematic-isotropic transition occuring at a temperature equivalent to an X^*_a value of about 1.5.

Lambda C (λ_c, X_c/X_a) : The ratio of the strength parameter for the chain segment to that of the aromatic mesogenic unit. The value of this ratio varies from almost zero, where the effect of the chain is purely a dilution of the core interactions, to approximately 0.4 where the interactions due to the chain segments are a significant proportion of the total interaction. In 4-*n*-pentyl-4'-cyanobiphenyl and 4-*n*-octyl-4'-cyanobiphenyl this ratio takes a value between 0.2 and 0.3, in the cyano-*p*-terphenyl systems the value is expected to be lower. This implies that the dilution of core interactions by increasing the chain length will be more in for the larger mesogenic core.

E^*_{tg} : The difference in energy of the *trans* and *gauche* conformers scaled with kT, is E_{tg}/kT. The energy difference is defined such that a value of one is used in most systems. This is consistent with Raman spectroscopy studies of liquid *n*-alkanes in which E_{tg} was found to be approximately 3.2 $kJmol^{-1}$ at room temperature [61]. Within the calculations E^*_{tg} is assumed to be temperature independent, an assumption which in certain systems may not be reasonable.

E^{*}_{12} ($E_{g\pm g\mp}$) : The energy penalty of a *gauche-gauche* link relative to 2 E_{tg}. As with all of the energy quantities this parameter is scaled with kT, as $E_{g\pm g\mp}/kT$. Within the calculation this quantity is always considered relative to E_{tg} and consequently is temperature independent. The ratio of $E_{g\pm g\mp}/E_{tg}$ is equal to four.

VCA : The volume ratio of a chain segment to that of the aromatic core unit, is given by

$$\mathbf{VCA} = \frac{\text{Volume of a methylene group (-CH}_2\text{-)}}{\text{Volume of the aromatic core system}} .$$

For the 4-*n*-alkoxy-4"-cyano-*p*-terphenyls (*n*-OCT) this ratio is 0.067 and for the 4-*n*-alkoxy-4'-cyanobiphenyls (*n*-OCB) it is slightly larger at 0.096 [59]. Consequently the addition of a methylene unit has a proportionally smaller effect on the *n*-OCTs than on the *n*-OCBs.

In order to obtain a set of transition temperatures and entropy changes for the model *n*-OCT system which can be compared with the experimental values the theoretical parameters where scaled to the ratio of the core strength parameters, ϵ_{aa}, for the biphenyl and terphenyl systems. The 4-*n*-alkoxy-4'-cyanobiphenyl systems have been extensively studied by molecular field theories [62] and the parameters required to predict the various properties of the system obtained. Equation (47) gives the ratio as

$$v^{BI}_{m}\, T^{BI}_{NI} / v^{TER}_{m}\, T^{TER}_{NI} = \epsilon^{BI}_{aa} / \epsilon^{TER}_{aa} \qquad (49)$$

By using the experimental transition temperatures from section 2.3, in kelvin, and molar volume tabulations in equation (49) and then extrapolating the ratio to zero chain length gives a ratio of

$$\epsilon^{BI}_{aa} / \epsilon^{TER}_{aa} = 0.419.$$

Using this ratio the values of the parameters λ_c and E_{tg} shown to give a good fit to experimental data in the *n*-OCB systems can be scaled to give parameters appropriate for the *n*-OCT systems.

3.3 Predictions for the Molecular Field Theory of Flexible Molecules.

The properties of interest which are obtained from the Marcelja-Luckhurst molecular field theory are the properties of the system at the nematic to isotropic transition. In order to locate the phase transition using the theory the necessary parameters are set to appropriate values, as outlined in the previous section. The scaled value of the aromatic core strength parameter, x^*_a, is then varied over an appropriate range (zero to four) in steps of 0.1, this is equivalent to varying the temperature of the system on the scale indicated in equation (46). At each value of the aromatic core strength parameter, x^*_a, the difference in Helmholtz free energy between the nematic and isotropic phases is calculated, using equation (37), a free energy difference of zero corresponding to the nematic to isotropic transition. Once the transition has been located the required thermodynamic properties of the system can be calculated. The properties of interest include the transition temperature, the entropy change at the transition and the order parameter profiles for the mesogenic core and C-D bonds. By repeating this cycle and incrementing the chain length the variation of these properties with increasing alkyl/alkoxy chain length can be obtained.

In the 4-*n*-alkoxy-4'-cyanobiphenyls (*n*-OCB) the ratio of the strength parameters for the chain and aromatic core, $\lambda_c = x^*_c/x^*_a$, has been estimated to be in the range 0.2 to 0.3 [60][63] from a comparison of the predicted order parameter profile with experiment. It is expected that the increase in the mesogenic core size in the 4-*n*-alkoxy-4"-cyano-*p*-terphenyls (*n*-OCT) will lead to an increase in the value of the anisotropic core-core interaction parameter, ϵ_{aa}, and as the value of the chain-chain interaction parameter ϵ_{cc} is expected to remain constant this will result in a reduction in λ_c the ratio of the segmental interaction parameters. The core-core interactions will be the dominant term in the total interaction energy. In order to test this expectation each simulation

run was carried out with a range of λ_c values, the values used range from zero through 0.05, 0.10, 0.20, 0.25, to 0.29. The first three of these values are expected to provide the better fit to the larger mesogenic core of the *n*-OCTs, the last three have been used in previous calculations [60][63] to effectively model properties of the *n*-CBs and *n*-OCBs.
The predicted values of the transition temperature for the 4-*n*-alkoxy-4"-cyano-*p*-terphenyls are shown in figure 3.3a with those for the 4-*n*-alkoxy-4'-cyanobiphenyls shown in figure 3.3b.

The plots shown in figures 3.3a and 3.3b clearly demonstrate that for a given value of λ_c the variation of the reduced temperature is different, this is a consequence of the different volume ratio terms, VCA, for the mesogenic groups. The graphs both show similarities, as expected for two such analogous systems, and differences. Both systems show a tendency for the longer alkoxy chain homologues to have lower transition temperatures as the value of λ_c is reduced. This effect is slightly less pronounced for the 4-*n*-alkoxy-4"-cyano-*p*-terphenyl compounds as a result of the proportionally smaller dilution of the interactions on adding a methylene unit.

In the *n*-OCTs the *odd-even* alternation is significantly less than in the *n*-OCBs, this is a consequence of the lower E^*_{tg} value allowing the chain to adopt more conformations thereby reducing the shape anisotropy difference between *odd* and *even* homologues. In both systems the *odd-even* alternation is reduced as λ_c is reduced and the mesogenic core interactions become dominant. This is consistent with the illustration given in figure 1.4c, with the *odd-even* effect being the result of shape anisotropy changes on increasing the chain length, *odd* chain lengths widening the molecule while *even* alkoxy chains increase only the molecular length.
Comparison of figure 3.3b with the experimentally observed transition temperatures, given in figure 2.3c, suggests that the appropriate value of λ_c to

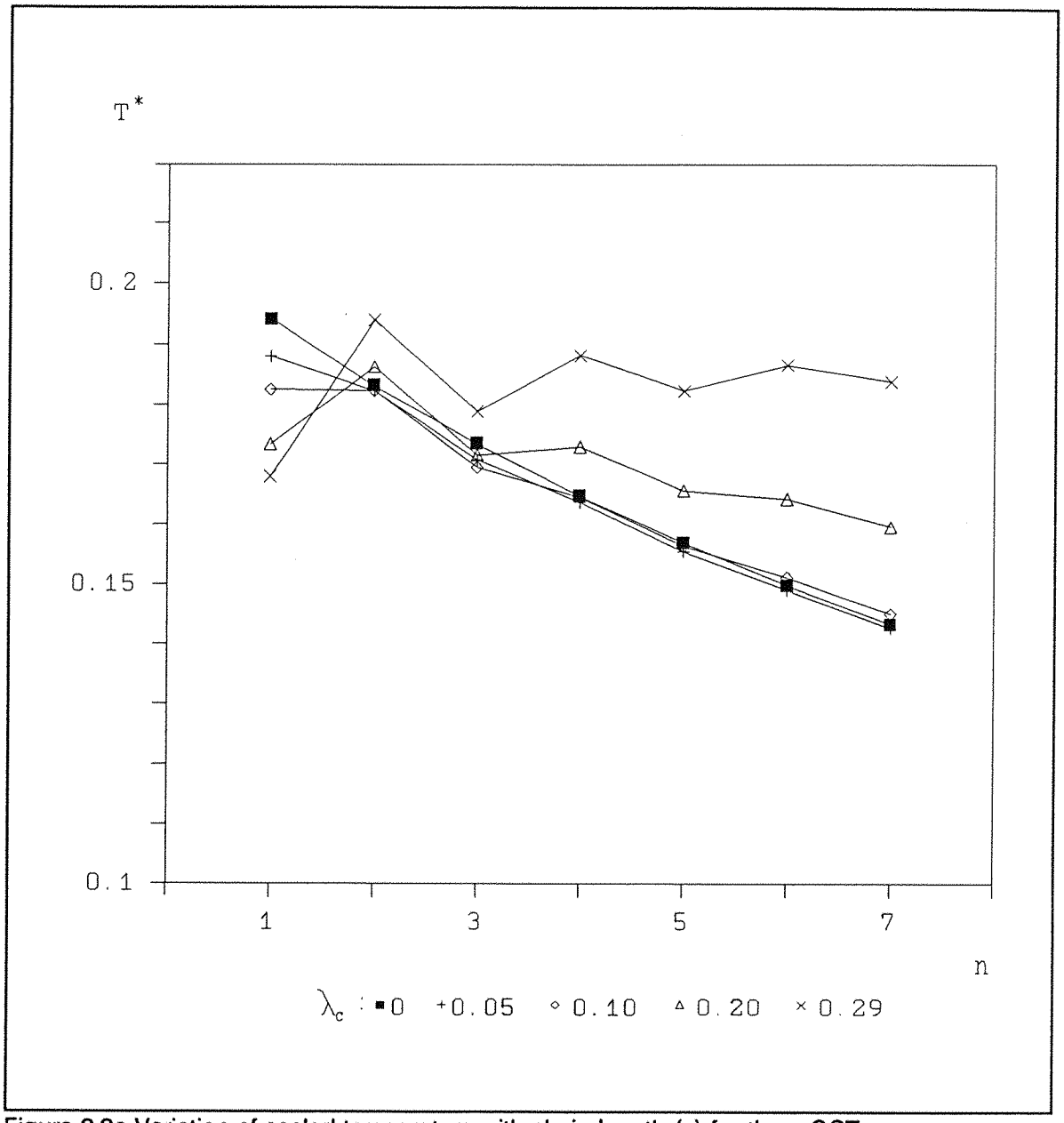

Figure 3.3a Variation of scaled temperature with chain length (n) for the *n*-OCTs.

give a qualitative fit is between 0.25 and 0.29. In the case of the *n*-OCTs the best fit is obtained with a value of approximately 0.10. A direct comparison of the theoretical results with those of experiment can be obtained by scaling the best fit values for the *n*-OCBs, in agreement with the value, λ_c=0.29, obtained by Emsley *et al.* for modelling the order parameter profile [63], to the ratio of $\epsilon^{BI}_{aa}/\epsilon^{TER}_{aa}$ as calculated in section 3.2. The resulting scaled temperatures are shown in figure 3.3c.

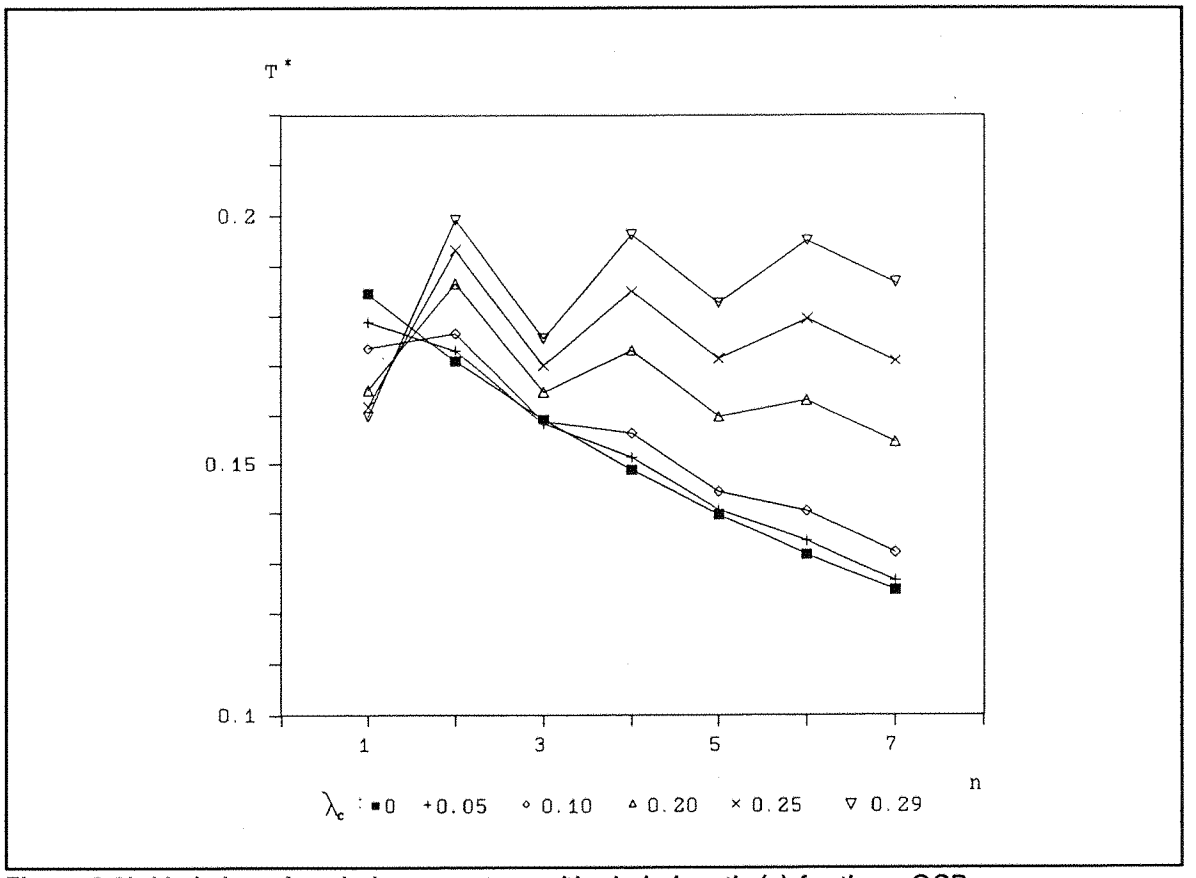

Figure 3.3b Variation of scaled temperature with chain length (n) for the *n*-OCBs.

It should be noted that the theory used here is based on a tetrahedral geometry with a C-C-C bond angle of 109.5° and a dihedral angle (ϕ_g) of 60°. Work by Counsell *et al.* [63][64] has shown that in real systems a better approximation to the angles are

C-O-C 126.4°: C-C-C 113.5°: $\phi_g \pm 68°$.

The use of these angles within the theory leads to higher transition temperatures and reduces the *odd-even* alternation [60]. Such values were not used as they increase the calculation times and in this work we are interested more in a qualitative overall view of the trends than quantitative predictions of the actual transition temperatures and transition entropies.

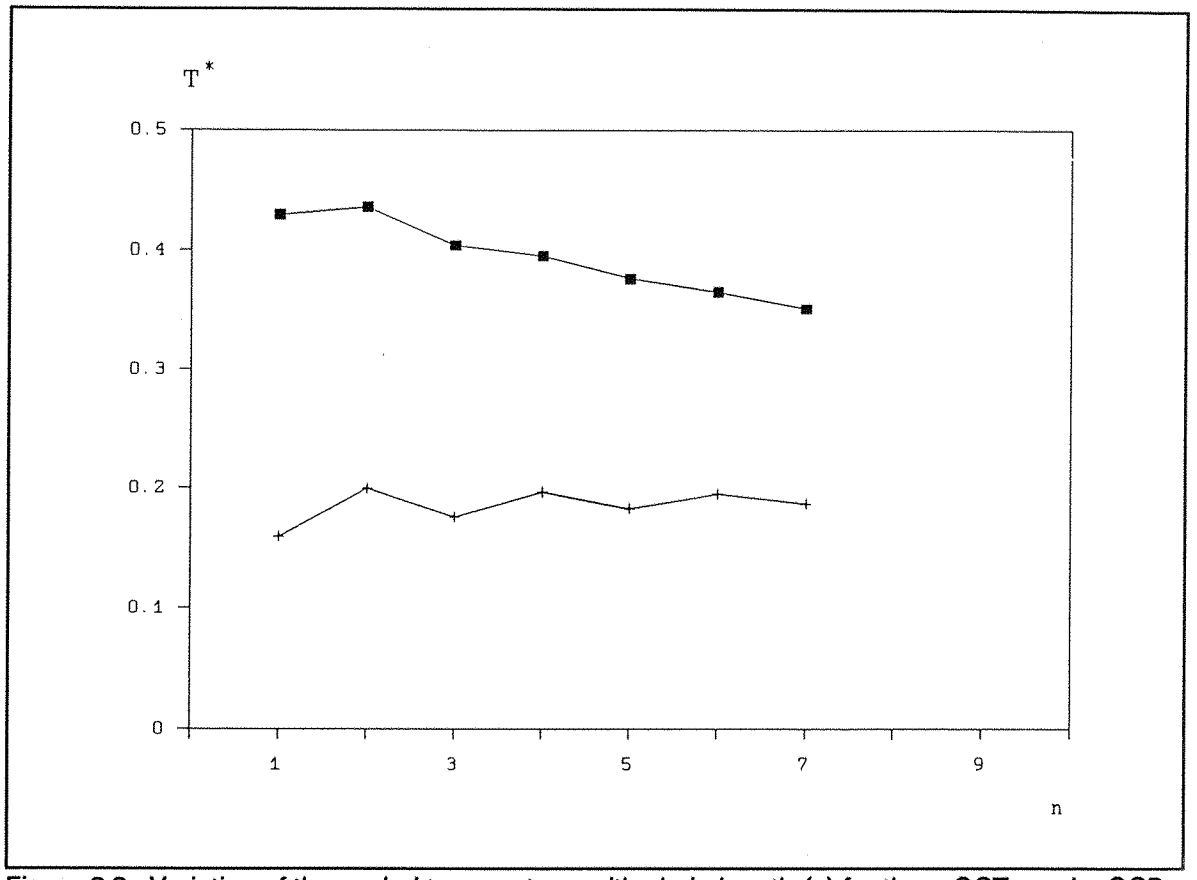

Figure 3.3c Variation of the scaled temperature with chain length (n) for the *n*-OCTs and *n*-OCBs.

Comparison of figure 3.3c with the experimental T_{NI}, shown in figure 3.3d, show extremely good agreement for the *n*-OCTs with not quite such good agreement for the *n*-OCBs. Indeed because of the minimum in the T_{NI} profile at $n=3$ the *n*-OCBs are extremely difficult to model effectively, but this is not clear why. Shown in figure 3.3e and figure 3.3f are the theoretical values for the entropies of transition of the *n*-OCTs and the *n*-OCBs, as given by equation (40). The profiles are very similar for both systems as the entropy change unlike the transition temperature depends only on the order of the system and not on the molar volume.

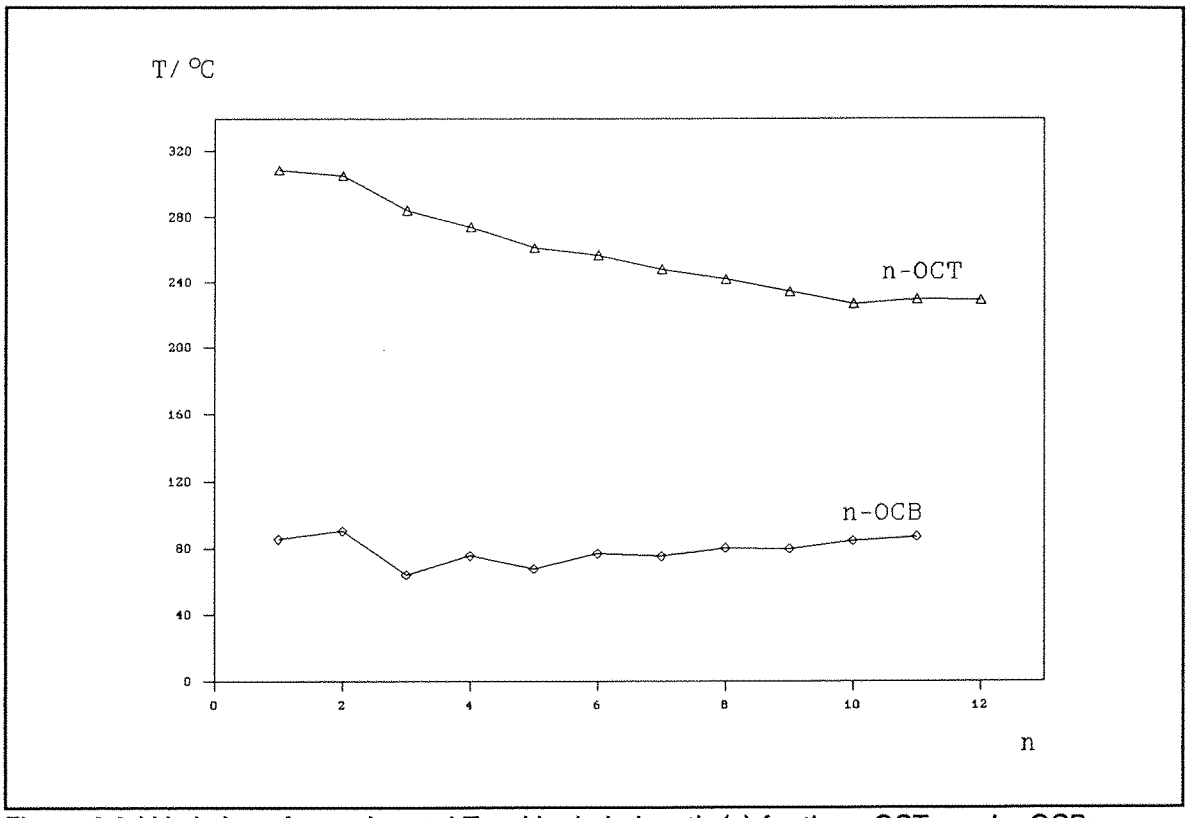

Figure 3.3d Variation of experimental T_{NI} with chain length (n) for the *n*-OCTs and *n*-OCBs.

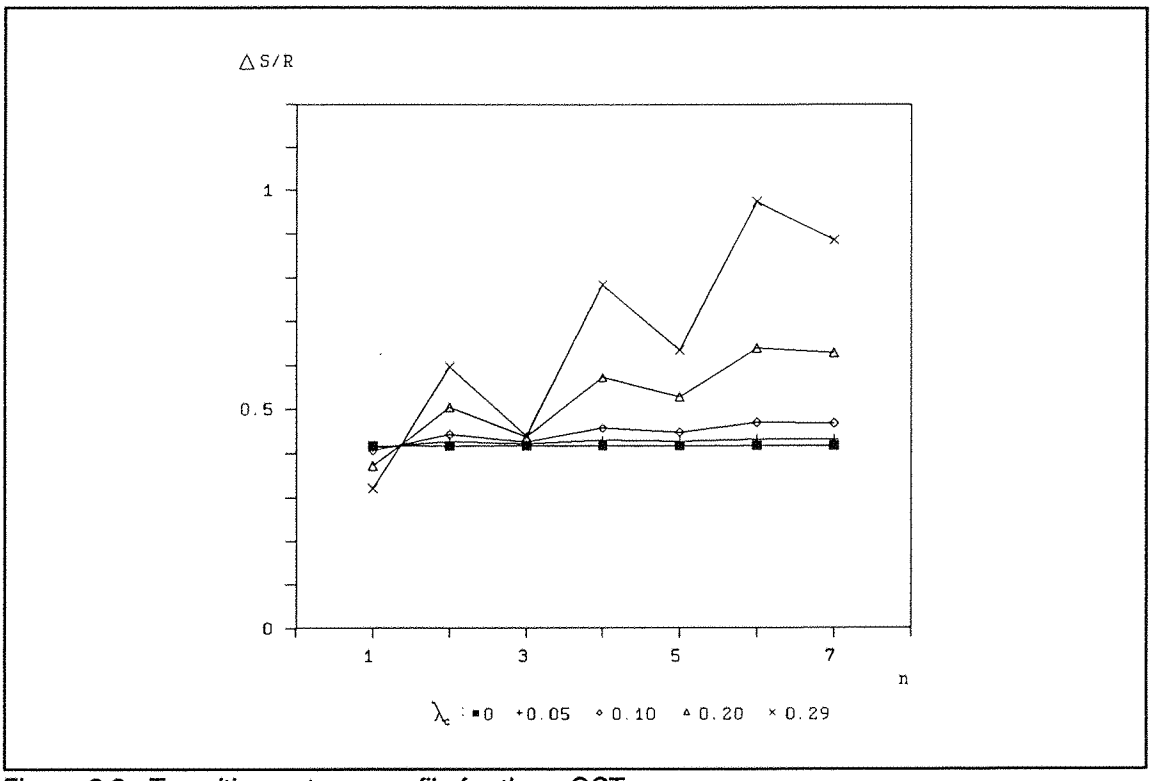

Figure 3.3e Transition entropy profile for the *n*-OCTs.

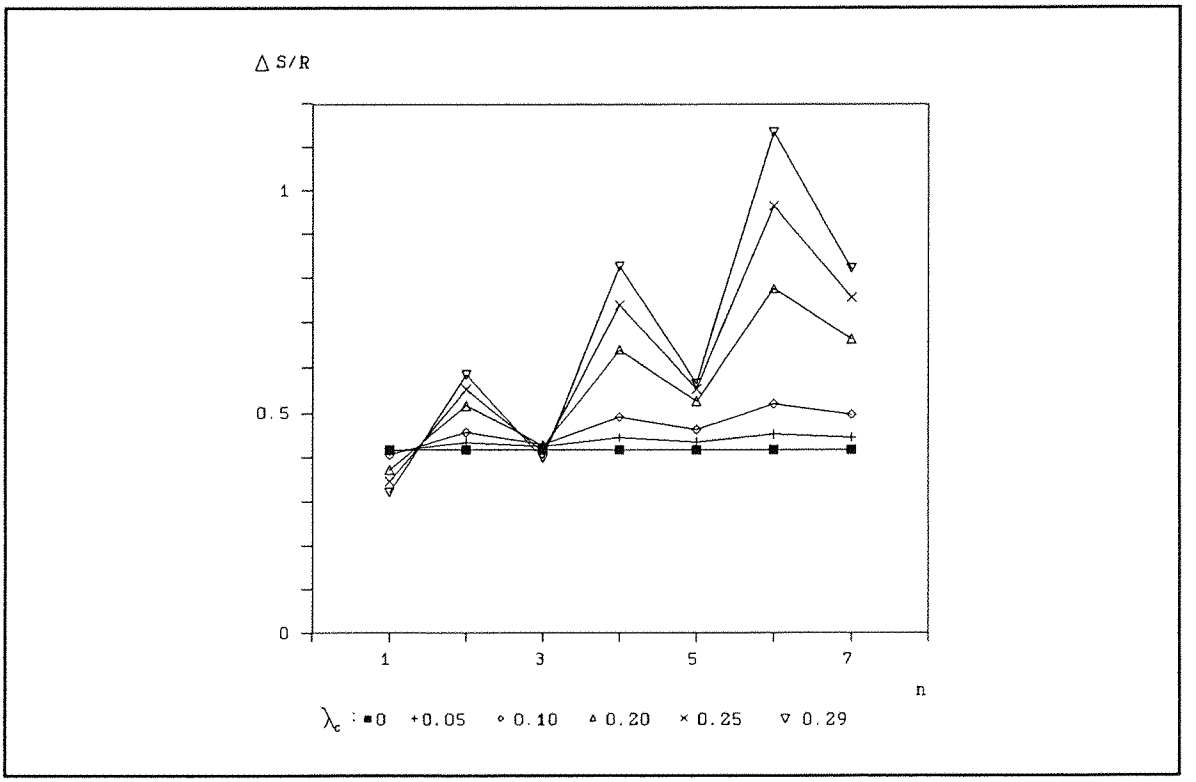

Figure 3.3f Transition entropy profile for the *n*-OCBs.

The graph shows a dramatic reduction in the *odd-even* alternation as the ratio of the chain to core strength parameters is reduced. Comparison between the experimental values, given in table 2.3b and figures 2.3e and 2.3g(a), and those predicted by the theory, concentrating on the value of λ_c giving best fit to the transition temperature profile, show the agreement to be far from good. In the case of the *n*-OCTs the *odd-even* alternation is in the correct sense, with those homologous having *even* alkoxy chain lengths having higher entropies of transition than adjacent *odd* homologues. In the *n*-OCB systems the predicted values are significantly higher than those observed experimentally, and the predicted regular *odd-even* alternation of between 0.3 and 0.4, for λ_c=0.29 is approximately ten times that observed experimentally. The predicted entropy change is made up of an orientational and a conformational contribution. In all cases the orientational entropy is the dominant term [60], as illustrated in figure 3.3g, being on average ninety per cent of the total. The entropy of transition arises primarily from the increased order in the nematic phase. In both cases the molecular field theory has considerably overestimated the entropy change at the nematic to isotropic transition. This problem is frequently encountered when using such theories [35] as the isotropic phase is considered to be totally disordered. In reality, however, short range correlations exist within the isotropic phase consequently the transition to the orientational ordered nematic phase is predicted to have a greater increase in order than is seen experimentally.

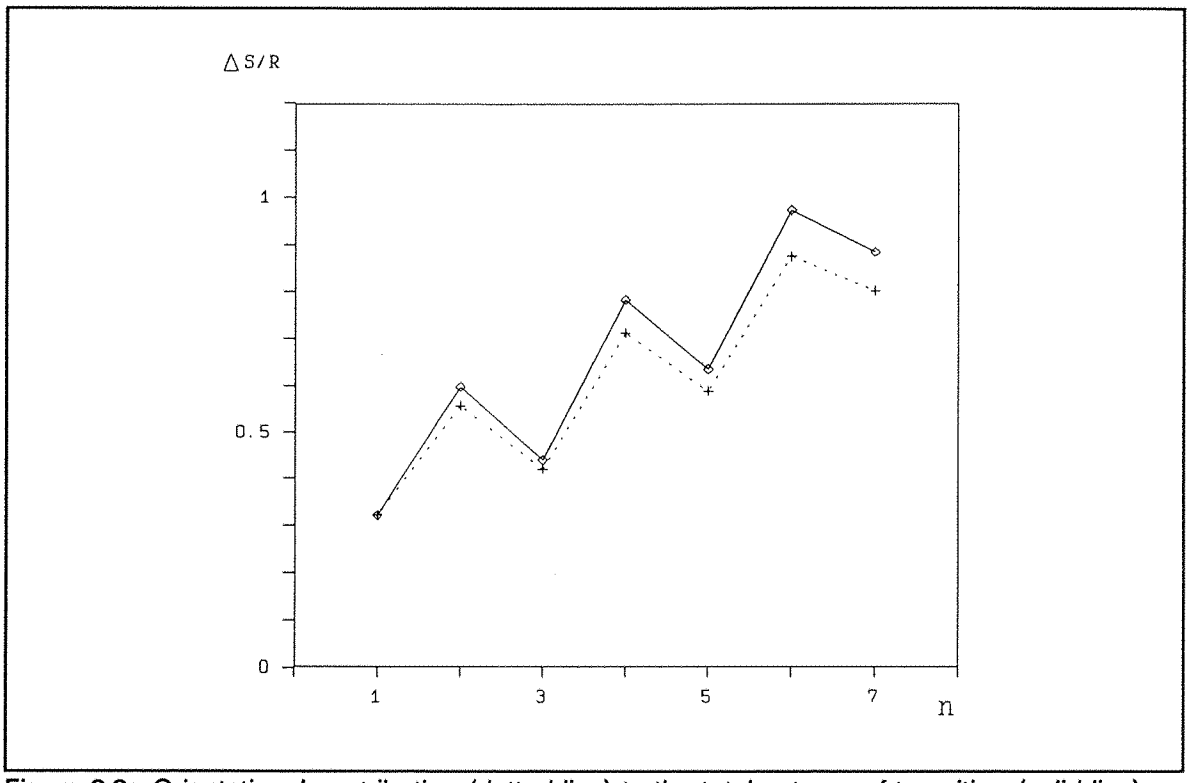

Figure 3.3g Orientational contribution (dotted line) to the total entropy of transition (solid line).

3.4 Conclusions

In this chapter the molecular field theory for flexible molecules has been used to calculate the nematic to isotropic transition properties of the *n*-OCBs and the *n*-OCTs. Comparison of these results with experimental observations show good qualitative agreement for the transition temperatures. The agreement is especially good in the case of the *n*-OCTs where the values of λ_c and E^*_{tg} giving the best fit to the *n*-OCB data have been scaled with the ratio $\epsilon^{BI}_{aa}/\epsilon^{TER}_{aa}$.

The agreement in the entropies of transition is less good especially for the *n*-OCBs where the predicted values are significantly higher and show a considerably greater *odd-even* alternation. The values obtained for the *n*-OCTs are qualitatively correct, showing a small alternation with the *even* values higher than the adjacent *odd*. In general there is an overestimation of the entropy changes for the nematic to isotropic transition.

These observations are all consistent with the alkoxy chain of the 4-*n*-alkoxy-4"-cyano-*p*-terphenyls contributing less to the total interaction energy because of the increase in the core interaction parameter, ϵ_{aa}.

REFERENCES

[1]. Reinitzer,F., *Montash. Chem.* 9, 421, (1888).

[2]. Kelker, H., and Knoll, P.M., *Liq. Crystals*, 5, 19, (1989).

[3]. See for example,
Demus, D., Demus, H., and Zaschke, H., *Flüssige Kristalle in Tabellen I*, VEB Deutscher Verlag für Grundstoffindustrie, 1974.

Demus, D., and Zaschke, H., *Flüssige Kristalle in Tabellen II*, VEB Deutscher Verlag für Grundstoffindustrie, 1984.

Attard, G.S., and West, Y.D., *Liq. Crystals*, 7, 487, (1990).

Adams, H., Bailey, N.A., Bruce, D.W., Dunmur, D.A., Lalinde, E., Marcos, M., Ridgway, C., Smith A.J., Styring, P., and Maitus, P.M., *Liq. Crystals*, 2, 381, (1987).

[4]. See for example,
Brown, G.H., Doane, J.W., and Neff, V.D., *A Review of the Structure and Properties of Liquid Crystals*, Butterworth Group, (1971).

Tanford, C., *The Hydrophobic Effect*, Wiley Interscience, New York, (1980).

Kelker, H., and Hatz, R., *The Handbook of Liquid Crystals*, Verlag Chemie, (1980).

Winsor, P.A., *Chem. Rev.*, 68, 1, (1968).

Freiburg, S.E., and Chapman, D., *Liquid Crystals: Applications and Uses*, Vol.2, Ed. Bahadur, B., World Scientific (1991).

[5]. Howell, O.T., unpublished work.

Bazuin, C.G., Guillon, D., Skoulios, A., and Nicoud, J.F., *Liq. Crystals*, 1, 188, (1986).

[6]. Gray, G.W., *Advances in Liquid Crystals*, 2, 1, (1976).

[7]. Schadt, M., *Liq. Crystals*, 5, 57, (1989).

[8]. Demus, D., and Richter, L., *Textures of Liquid Crystals*, Verlag Chemie, Weinheim, New York, (1978).

[9]. Attard, G.S., and Luckhurst, G.R., *Liq. Crystals*, 2, 441, (1987).

Van der Veen, J., de Jeu, W.H., Wanninkhof, M.W.M., and Teinhoven, C.A.M., *J. Phys. Chem.*, 77, 2153, (1973).

[10]. Leadbetter, A.J. (Chapter 1), *Thermotropic Liquid Crystals*, Ed. Gray, G.W., John Wiley & Sons, Chichester (1987).

[11]. See for example,
Reference [8].

Collings, P.J., *Liquid Crystals: Natures Delicate Phase of Matter*, Adam Hilger, Bristol (1990).

[12]. Gray, G.W., and Goodby, J.W., *Smectic Liquid Crystals: Textures and Structures*, Leonard Hill, London, Glasgow (1984).

[13]. Prost, J., *Advances in Physics*, 33, 46 (1984).

[14]. Date, R.W., Ph.D. Thesis, University of Southampton, (1991).

[15]. Luz, Z., Hewitt, R.C., and Meiboon, S., *J. Chem. Phys.*, 61, 1758, (1974).

[16]. Birgeneau, R.J., and Litster, J.D., *J. Phys.(Paris) Lett.*, 39, L-399, (1978).

Nelson, D.R., and Malpern, B.I., *Phys. Rev.*, B19, 2457, (1979).

[17]. Leadbetter, A.J., Richardson, R.M., and Frost, J.C., *J. Phys.(Paris)*, 40, C3-125, (1979).

[18]. Barbarin, F., Dugay, M., Piovesan, A., Fadel, H., Guillon, D., and Skoulious, A., *Liq. Crystals*, 2, 815, (1987).

[19]. Leadbetter, A.J., Frost, J., Gaughan, J.P., and Mazid, M.A., *J. Phys.(Paris)*, 40, C3-185, (1979).

[20]. Etherington, G., Leadbetter, A.J., Wang, X.J., Gray, G.W., and Tajbakhsh, A., *Liq. Crystals*, 1, 209, (1986).

[21]. Benattar, J.J., Moussa, F., and Lambert, M., *J. Phys.(Paris)*, 41, 1371, (1980).

[22]. Ehrenfest, P., *Proc. Acad. Sci. Amsterdam*, 36, 153, (1933).

[23]. Atkins, P.W., *Physical Chemistry*, 3rd Edition, Oxford University Press, Oxford (1986).

[24].See for example,
Doucet, J. (Chapter 14), and Leadbetter, A.J. (Chapter 13), *Molecular Physics of Liquid Crystals*, Ed. Luckhurst, G.R., and Gray, G.W., Academic Press, London, (1979).

Brown, J.G., *X-rays and their Applications*, Iliffe books limited, London, (1966).

Hukins, D.W.L., *X-ray diffraction by Disordered and Ordered systems*, Pergamon Press, Oxford, New York, (1981).

Sherwood, D., *Crystals, X-rays and Proteins*, Longmann, London, (1976).

[25]. See for example,
Demus, D., *Liq. Crystals*, 5, 75, (1989).

Ebert, M., Jungbauer, D.A., Kledringer, R., Wendorff, J.H., Kohne, B., and Praefcke, K., *Liq. Crystals*, 4, 53, (1989).

Chandrasekhar, S., *Phil. Trans. R. Soc. Lond. A.*, 309, 93, (1983).

[26]. See for example,
Gray, G.W., *Liquid Crystals and Plastic Crystals*, Vol.1, Ed. Gray, G.W., and Winsor, P.A., Ellis Horwood Ltd., (1974).

Gray, G.W., *Phil. Trans. R. Soc. Lond. A.*, 309, 77, (1983).

Gray, G.W. (Chapters 1 & 12), *Molecular Physics of Liquid Crystals*, Ed. Luckhurst, G.R., and Gray, G.W., Academic Press, London, New York, (1979).

[27]. de Jeu, W.H., and Van der Veen, J., *Phillips Res. Repts.*, 27, 172, (1972).

[28]. Maier, W., and Saupe, A., *Z. Naturforsch*, 13a, 564, (1958).

Maier, W., and Saupe, A., *Z. Naturforsch*, 14a, 882, (1959).

[29]. See for example,
Schultz, T.D., in *Liquid Crystals 3: Proceedings of the Third International Conference*, Ed. Brown, G.H., and Labes, M.M., p.263, Gordon and Breach, (1972).

Wulf, A., *J. Chem. Phys.*, 55, 4512, (1971).

[30]. Luckhurst, G.R. (Chapter 4), *Molecular Physics of Liquid Crystals*, Ed. Luckhurst, G.R., and Gray, G.W., Academic Press, London, New York, (1979).

[31]. Lee, M.A., and Woo, C-W., *Phys. Rev. A.*, 16, 750, (1977).

Shen, L., Sim, H.K., Shim, Y.H., and Woo, C-W., *Mol. Cryst. Liq. Cryst.*, 39, 229, (1977).

[32]. Hansen, J.P., and MacDonald, I.R., *Theory of Simple Liquids*, Academic Press, London, (1976).

[33]. Hill, T.C., *Statistical Mechanics: Principles and Selected Applications*, McGraw-Hill book Co Inc., New York, London, (1956).

[34]. Brink, D.M., and Satchler, G.R., *Angular Momentum*, Oxford University Press, London, New York, (1962).

[35]. Marcelja, S., *J. Chem. Phys.*, 60, 3599, (1974).

[36]. Flory, P.J., *Statistical Mechanics of Chain Molecules*, Interscience, New York, (1969).

[37]. Gray, G.W., and Mosley, A., *J. Chem. Soc. Perkin Trans. II*, 97, (1976).

[38]. Gray, G.W., *J. Phys.(Paris)*, 36, C1-337, (1975).

Gray, G.W., Harrison, K.J., Nash, J.A., *J. Chem. Soc. Chem. Commun.*, 431, (1974).

[39]. Leadbetter, A.J., Tucker, P.A., Gray, G.W., and Tajbakhsh, A.R., *Liq. Crystals*, 8, 1, (1990).

[40]. Morrison, F.A., Friedrich, C., Noel, C., Davidson, P., and Levelut, A.M., *Liq. Crystals*, 8, 153, (1990).

[41]. See for example,
Sadashiva, B.K., Ra, O., and Subba, G.S.R., *Mol. Cryst. Liq. Cryst.*, 38, 345, (1977).

Gray, G.W., and McDonnell, D.G., *Mol. Cryst. Liq. Cryst.*, 37, 189, (1976).

[42]. Miyaura, N., Yanagi, T., and Suzuki, A., *Syn. Commun.*, 11, 513, (1981).

[43]. Gray, G.W., Hird, M., and Toyne, K.J., *Mol. Cryst. Liq. Cryst.*, 204, 34, (1991).

[44]. Gray, G.W., Hird, M., and Toyne, K.J., *Mol. Cryst. Liq. Cryst.*, 204, 91, (1991).

[45]. Hoshino, Y., Miyaura, N., and Suzuki, A., *Bull. Chem. Soc. Jpn.*, 61, 3008, (1988).

[46]. Williams, D.H., and Fleming I., *Spectroscopic Methods in Organic Chemistry*, 4th Edition, McGraw-Hill book Co.(UK)Ltd. (1987).

[47]. Pouchert, C.J., *The Aldrich Library of Infrared Spectra*, 2nd Edition, Aldrich Chemical Company Ltd.

[48]. Demus, D., and Zaschke, H., *Flüssige Kristalle in Tabellen II*, VEB Deutscher Verlag für Grundstoffindustrie, Leipzig, (1984).

[49]. Wiltshire, S.P., Seddon, J.M., and Luckhurst, G.R., unpublished work.

[50]. Doucet, J. (Chapter 14), *Molecular Physics of Liquid Crystals*, Ed. Luckhurst, G.R., and Gray, G.W., Academic Press, London, New York (1979).

[51]. Luckhurst, G.R., Simpson, P., Zannoni, C., *Liq. Crystals*, 2, 313, (1987).

[52]. Leadbetter, A.J., Frost, J., Gaughan, J.P., Gray, G.W., and Mosley, A., *J. Phys.(Paris)*, 40, 375, (1979).

[53]. Luckhurst, G.R. (Chapter 7), *Recent Advances in Liquid Crystalline Polymers*, Ed. Chapoy, L.L., Elsevier Applied Science Publishers, London, (1985).

[54]. Zannoni, C. (Chapter 9), *Molecular Physics of Liquid Crystals*, Ed. Luckhurst, G.R., and Gray, G.W., Academic Press, London, New York (1979).

[55]. Emsley, J.W., Luckhurst, G.R., and Stockley, C.P., *Proc. R. Soc. A.*, 381, 117, (1982).

[56]. Photinos, D.J., Samulski, E.T., and Toriumi, H., *J. Chem. Phys.*, 94, 2758, (1991).

[57]. Marcelja, S., *Nature*, 241, 451, (1973).

Marcelja, S., *Biochim. Biophys. Acta.*, 367, 165, (1974).

[58]. Humphries, R.L., James, P.G., and Luckhurst, G.R., *J. Chem. Soc. Faraday Trans II*, 68, 1031, (1972).

[59]. Bondi, A., *J. Phys. Chem.*, 68, 441, (1964).

[60]. Emerson, A.P.J., Ph.D. Thesis, University of Southampton, (1991).

[61]. Kanesaka, I., Snyder, R.G., and Strauss, H.L., *J. Chem. Phys.*, 84, 395, (1986).

Wong, T.T., Mansch, H.H., and Snyder, R.G., *J. Chem. Phys.*, 79, 2369, (1983).

[62]. Counsell, C.J.R., Ph.D. Thesis, University of Southampton, (1984).

Stockley, C.P., Ph.D. Thesis, University of Southampton, (1981).

Heaton, N.J., and Luckhurst, G.R., *Mol. Phys.*, 66, 65, (1989).

Counsell, C.J.R., Emsley, J.W., Luckhurst, G.R., and Sachdev, H.S., *Mol. Phys.*, 63, 33, (1988).

[63]. Counsell, C.J.R., Emsley, J.W., Heaton, N.J., and Luckhurst, G.R., *Mol. Phys.*, 54, 847, (1985).

[64]. Heaton, N.J., Ph.D. Thesis, University of Southampton, (1987).